AD-A166 140 AN INTRODUCTION TO ICE IN THE POLAR OCEANS(U) 1/2
WASHINGTON UNIV SEATTLE APPLIED PHYSICS LAB G A MAYKUT
SEP 85 APL-UW-8510 N00014-84-C-0111

UNCLASSIFIED F/G 8/12 NL

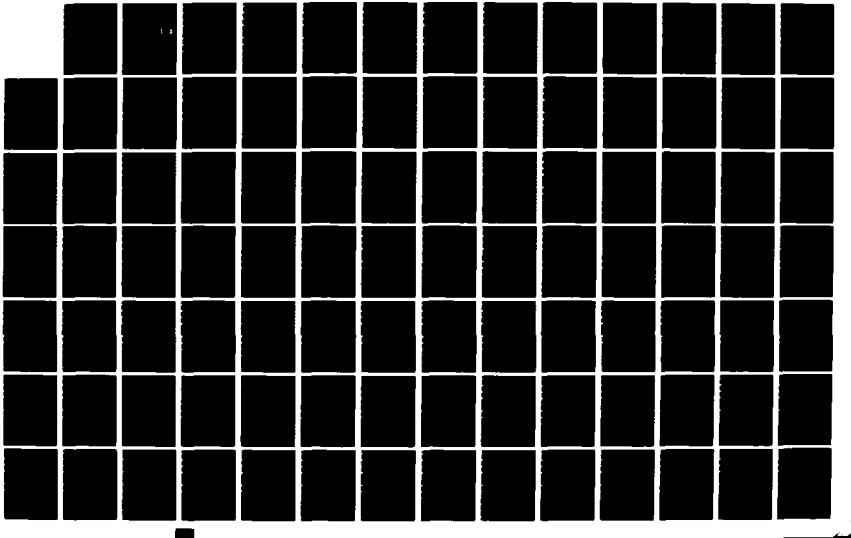

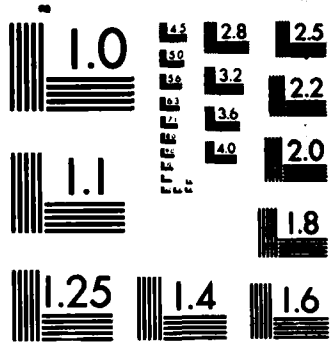

(12)

AD-A166 140

An Introduction to Ice in the Polar Oceans

APL-UW 8510
September 1985

SECURITY CLASSIFICATION OF THIS PAGE (When Data Entered)

REPORT DOCUMENTATION PAGE

READ INSTRUCTIONS BEFORE COMPLETING FORM

1. REPORT NUMBER: APL-UW 8510	2. GOVT ACCESSION NO.
3. RECIPIENT'S CATALOG NUMBER	
4. TITLE (and Subtitle): AN INTRODUCTION TO ICE IN THE POLAR OCEANS	5. TYPE OF REPORT & PERIOD COVERED: TECHNICAL REPORT
6. PERFORMING ORG. REPORT NUMBER: APL-UW 8510	
7. AUTHOR(s): GARY A MAYKUT	8. CONTRACT OR GRANT NUMBER(s): N00014-84-C-0111
9. PERFORMING ORGANIZATION NAME AND ADDRESS: DEPARTMENT ATMOSPHERIC SCIENCES AK-40 UNIVERSITY OF WASHINGTON SEATTLE, WA 98195	10. PROGRAM ELEMENT, PROJECT, TASK AREA & WORK UNIT NUMBERS: 307 252
11. CONTROLLING OFFICE NAME AND ADDRESS: OFFICE OF NAVAL RESEARCH ARCTIC SCIENCES, CODE 1125AR ARLINGTON, VA 22217	12. REPORT DATE: September 1985 13. NUMBER OF PAGES: 107
14. MONITORING AGENCY NAME & ADDRESS (if different from Controlling Office)	15. SECURITY CLASS. (of this report): UNCLASSIFIED 15a. DECLASSIFICATION/DOWNGRADING SCHEDULE

16. DISTRIBUTION STATEMENT (of this Report)

DISTRIBUTION OF THIS REPORT IS UNLIMITED

17. DISTRIBUTION STATEMENT (of the abstract entered in Block 20, if different from Report)

18. SUPPLEMENTARY NOTES

19. KEY WORDS (Continue on reverse side if necessary and identify by block number)

SEA ICE

extent	mass balance	salinity
formation	mechanical properties	structure
growth	morphology	thermal properties
heat balance	optical properties	thickness distribution

20. ABSTRACT (Continue on reverse side if necessary and identify by block number)

This report provides a general review of the formation, growth, distribution, properties, and behavior of sea ice in the polar oceans.

DD FORM 1 JAN 73 1473 EDITION OF 1 NOV 65 IS OBSOLETE
S/N 0102-014-6601

SECURITY CLASSIFICATION OF THIS PAGE (When Data Entered)

An Introduction to Ice in the Polar Oceans

by
Gary A. Maykut

APL-UW 8510
September 1985

Department of Atmospheric Sciences/Geophysics Program
University of Washington
Seattle, Washington 98195

PREFACE

This report is intended to provide a general review of the formation, growth, distribution, properties, and behavior of sea ice in the polar oceans. Special emphasis is given to factors that directly affect biological activity beneath the ice, so that the treatment of some topics (e.g., mechanical properties, ice dynamics) is less complete than that of others (e.g., optical properties, ice growth). Although written primarily for the nonspecialist, the report includes an extensive bibliography where more detailed information can be obtained. A slightly modified version of this report will also appear as Chapter 2, "The ice environment," in *Sea Ice Biota*, edited by Rita A. Horner. The material here is reprinted with permission from *Sea Ice Biota*, copyright CRC Press, Inc., Boca Raton, Florida.

I am indebted to Steve Ackley, Don Perovich, and Ed Waddington for technically reviewing the material in this report. Special thanks go to Rita Horner for her patience and many helpful suggestions during preparation of the manuscript. Finally, I would like to acknowledge the contribution made by the Office of Naval Research whose long-term commitment to sea ice research produced much of the information summarized here, and whose support under Contract N00014-84-C-0111 made possible this review.

TABLE OF CONTENTS

LIST OF FIGURES

LIST OF TABLES

1. EXTENT AND MORPHOLOGY OF THE POLAR ICE PACK

Sea ice interacts thermodynamically with both the atmosphere and ocean, giving rise to a climate over the polar oceans that is more characteristic of the continental ice sheets than of a marine environment. By area, sea ice accounts for roughly two-thirds of the earth's permanent ice cover, but only about 0.1% of its volume. Thus, unlike the polar ice caps, sea ice is only a thin veneer whose thickness and extent can undergo large changes in response to small changes in climate or oceanic heat transport. Not only does a sea ice cover greatly reduce heat exchange between the surface and the atmospheric boundary layer, but it also affects the temperature and salinity structure of the underlying ocean. In particular, growth and melting of the ice causes continual salinity changes at the top of the mixed layer, while variations in ice thickness and concentration complicate the input of solar energy to the water. Because of its impact on the ocean and atmosphere and because of a positive feedback between ice extent and surface albedo, sea ice is generally considered to be an important element in the earth's climate system.

A. Geographical Distribution

At maximum extent sea ice covers some 8% of the Southern Hemisphere and 5% of the Northern Hemisphere. The nature of the ice pack in the two hemispheres is, however, quite different primarily because of differences in the distribution of the polar land masses. In the south the Antarctic Continent occupies most of the area poleward of 70°S, so that sea ice forms a seasonally varying annulus in the region between 55° and 70°S (Fig. 1). Meridional variations are relatively small, the greatest northward extent occurring in the Weddell Sea sector. Most of the antarctic ice pack is seasonal, covering $20 \cdot 10^6$ km^2 at maximum extent and only $4 \cdot 10^6$ km^2 at the end of summer (*Zwally et al.*, 1983).

In the Northern Hemisphere the area poleward of 70°N is in large part a landlocked ocean basin which is ice covered during most of the year. Seasonal ice forms in many of the peripheral seas surrounding the

Arctic Basin (Fig. 2). At minimum extent (August) the ice covers about $7 \cdot 10^6$ km^2, almost double that in the Antarctic, while at maximum extent (March) the area expands to $14 \cdot 10^6$ km^2 (*Walsh and Johnson*, 1979).

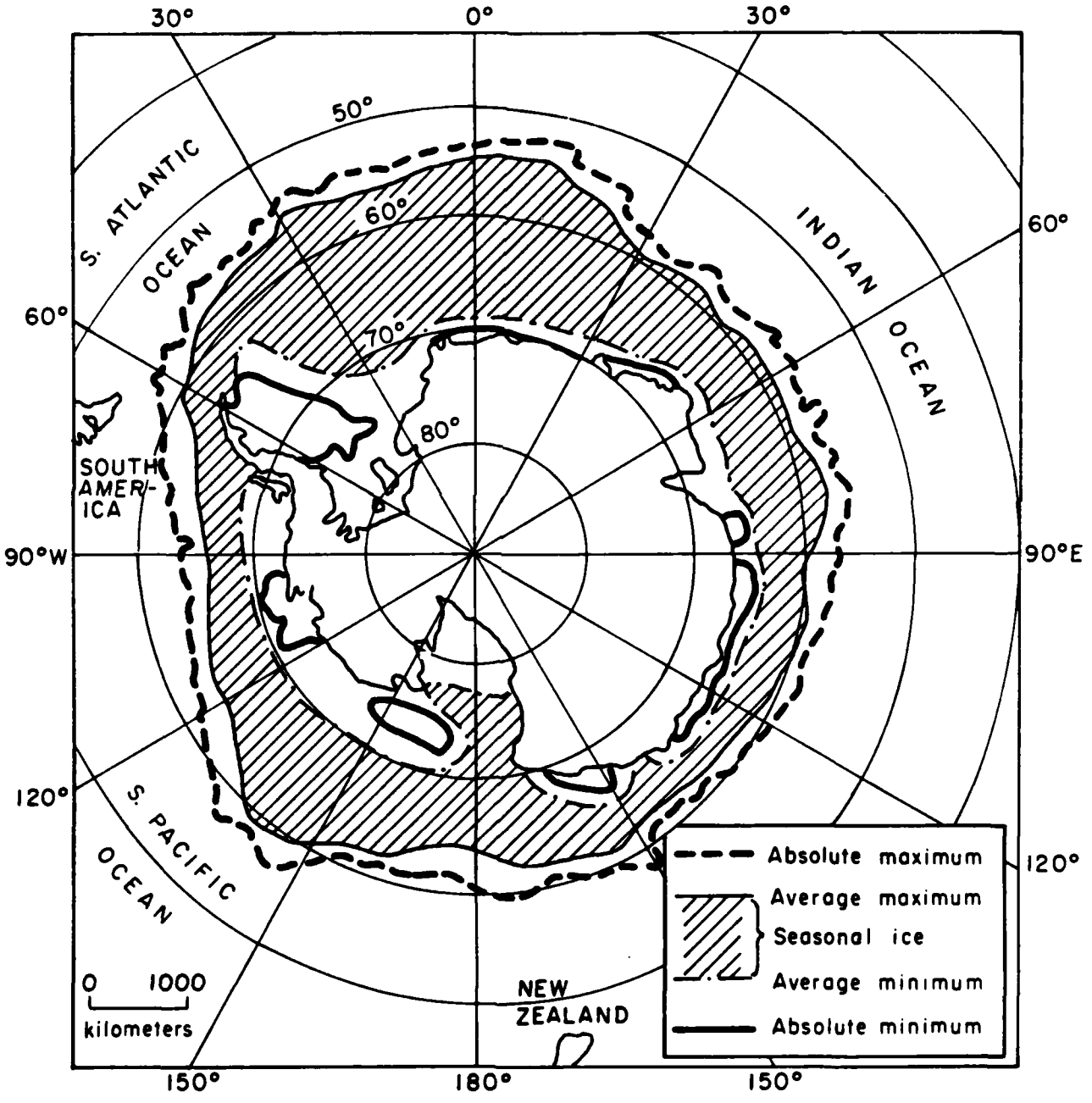

Fig. 1. The extent of sea ice in the Southern Hemisphere with greater than 1/8 concentration (after *CIA*, 1978).

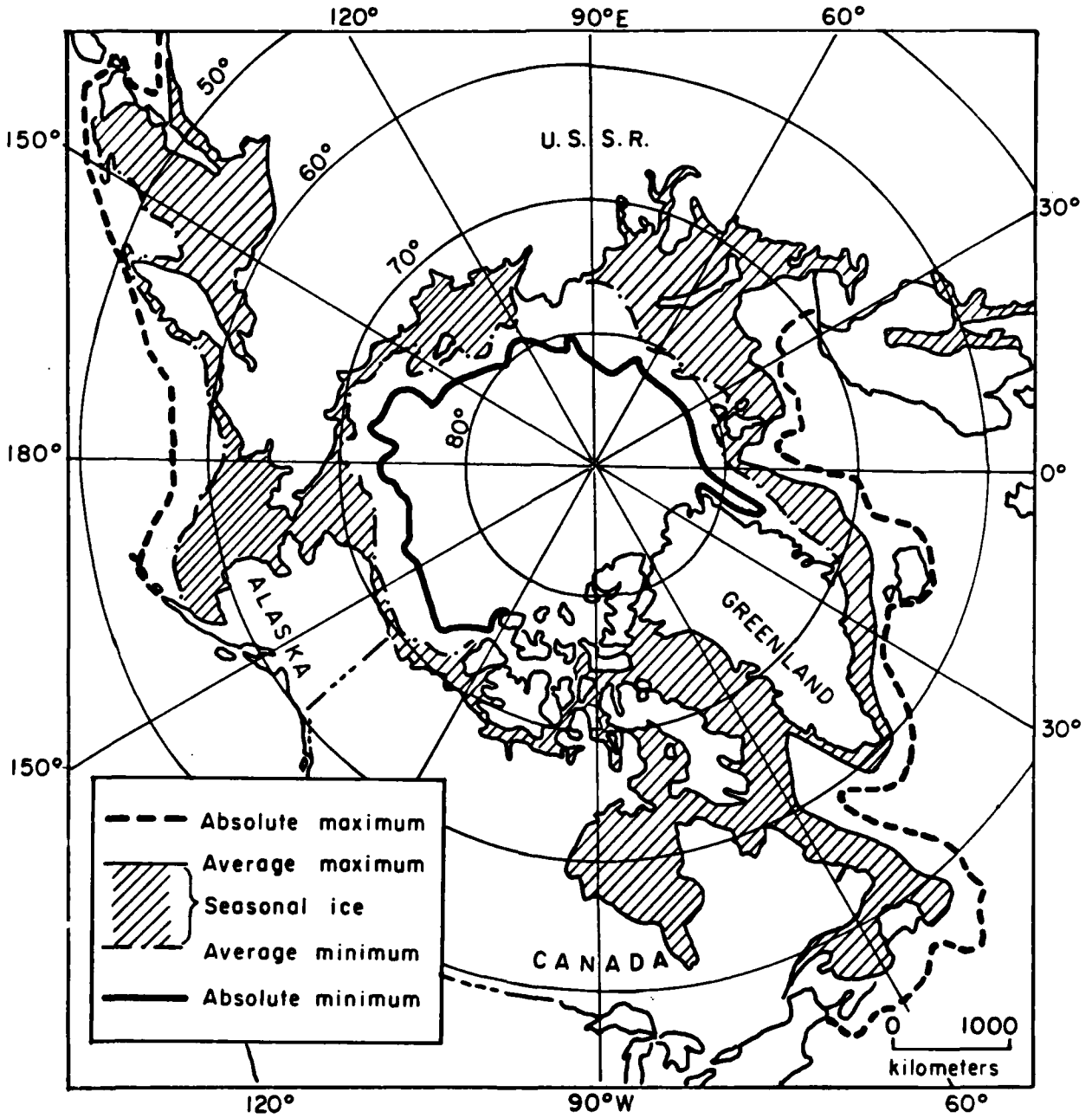

Fig. 2. The extent of sea ice in the Northern Hemisphere with greater than 1/8 concentration (after *CIA*, 1978).

Variations in oceanic circulation and the complex configuration of the land masses cause meridional variations in winter ice extent of up to 35 degrees of latitude. Cold air flowing over the Sea of Okhotsk from the Asian Continent results in the formation of a seasonal ice cover which

typically extends to the north coast of Japan (44°-45°N). At the other extreme is the area west of Spitsbergen (0°, 80°N) where warm Atlantic water flowing into the Arctic Basin and the southward drift of the ice combine to maintain the ice edge at a nearly constant position throughout the year. The economic, military, and scientific importance of the region, together with its relative accessibility, have stimulated extensive research efforts and we now have a good general picture of the ice-ocean-atmosphere system in the Arctic. Such is not the case in the Antarctic. Although some satellite-derived data are available regarding the drift, extent, and physical characteristics of antarctic pack ice (e.g., *Ackley*, 1979), conditions in most ice covered portions of the Southern Ocean are poorly known.

B. Ice Movement

Sea ice, driven principally by winds and currents, is in almost continual motion. As will be discussed later, these motions affect not only the extent of the ice, but also its physical properties and the way in which it interacts with the atmosphere and ocean. Ice motion in the Arctic Basin has been well documented from the trajectories of manned drifting stations and automatic data buoys. Most references describe the two major drift features identified by *Gordienko* (1958): (i) the Transpolar Drift Stream which transports ice from the western side of the basin across the pole and through Fram Strait between Greenland and Spitsbergen, and (ii) a clockwise gyre in the Beaufort Sea region. However, a recent analysis of the mean drift field by *Colony and Thorndike* (1983) shows a somewhat different pattern with anticyclonic motions throughout the Amerasian Basin and southward drift toward Fram Strait in the Eurasian Basin. Average displacements are approximately 7 km/day. Ice movement in the Greenland and Bering seas tends to be southerly with average velocities on the order of 15 km/day (*Muench and Ahlnas*, 1976). While some ice is lost from the Arctic Basin through the Bering Strait, this is small compared to the export through Fram Strait. On an annual basis roughly 10% of the ice in the basin drifts into the Greenland Sea where it eventually melts, providing a significant heat gain for the

basin. Ice movements in the Antarctic are much simpler, being generally clockwise around the continent. A major drift feature exists in the Weddell Sea in the form of a cyclonic gyre which advects ice along the Antarctic Peninsula and allows multiyear ice to develop in the region.

Diverging motions in the ice cause it to break apart and expose the underlying water. These cracks, called *leads*, tend to be narrow (tens to hundreds of meters in width), but may extend for many kilometers. In some situations leads may reach several kilometers in width and are termed *polynyas*. The steep temperature gradients which exist over winter leads result in large turbulent heat losses to the atmosphere and rapid ice production. During the summer, leads act as moving windows which admit substantial amounts of solar energy to the upper ocean. Leads are common in most regions. In the Arctic Basin winter leads occur with an average spacing of about 300 m. Leads tend to freeze over quickly and open water rarely makes up more than 0.5% of the winter ice cover. Young ice ($h < 1$ m) in refrozen leads typically accounts for 5-10% of the area. During the summer decay cycle the area of open water increases greatly, reaching maximum values of 10-20% in the Central Arctic.

In marginal seas where the ice edge is not confined by land, ice concentration patterns are complex and can vary rapidly with time. Over the interior of the Bering Sea ice pack, for example, *Cavalieri et al.* (1983) found winter concentrations ranging between 85% and 100% with cold northeast winds, but these values dropped to as low as 45% following the onset of warm southerly winds. Ice concentrations in the Antarctic are also fairly low, averaging 60-80% throughout most of the year (*Zwally et al.*, 1983). The large amount of open water suggests that antarctic ice undergoes substantial divergence. In fact, analysis of satellite imagery indicates that the antarctic ice pack is everywhere divergent in its mean motion and that northward advection of the ice must result in the continual production of new leads and polynyas (*Budd*, 1975; *Ackley and Keliher*, 1976).

Convergence and shearing motions cause the ice to fracture and pile up into a variety of deformation features, the most notable being pres-

sure ridges. Pressure ridges form linear features up to several kilometers in length which consist of a *keel* beneath the ice and a *sail* on the surface of the ice. Keels are typically about five times thicker than sails. Most ridges in the Central Arctic appear to be built out of ice that was originally less than 1 m thick (*Herbert*, 1970). This may not be true in all areas, however, as detailed morphological studies north of Prudhoe Bay, Alaska, indicated that nearly 50% of the ridges there were composed of blocks between 1.0 and 1.6 m thick (*Tucker and Govoni*, 1981). Ridge frequency in the Arctic Basin varies with season and location, but generally ranges from two to six per kilometer. Keel depths are usually less than 20 m. It has been estimated (*Wadhams*, 1980) that as much as 40% of the total mass in the arctic ice pack may be contained in deformation structures. In contrast to the arctic situation, ridges are generally believed to be uncommon in most parts of the Antarctic because of the divergent nature of the velocity field there. A notable exception is the Weddell Sea where ridged ice may account for more than 15% of the area (*Ackley*, 1979).

Without continued deformations the polar ice pack would assume a much more uniform character. In areas of seasonal ice the thickness would increase smoothly inward from the edge, while in areas of perennial ice the thickness within a particular climatic regime would be essentially constant. The reality is that a typical sea ice cover contains a great range of thicknesses, all temporarily coexisting under similar thermal forcing. Thicknesses tend to be distributed chaotically with large variations occurring on horizontal scales of only a few meters. Ice motion enhances the transfer of momentum from the atmosphere to the ocean and causes thermodynamic interactions between the air and water to be much more vigorous than would otherwise be the case. Mechanical breakup and advection also act to accelerate the decay and retreat of the ice cover, allowing larger portions of the polar oceans to become ice free each summer.

C. Ice Zones

Because of differences in the properties of the ice, in the dominant ice-ocean interaction processes, and in the nature of the

scientific problems encountered, the polar ice pack is frequently subdivided into different zones. The most basic distinction is between regions that are perennially ice covered and those with seasonal ice. Other ice regimes frequently mentioned in the literature include the *fast ice zone*, the *shear zone*, and the *marginal ice zone*.

1. Perennial Ice Zone

Areas of year-round ice are found in both the Arctic and Antarctic; however, the characteristics of this ice differ substantially in the two hemispheres. The *perennial ice zone* in the Arctic, located largely poleward of 75-80°N (Fig. 2), contains about two-thirds of all the multiyear sea ice found in the World Ocean. Thickness averages 3-4 m in the central part of the basin, but increases significantly north of Greenland and Ellesmere Island as the motion of the ice toward the land causes extensive ridging. The age of this ice is uncertain, but may reach tens of years in the Beaufort sector and at least several years on the Soviet side of the basin.

Multiyear ice in the Antarctic is restricted to the Weddell Sea and parts of the Ross, Amundsen, and Bellingshausen seas (Fig. 1). The age of this ice is probably much less than in the Arctic. What is known of drift patterns in the Weddell Sea suggests that the residence time of the ice is not more than 2-3 years. Nevertheless, ice thicknesses of up to 5 m have been observed in undeformed ice there (*Weeks and Ackley*, 1982). The structure of this ice, however, was quite different from that in the Central Arctic. Some 60-70% of the thickness was made up of layers of small ice crystals a few millimeters across rather than the organized columnar structure commonly observed in most arctic ice. These so-called "frazil" crystals could originate in the water column beneath the ice or in nearby leads, but the exact mechanisms involved have not yet been positively identified. In addition to the more complex internal structure, weak surface melting during the antarctic summer allows the salinity of the ice near the surface to remain high.

As a result, microwave techniques that rely on differences in near-surface salinity to distinguish between first-year and multiyear ice are much less successful in the Antarctic than in the Arctic (see Section 4E).

2. Seasonal Sea Ice Zone

The *seasonal sea ice zone* (SSIZ) covers about $25 \cdot 10^6$ km^2, roughly 7% of the World Ocean. The area covered by the SSIZ in the Arctic is about the same as that of the perennial ice. While undeformed ice in the arctic SSIZ is generally less than 2 m thick, large amounts of ridged ice are present so that average thicknesses can be much greater, particularly near the coasts. As pointed out previously, 80% of the highly mobile antarctic ice pack is seasonal. It has been reported (*Paige*, 1966) that seasonal ice in the Antarctic can grow to thicknesses at least 50% greater than in the Arctic. This ice has frequently been observed to possess not only layers of frazil crystals, but also a layer of infiltration ice formed by flooding of the ice surface in response to snow loading in the early stages of growth. The generality of these observations, however, has not been established, and it is not known whether they apply throughout the southern SSIZ or only to certain regions near the continent. The relative importance of various ice decay processes also differs in the two hemispheres. Surface melting, for example, is a major factor in the summer disappearance of arctic ice. Antarctic ice, on the other hand, is characterized by minimal surface melting and an absence of melt ponds, probably owing to lower relative humidity in the atmosphere (*Andreas and Ackley*, 1982). This means that heat from the water must be largely responsible for seasonal ice retreat in the Southern Ocean. In addition, higher biological activity in antarctic ice enhances internal melting, weakening the ice and accelerating the breakup.

Ice-ocean-atmosphere interactions in the shelf regions of the SSIZ appear to have an important effect on the large-scale structure and circulation of the World Ocean (e.g., *Gill*, 1973). It has long been suspected that salt fractionation during freezing leads to the formation

of cold, dense water on the shelves. Such water appears to be the precursor to the Antarctic Bottom Water which fills much of the deep World Ocean. Few details are known regarding production sites, rates, or mechanisms for the formation of this water. Offshore winds produce a number of large recurrent polynyas around the Antarctic Continent, especially in the Ross, Weddell, and Amundsen seas (*Streten*, 1973; *Carsey*, 1980). Rapid ice growth in such polynyas and the resulting increase in density leads to vertical haline convection, possibly all the way to the sea floor in some areas. It is probable that much of the Antarctic Bottom Water originates in this way. Similar processes on certain of the arctic shelves also appear to produce dense water which is critical in maintaining the thermohaline structure of the Arctic Ocean (*McPhee*, 1980).

3. Fast Ice Zone

Shorefast ice occurs along most coasts in the Arctic and Antarctic. It forms early in the winter in shallow water where the water column can cool rapidly to the freezing point. It is anchored to the bottom at the shoreline and frequently at depths of up to 20 m by grounded pressure ridge keels (*Kovacs and Mellor*, 1974). Although rigidly anchored, fast ice may move tens of meters in response to thermal and mechanical stresses (*Tucker et al.*, 1980). Such motions are important because of their potential impact on offshore structures. Salinities beneath ice in lagoons and basins where circulation is restricted can reach values in excess of $100\,^{o}/_{oo}$. The extent of fast ice is determined primarily by sea bottom and shoreline topography and is highly variable. Near Point Barrow, for example, the zone is about 15 km in width while at nearby Harrison Bay it extends some 60 km offshore. Fast ice development is most extensive in areas where the shelf slope is gentle (e.g., MacKenzie Delta and Laptev Sea). Also usually classified as landfast is much of the ice that fills constricted bays and channels in regions like the Canadian Archipelago. A review of landfast ice and biological characteristics of the underlying water has recently been given by *Newbury* (1983).

4. *Shear Zone*

Aircraft and submarine sonar observations indicate the existence of a zone of highly deformed ice in coastal regions along the Alaskan North Slope and Canadian Archipelago (*Tucker et al.*, 1979; *Weeks and Ackley*, 1982). The origin of this so-called *shear zone* is landward movement of the ice pack, causing the ice to converge, shear, and ridge. The frequency of ridges in the shear zone is several times greater than in the central pack, but keel depths are not appreciably larger. The size of the shear zone depends on definition. *Wadhams* (1980) defines the shear zone as the region where ice characteristics differ significantly from those in the Central Arctic. His analysis of submarine data suggests that the shear zone extends some 400 km off the coast of Ellesmere Island where ice motion is normal to the coast, and about 160 km off Alaska where the motion is more parallel to the land. Microwave imagery (*Campbell et al.*, 1976) shows that the landward part of this zone is made up largely of first-year ice and that, as might be expected, the outer part contains a substantial amount of multiyear ice. The shear zone is clearly a boundary layer between the fast ice and central pack and, as such, understanding its behavior is of particular importance in efforts to develop large-scale dynamic models of sea ice.

5. *Marginal Ice Zone*

One of the most complex and scientifically interesting regions, the *marginal ice zone* (MIZ), is located near the boundary between the ice and open ocean. Here, penetration of surface waves into the pack breaks the ice into numerous small floes whose average size increases rapidly with distance from the edge. In regions like the Bering Sea, where floes are usually thin (< 0.5 m), ice in the outer 5-15 km is often heavily rafted and many reach thicknesses of up to 5 m (*Bauer and Martin*, 1980). The MIZ is usually taken to include that part of the ice that is in some way affected by the presence of the open ocean, a region some 150-200 km in width. The outer part of the MIZ is characterized by large horizontal gradients in the properties of the ice, ocean, and

atmosphere. Advection of air across the ice edge can produce large changes in turbulent heat transfer, surface stress, cloudiness, and the radiative fluxes. Comparable changes also occur in the mechanical properties of the ice, surface roughness, and solar input to the ocean. Horizontal variations in density structure and surface stress can give rise to a variety of mesoscale phenomena in the ocean (eddies, jets, upwelling) which impact biological activity and acoustical properties across the MIZ. During the summer, floe breakup and increasing stratification beneath the ice affect the response of the ice to winds and currents and the rate at which heat is transferred from the water to the ice. Biological activity in the MIZ is high (*Alexander*, 1980). Substantial research efforts are currently under way in the Bering and Greenland seas to investigate not only the properties of the ice cover, but also oceanographic, atmospheric, biological, and acoustical characteristics of the MIZ (*McPhee*, 1983; *MIZEX West Study Group*, 1983).

2. FORMATION AND GROWTH OF SEA ICE

A. The Freezing of Seawater

The presence of salt causes seawater to respond somewhat differently to atmospheric cooling than freshwater. A density vs. temperature plot of freshwater (Fig. 3a) shows the existence of a density maximum at 3.98°C. Surface cooling in a freshwater body whose temperature is above this value causes a density increase, generating vertical convection that continues until all the water reaches the temperature of maximum density (T_m). Further cooling then produces a density decrease in the surface layer, allowing the water to become thermally stratified. Since conduction rather than convection is then the dominant heat transport mechanism in the water, there is a sharp decrease in the upward flux of heat to the surface, and cooling proceeds rapidly. Ice can thus form in freshwater when most of the water column is significantly above the freezing point.

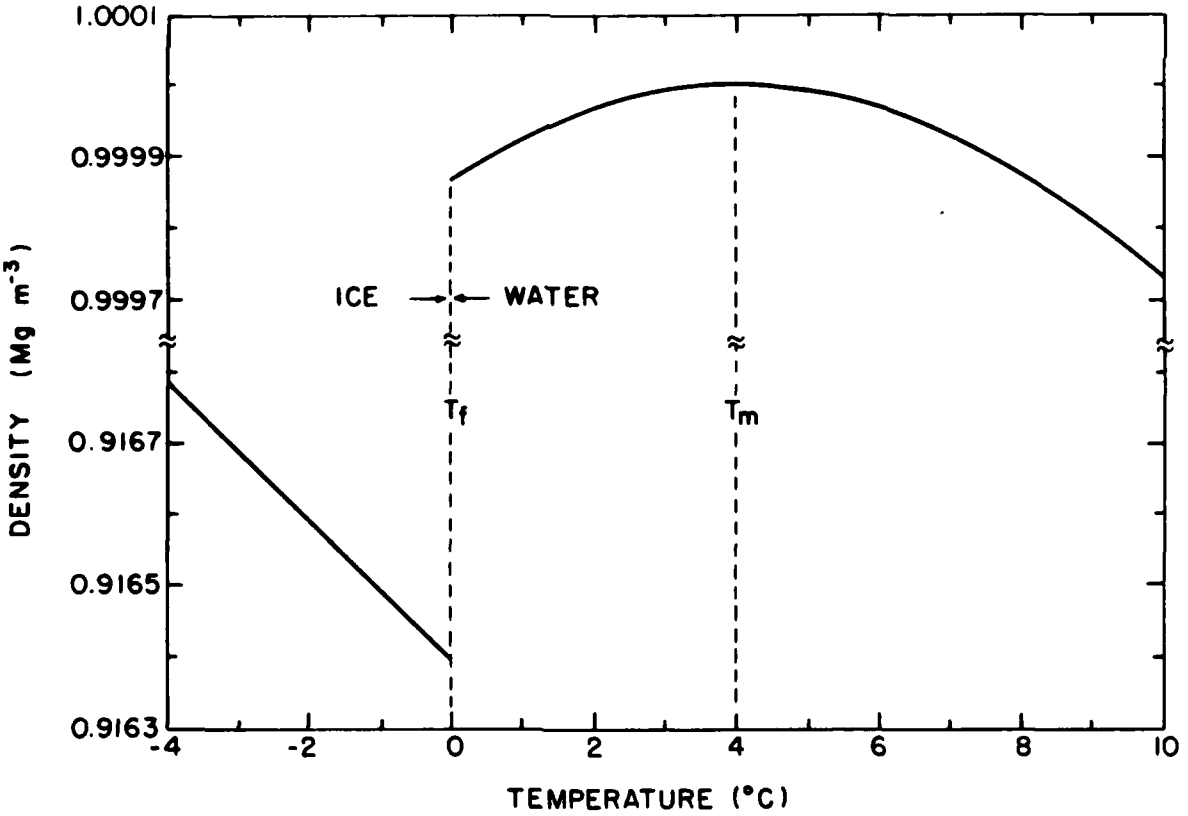

Fig. 3a. Density vs. temperature diagram for freshwater and ice at atmospheric pressure.

Addition of salt to the water depresses the freezing point of the solution (T_f) according to the relation (*Neumann and Pierson*, 1966)

$$T_f = -0.003 - 0.0527S_w - 0.00004S_w^2, \quad (1)$$

where temperature is in °C and the salinity of the water (S_w) is in °/oo. For many purposes Eq. (1) can be approximated simply by $T_f = -0.055S_w$. Salt also reduces T_m, but at a more rapid rate than T_f (Fig. 3b). If $S_w > 24.7$ °/oo, $T_m = T_f$. As this is the case in normal seawater, surface cooling results in a density increase and vertical mixing which continues until the water reaches T_f. Unlike freshwater lakes, however, density gradients in the upper ocean usually limit the depth (z_c) to which the water must be cooled before freezing can commence. Soviet data (*Doronin and Kheisin*, 1975) indicate that z_c is

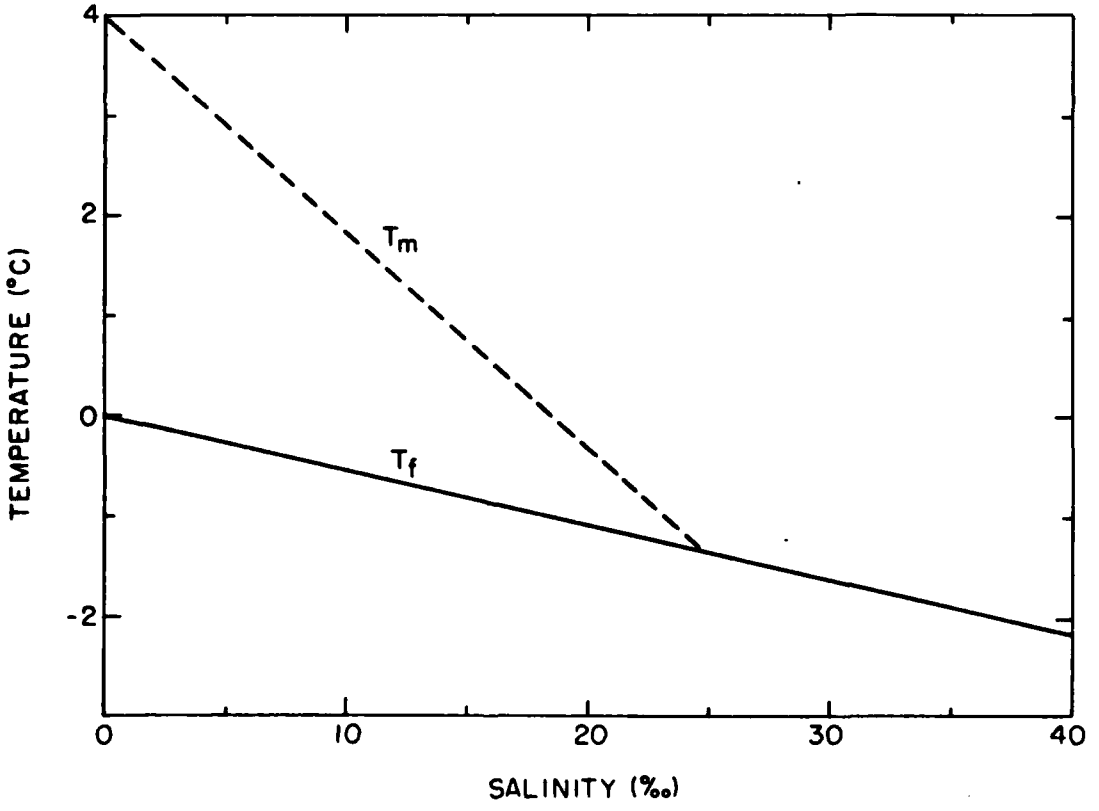

Fig. 3b. Effect of salinity on the temperature of maximum density (dashed curve) and the freezing point temperature (solid curve).

usually in the 10-40 m range, although values in excess of 70 m have been observed. The density structure of the ocean is thus a major factor in determining the onset of freezing. Observations (*Doronin and Kheisin*, 1975) show a delay of as much as two months in the date of initial ice formation in regions where z_c = 50 m compared to those where z_c = 10 m.

B. Initial Ice Formation

Once the upper ocean reaches the freezing point, additional heat loss produces slight supercooling of the water and ice formation begins. The amount of supercooling necessary to initiate ice growth is usually small, probably on the order of a few hundredths of a degree Celsius, although observations in some antarctic polynyas and near Greenland have shown a supercooling of 0.2-0.4°C down to depths of tens of meters (*Doronin and Kheisin*, 1975). Initial ice formation occurs at or near the surface of the water in the form of small platelets and needles which are termed *frazil ice*. Frazil crystals do not generally exceed 3-4 mm in diameter. Continued freezing results in the production of *grease ice*, a soupy mixture of unconsolidated frazil crystals. Because grease ice suppresses capillary wave action, it appears as a smooth, grayish layer whose albedo is only slightly above that of open water. Under quiescent conditions the frazil crystals quickly freeze together to form a solid, continuous ice cover with a thickness between 1 and 10 cm. More typically, wind waves induce turbulence in the water and abrasion between the crystals which inhibit development of a solid cover. Wind and wave action advect frazil crystals downwind where accumulations up to 1 m thick can form in front of obstacles (e.g., floe edges). Laboratory experiments (*Martin and Kauffman*, 1981) indicate that when the ice volume is low, grease ice behaves as a fluid whose viscosity increases as the proportion of ice increases. Once the ice fraction exceeds 30-40%, sintering and regelation create sufficient bonding between individual crystals that their mobility is drastically reduced and the transition to a solid cover begins. In the presence of

a wave field, this transition is usually marked by the formation of *pancakes*, rounded masses of semiconsolidated slush 0.3-3.0 m in diameter. Pancakes often display irregular ice rims around their perimeters, built up as a result of continual bumping into one another. With time, the pancakes consolidate and are welded together into a composite ice sheet by the freezing of grease ice that forms between them. A detailed review of initial freezing processes, together with photographs of different stages of ice development, appears in *Weeks and Ackley* (1982).

C. Young Ice Growth

In the early stages of growth (grease ice, pancake ice) the surface of the ice is wet and its temperature stays close to the freezing point. With air temperatures often in the -10 to -20°C range, turbulent and longwave radiation losses are large and ice formation rapid. However, once the ice becomes consolidated, free water is no longer available at the surface and its temperature begins to approach that of the atmosphere. Additional growth then occurs by accretion on the underside of the sheet, the rate depending on how rapidly heat can be conducted from the ice-water interface toward the surface, i.e., on the thermal conductivity and temperature gradient in the ice.

While winds, cloudiness, relative humidity, snowfall, and oceanic heat flux all affect the rate of ice growth, field measurements suggest that reasonable growth estimates can be obtained from air temperature data alone. Figure 4 shows ice thicknesses observed by *Anderson* (1961) near Thule, Greenland, plotted against the cumulative number of freezing-degree days θ, where

$$\theta \equiv \int_o^t (T_f - T_a)dt \quad , \tag{2}$$

t is time, and T_a is the air temperature. Anderson found that in the thickness range $10 < h < 80$ cm his data could be fit by a simple power law,

$$h^2 + 5.1\ h = 6.7\theta \quad . \tag{3}$$

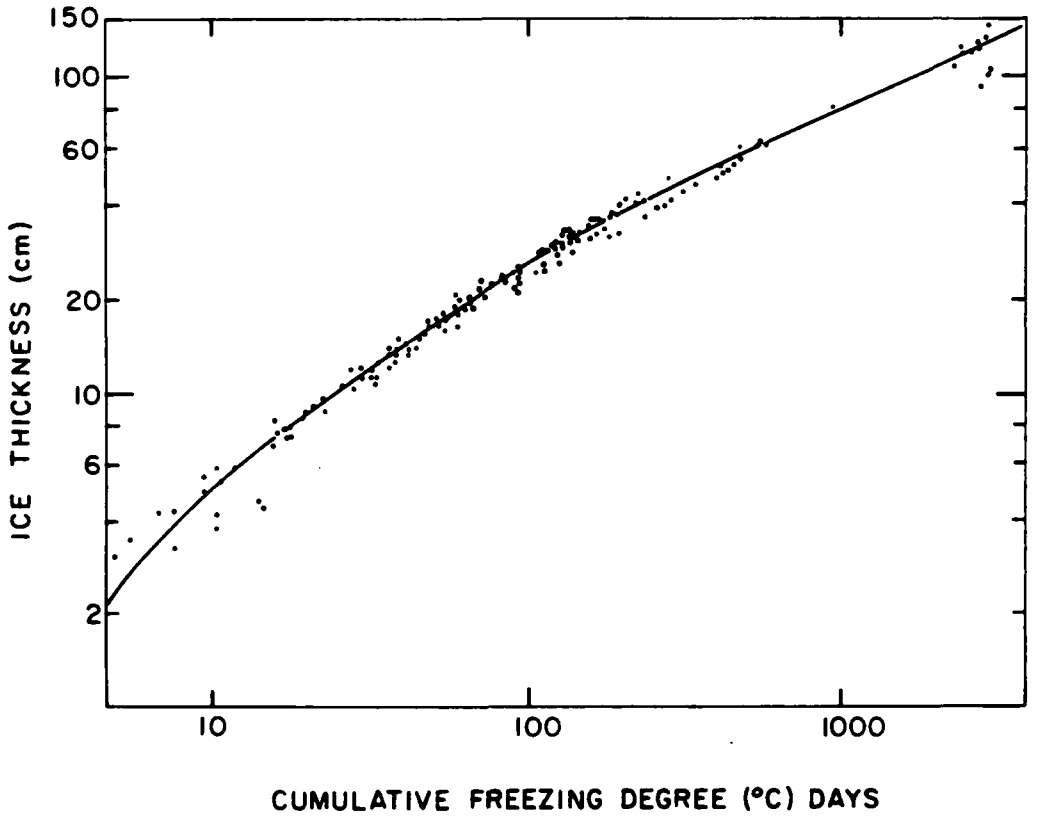

Fig. 4. Relationship between the thickness of young sea ice with minimal snow cover and the cumulative number of freezing-degree days (after *Anderson*, 1961).

As the ice becomes thicker, the close relationship between θ and h begins to break down. Figure 4, for example, shows that when θ = 3000 degree-days, the observed h varies between 90 and 140 cm. Factors contributing to this breakdown are the increasing thermal mass of the ice, the decreasing magnitude of the heat flux in the ice relative to that in the ocean, and increasing snow cover. The term *young ice* has been somewhat narrowly defined in the *Glossary of Snow and Ice* (*Armstrong et al.*, 1973) as ice in the 10-30 cm category. Here the term will be used in a broader sense to refer to ice whose temperature profile is nearly linear and whose growth can usually be described by some simple function of θ, i.e., h < 80-100 cm.

Alternate expressions for $h(\theta)$ have been derived by investigators working in other regions (see *Bilello*, 1961). Implicit in such formulations is the idea that the exact form of $T_a(t)$ is unimportant in determining h; rather it is only the area under the curve that needs to be known. This is equivalent to saying that the ice would, for example, attain the same thickness in 10 days at -20°C as it would in 20 days at -10°C (assuming that T_f = 0°C). Differences in growth predicted by the various empirical formulas presumably reflect differences in environmental parameters (snowfall, heat content of the underlying water column, etc.) which are not explicitly treated in the formulas. As a result such equations must be considered at least partially site-specific and their utilization approached with caution. Applying an equation obtained from data in the Central Arctic to coastal conditions or to conditions in the Southern Ocean could lead to substantial errors.

To establish a more general relationship, it is necessary to consider the physics governing the situation. The usual approach is to formulate a model using energy balance equations at the top and bottom of the ice (see Section 5B) which are coupled by an equation describing the rate of heat transport between the two boundaries. The problem is greatly simplified in the case of young ice because the conductive flux is directly proportional to the temperature difference between the boundaries. It can easily be shown (e.g., *Maykut*, in press) that the form of Anderson's equation follows from the assumption of a linear temperature gradient in the ice and negligible heat flux in the water. The theoretical expression can be written

$$h^2 - h_o^2 + \left(\frac{2k_i}{k_s} h_s + \frac{2k_i}{C_t}\right)(h - h_o) = \frac{2k_i}{\rho_i L}\theta \,, \qquad (4)$$

where h_o is the initial thickness of the ice, k_i is the average thermal conductivity of the ice, k_s is the thermal conductivity of the snow, ρ_i is the density of the ice, L is the latent heat of fusion, C_t is a bulk transfer coefficient parameterizing turbulent heat transfer between the

ice and atmosphere, and h_s is the snow depth which is assumed to remain constant over the period of integration. The net radiation balance is assumed to be zero. When $h_s = 0$ and the surface temperature of the ice (T_o) is equal to T_a, Eq. (4) yields the classic result that h is a simple function of $\theta^{1/2}$. Taking into account the difference between T_a and T_o gives rise to the linear term in (4). With no snow, the linear term rapidly decreases in importance once h exceeds about 20 cm. A small amount of snow, however, greatly extends the range over which the linear term dominates the growth.

With nominal values for the thermal properties and $h_o = 0$, (4) can be written as $h^2 + (13.1h_s + 16.8)h = 12.9\theta$. Comparison with (3) shows that the theoretical coefficients multiplying the h and θ terms are substantially larger than the ones found empirically. If $h_s = 0$, (4) predicts much too rapid a growth. With a few centimeters of snow the theoretical growth is too slow initially and too rapid once the ice becomes thicker. One factor contributing to this problem is that, contrary to what was assumed in the derivation of (4), heat conduction in the ice is not usually the dominant heat transfer mechanism in the early stages of ice formation. Strictly, then, (4) should be applied only after a solid ice cover has been established. Another complication is the fact that h_s cannot be expected to remain constant over extended periods of time. It is, however, possible to take into account $h_s(t)$ by applying (4) in a stepwise fashion between periods of snow accumulation. Such an approach was taken by *Nakawo and Sinha* (1981) in analyzing ice growth data from the Canadian Arctic. Surprisingly, they found that growth predictions made by including observed variations in h_s were less accurate than those obtained using a large constant snow depth. The reason for the apparent failure of the more rigorous method was probably due to the oceanic heat flux at the bottom of the ice (F_w). *Allison* (1981) reports values of F_w as high as 50 W m^{-2} under young, rapidly growing ice, which would be sufficient to decrease growth rates by 1-2 cm/day.

Unfortunately, a simple analytic solution to the heat balance equations cannot be obtained when F_w is nonzero, making it necessary to employ numerical techniques to estimate the ice growth. In the case of young ice the numerical procedures are relatively simple and growth calculations straightforward. Using a numerical model to describe the thermodynamics of young ice (e.g., *Maykut*, 1978) has the advantage that many of the simplifying assumptions (e.g., zero radiation balance) that were needed to obtain an analytical expression are unnecessary. Moreover, such a model is general in that it is not restricted to a particular location or season, provided that sufficient information on the thermal forcing is known. If actual data on snowfall, T_a, F_w, wind speed, and the radiative fluxes are available, very accurate growth calculations can be made. Even if direct observations are lacking, it is possible to improve on empirical predictions through the use of climatological data and suitable parameterizations for the radiative fluxes (*Maykut*, in press). The most serious source of error in such a calculation would probably be uncertainties in F_w. If only a crude estimate of ice growth is needed, then the formula given by *Zubov* (1945), $h^2 + 50h = 8\theta$, will probably yield acceptable results as it represents an average of many years of observation from the Soviet Arctic. Because it contains implicit assumptions regarding $F_w(t)$ and $h_s(t)$, its applicability to the Southern Ocean is doubtful.

Although estimating the thickness of the ice is of primary importance in many practical problems, the *rate* at which it grows affects the level of convective activity and the structure of the underlying ocean. This is because freezing removes freshwater from the surface of the water column, producing in effect a salt flux at the bottom of the ice. The rate of ice production is extremely sensitive to ice thickness, dropping by roughly an order of magnitude in the first 50 cm of growth. Figure 5, based on Anderson's observations, shows growth rate f as a function of h for several different air temperatures. Note that the sensitivity of f to T_a tends to decrease as h increases.

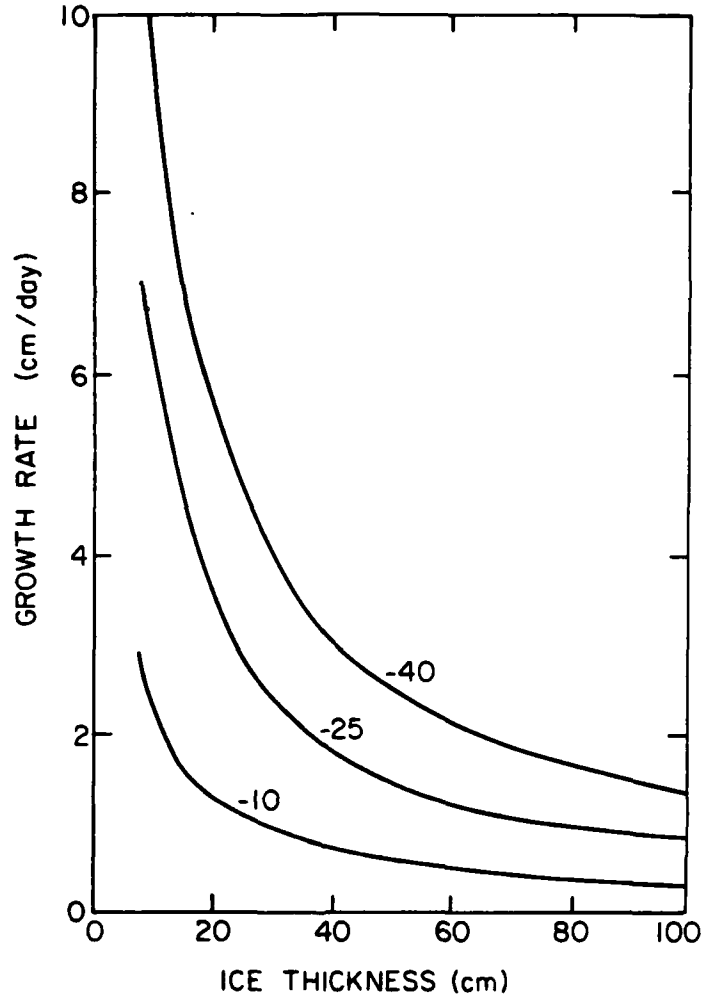

Fig. 5. Dependence of growth rates in young sea ice on ice thickness and air temperature (°C) (after *Maykut*, in press).

Because of its low thermal conductivity, snow insulates the ice and decreases the rate at which it can lose heat to the atmosphere. With a numerical model it is possible to quantify the response of young ice to changes in h_s (Fig. 6). Increasing h_s decreases f, the effect being much more pronounced for the thinner ice. For the case illustrated, f is essentially constant if $h_s > 15$ cm. The reason for this behavior is best explained in terms of the *thermal conductance* (γ) of the combined

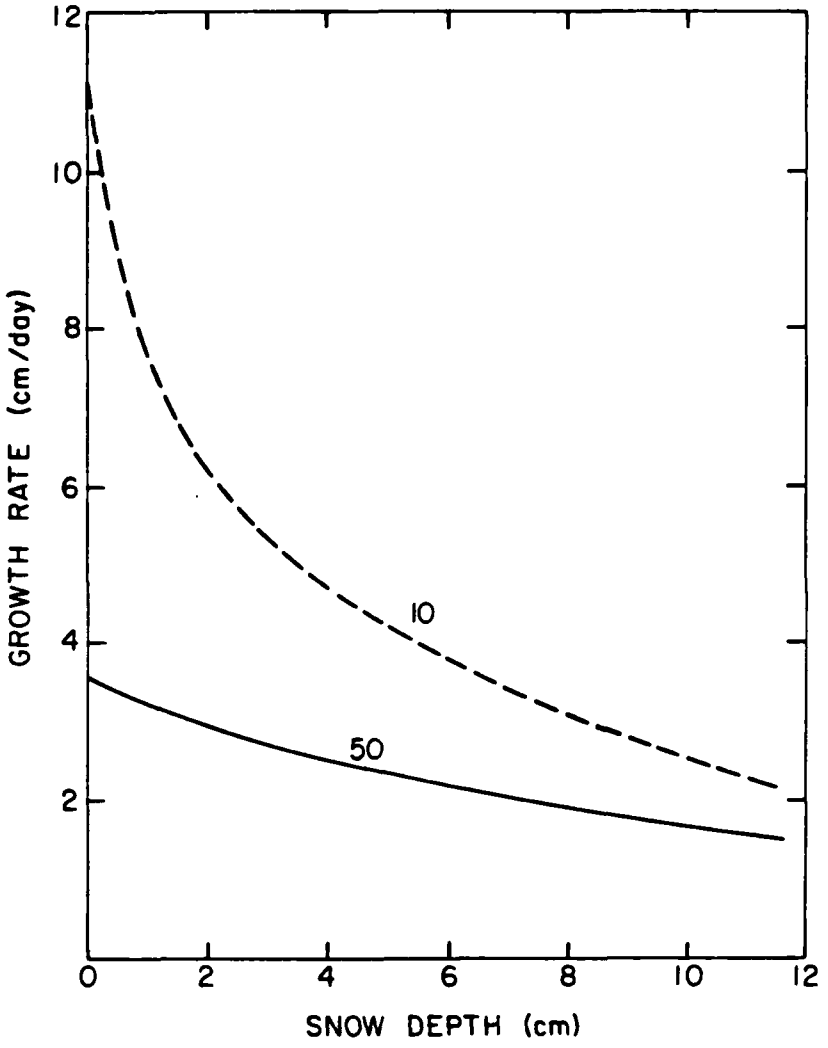

Fig. 6. Growth rates as a function of snow depth for ice thicknesses of 10 and 50 cm.

ice-snow slab. The magnitude of f depends on the rate at which heat is conducted through the slab (F_c), which for young ice can be written

$$F_c = \gamma(T_s - T_f) \quad , \tag{5}$$

where T_s is the surface temperature of the slab and $\gamma \equiv k_i k_s/(k_i h_s + k_s h_i)$. Values of $\gamma(h,h_s)$ are presented in Section 4 (see Fig. 14). When h_s is small, γ (and hence f) decreases rapidly with increasing h; when h_s is large, γ is small and changes slowly with both h and h_s.

D. Multiyear and Thick First-Year Ice Growth

The principal simplification used in treating the growth of young ice was the assumption of a linear temperature gradient in the ice, causing f to respond immediately to changes in thermal forcing at the surface. However, measurements of the temperature field in multiyear ice (*Untersteiner*, 1961) indicate significant departures from linearity, even during midwinter when temperature fluctuations are relatively small. Figure 7 shows theoretical predictions of f(h) as a function of season for thicker ice in the Central Arctic. The curves demonstrate that differences in thermal mass strongly affect how the ice responds to conditions at the upper surface. In November, over two months after

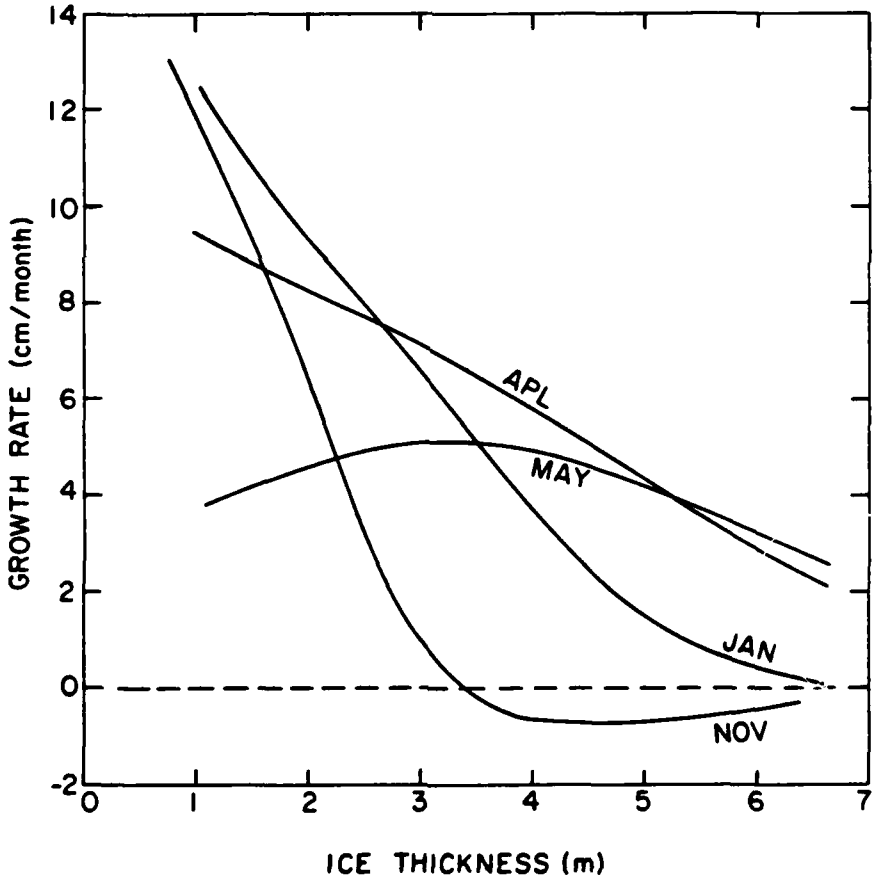

Fig. 7. Growth rates in multiyear and thick first-year sea ice as a function of season in the Central Arctic (after *Maykut*, in press).

freezeup, ice thicker than about 3 m continues to ablate because the fall cooling has had insufficient time to reach the lower part of the ice. Spring warming is reflected in decreasing values of f in the thinner ice during April and May, while ice thicker than 4 m continues to feel the effects of the winter cooling. In June, accretion can occur at the bottom of the ice while vigorous melting is taking place at the surface. Clearly the assumption of a linear temperature profile is invalid for thicker ice whose growth depends more on its thermal history than on the immediate heat balance at the surface.

Heat transport and temperature changes in thicker ice can be predicted by utilizing the standard second-order partial differential equation describing heat conduction in a solid. Combining this equation with heat balance equations at the upper and lower boundaries of the ice results in a model that can simulate the growth of any thickness of undeformed ice (see Section 5B). A detailed model of this type which takes into account effects of salinity and internal solar heating has been formulated and successfully tested under arctic conditions by *Maykut and Untersteiner* (1971). A serious drawback to incorporating the heat conduction equation into an ice model is that an accurate solution involves strong numerical constraints and substantial computer resources. The problem can, to a large extent, be overcome by only crudely resolving temperatures within the ice. Numerical experiments (*Semtner*, 1976; *Maykut*, in press) indicate that results of sufficient accuracy for climate studies or biological applications can be obtained with as few as three or four internal temperature points. Numerical difficulties in this case are minimal.

E. Equilibrium Growth

The concept of an *equilibrium thickness* (h_e) is frequently useful in discussing perennial ice in the Arctic. Such ice loses mass each summer by ablation at the upper and lower boundaries and gains mass the rest of the year by accretion at the bottom. The amount of ice accreted each year depends strongly on h. If interannual variations in atmospheric and oceanic forcing are small, the ice will ultimately attain a

steady-state thickness pattern where summer ablation essentially balances the net annual accretion. The ice is then in thermodynamic equilibrium with its environment, and ice thicker than equilibrium will experience net annual thinning while ice thinner than equilibrium will undergo net growth. Model simulations (Section 5B) indicate that the magnitude of h_e is especially sensitive to factors that affect the amount of surface melting: air temperature, ice albedo, incoming radiation, and turbulent heat exchange. Despite small year to year changes in the present climate and advection of ice between different climatic regimes, observations show that undeformed older ice in the Arctic Basin almost invariably has a thickness in the 3-4 m range, in agreement with theoretical expectations for h_e in the region (*Maykut and Untersteiner*, 1971). Although equilibrium ice in the Arctic may conceivably exist for any length of time, it is composed of ice whose age does not generally exceed 7-10 years. Over an annual cycle some 40-50 cm of ice are lost from the surface and replaced by an equal amount of new ice at the bottom. Thus an ice particle will necessarily move upward with time at a velocity of 40-50 cm per year until eventually melting away at the surface.

F. Underwater Frazil Production

To this point the discussions have focused on *congelation ice* (sometimes called *columnar ice*) which grows at the ice-water interface in response to conductive heat losses along the temperature gradient in the ice. It has been widely accepted that such ice makes up the vast majority of the polar ice pack; however, recent data suggest that there are some regions where other ice formation mechanisms may be important. As mentioned earlier, multiyear ice in the Weddell Sea appears to be substantially thicker than would be expected on the basis of congelation growth alone. Ice core data from the region indicate that congelation ice accounts for only about 20% of the multiyear ice and 47% of the first-year ice, with fine grained layers of frazil crystals making up most of the remainder. This means that 3-4 m of frazil crystals must accumulate and be incorporated into the ice cover over one or two annual

cycles. The higher percentage of frazil in thicker ice presumably reflects a decrease in the rate of congelation growth relative to frazil ice growth, suggesting that frazil production is not strongly dependent on ice thickness. The fact that frazil layers are often sandwiched between layers of congelation ice indicates that frazil production is episodic.

Underwater frazil ice also appears to be common along the antarctic coast. For example, *Dayton et al.* (1969) observed 1-4 m thick billows of frazil crystals beneath the ice in McMurdo Sound. On some occasions ice crystals appeared throughout the water column accompanied by the formation of anchor ice on the sea bottom and on lines hanging in the water. Similar conditions were also noted by *Morecki* (1965) near Mirny. It is suspected that periodic incursions of supercooled water generated at nearby ice shelves may be responsible for the coastal observations, but it does not seem likely that this mechanism could explain the extensive distribution of frazil in the Weddell Sea.

Because frazil crystals usually nucleate at some depth within the water column and then float to the surface, frazil accumulations tend to concentrate sediment and algae contained in the water. *Weeks and Ackley* (1982) mention that concentrations of algae in young Weddell Sea ice can be several times that in the water. Microscopic examination of the ice revealed considerable numbers of cells within individual crystals, suggesting that such cells are an effective nucleating agent for frazil ice. At the same time, one to two orders of magnitude more cells were located at grain boundaries than within crystals. Since the ice was too young for significant biological growth to have taken place within the ice, it follows that the algae loading was primarily the result of scavenging by the rising crystals.

Analogous phenomena also appear to be widespread in coastal portions of the Arctic where divers frequently encounter accumulations of slush on the underside of congelation ice. This "slush ice" can reach thicknesses of at least 2.5 m, but over 50% of the layer appears to consist of unfrozen water and divers can easily reach into it with

their hands (*Larsen*, 1980). Although frazil crystals form the bulk of this slush, large numbers of silt particles are often located in interstices between the frazil crystals. The source of many of these particles is likely to be scavenging from the water column, but direct entrainment by ice crystals forming on the sea floor could also be a factor. With time, upward loss of heat through the overlying congelation ice will cause interstitial water in the slush to freeze, producing a solid layer. Normal congelation ice may then form below the frozen slush. This was clearly the case in many of the Weddell Sea cores. Biological activity is severely impacted by the presence of silt-laden ice, light transmission and photosynthesis being negligible beneath it. Moreover, advection and subsequent melting of such ice after the spring breakup could represent an important sediment transport mechanism in the Arctic. Because most of the underice diving has taken place within a few kilometers of the coast, it is not known whether such intense frazil generation also occurs in deeper water where little if any sediment would be entrained. In the Central Arctic frazil production takes place in leads and in water below the ice, but there is little evidence from core data to suggest a significant effect on ice thickness.

Numerous mechanisms have been proposed to explain the occurrence of frazil ice in the ocean (*Larsen*, 1980; *Weeks and Ackley*, 1982; *Newbury*, 1983). All depend on having slight supercooling and some degree of turbulence in the water column. Wind induced mixing is one such mechanism. However, its effects are only felt near the surface and are rapidly damped out as the grease ice accumulates. In large leads and polynyas, wind and wave action herd the frazil crystals to the downwind side where it can accumulate to depths of up to 1 m (*Martin*, 1981). Currents and local circulations can carry some of these crystals beneath the surrounding ice but, except for regions with semipermanent polynyas, the process is self-limiting and does not seem capable of explaining the widespread distribution of frazil in areas like the Weddell Sea.

Another source of underwater frazil ice is the upward movement of water at its freezing point. Decreasing pressure as the water rises

raises the freezing point, producing supercooling and the potential for frazil formation. This mechanism is believed to be responsible for frazil generation near ice shelves, icebergs, and perhaps even pressure ridge keels. Likewise, contact between water masses of different salinity, but which are each at their freezing point, can cause ice to form at their interface through the process of double diffusion. Such ice is known to occur where rivers empty into the sea and during summer runoff of meltwater from the ice pack. In some areas like the Beaufort Sea coast, permafrost extends beneath the sea floor, promoting downward conduction of heat and the formation of anchor ice. Periodic release of anchor ice could thus contribute to sediment loading and ice accumulation at the bottom of the ice cover. While most of these mechanisms are restricted to very special situations, underwater frazil ice can also form as a result of thermohaline convection, a process associated with sea ice throughout the polar regions. Drainage of cold dense brine from the interior of sea ice occurs during much of the year and produces descending plumes of brine that cause supercooling in the adjacent water. Some of the resulting ice forms as hollow stalactites around the brine where it exits the ice, but laboratory studies indicate that as much as half of the ice production is in the form of frazil crystals (*Martin*, 1974). Similar plumes also exist under refreezing leads. *Weeks and Ackley* (1982) feel that there is a greater potential for frazil production in the Antarctic than in the Arctic and suggest that thermohaline convection could account for much of the frazil observed in the Weddell Sea. None of these processes have yet been studied in sufficient detail to allow quantitative calculations. It appears, however, that underwater frazil ice is much more widespread than previously thought and that no single mechanism is likely to explain all of the observed phenomena.

G. The Summer Melt Cycle

Existing data indicate significant differences in summer melt progression between regions of perennial ice, seasonal ice, and coastal ice, and between the Arctic and Antarctic. In the Arctic, melting of the

snow cover begins as the air temperature approaches the freezing point and typically takes 2-3 weeks. Accompanying the snow melt is a dramatic decrease in albedo due to the puddling of melt water on the surface. Melt pond coverage on multiyear ice may briefly reach values of 50-60%, but quickly decreases to about 30% once the snow cover has been removed. With the development of melt ponds, area-averaged albedos drop from about 0.7 to 0.5. Deepening and consolidation cause a continual decrease in the areal extent of the ponds throughout the summer. Values as low as 10% are common by the end of August. Albedos increase from about 0.50 to 0.55 during this period. Because turbulent heat fluxes and longwave radiation act to remove heat from the surface during the summer, the energy needed to drive the melt cycle in regions of perennial arctic ice comes almost entirely from shortwave radiation.

Initial melting on seasonal ice produces nearly complete pond coverage because of the lack of surface topography. Even when the melt cycle is well advanced, it is not unusual for shallow ponds to occupy 60% or more of the surface and average albedos to be in the 0.40-0.45 range. In coastal regions dust deposited from nearby land areas tends to lower the albedos even further. Areally averaged albedos as low as 20% have been reported from such regions (*Langleben*, 1966). Air temperatures in coastal areas are typically warmer than the ice, and the turbulent fluxes make a substantial contribution to the melting. Lower albedos and thinner ice also allow greater input of solar energy to the underlying ocean in areas of seasonal ice. Thus, even when the incoming radiation fluxes are similar, ice decay proceeds more rapidly in coastal regions and areas of first-year ice than in the interior pack.

The pattern of ice decay in the Southern Ocean appears to differ strikingly from that in the Arctic. Katabatic winds, higher latitudes, and lower oceanic heat fluxes cause melt rates near the continental boundaries to be small compared with those near the free boundary of the antarctic ice pack. Moreover, the melt ponds which are so characteristic of melting ice in the Arctic have rarely been observed in the Antarctic, and surface melting appears to be minimal. The reason appears to be related to differences in the meteorological variables

that control the surface heat balance. Surface melting in the Arctic often takes place with air temperatures significantly below freezing. In the Antarctic, however, *Andreas and Ackley* (1982) argue that lower relative humidities and stronger winds enhance turbulent heat losses from the ice and allow surface melting to occur only with air temperatures significantly above $0^{o}C$, a condition rarely encountered over the ice cover in the Southern Ocean. In spite of the near absence of surface melting, most of the antarctic ice pack disappears each summer, presumably as a result of melting at the ice-water interface. *Gordon* (1981) estimates that no more than half of the necessary energy could be derived from the relatively warm deep water below the Southern Ocean pycnocline. The remainder must come from shortwave radiation absorbed by the upper ocean, either through leads in the ice pack or near the ice edge.

An open lead absorbs over 90% of the incident shortwave radiation, about half of which is absorbed in the upper two meters of the water. Part of this energy goes to lateral melting on floe edges, causing an increase in the area of open water (A_w). This represents a positive feedback process which affects both the rate of retreat of the ice edge and the overall heat and mass balance of the ice pack. In sheltered bays and fjords along the arctic coast, for example, surface melting is generally inadequate to remove the 2-2.5 m of ice which grows each winter. The annual disappearance of this ice can only be explained by taking into account the accelerated decay produced by solar heating in leads (*Langleben*, 1972).

Both ice dynamics (diverging motions) and thermodynamics (lateral melting on floe edges) affect A_w, though field data are not yet adequate to identify their relative importance in the different regions. Except in areas like the Greenland Sea, ice divergence is believed to be much smaller in the Arctic than in the Antarctic. Nevertheless, substantial amounts of open water exist in the Arctic where the summer ice cover undergoes a dramatic increase in the number and size of leads. Even in regions of perennial ice, summer values of A_w can reach 10-15% (*Hall*, 1978). Clearly the effects of $A_w(t)$ on the input of solar energy and

meltwater to the upper ocean can have a substantial impact on biological processes there.

Various attempts have been made to relate the summer decrease in ice thickness to T_a through empirical equations analogous to those developed for young growing ice. *Bilello* (1961), for example, found a correlation of 0.93 between his data and thickness changes given by the equation

$$\Delta h = 0.55\theta' \quad , \tag{6}$$

where Δh = the total decrease in ice thickness and θ' = the accumulated degree-days above freezing. Bilello also mentions a similar relationship [$\Delta h = 0.51(\theta'' - 32)$, where θ'' ≡ accumulated degree-days above $-5^{\circ}C$] developed by Karelin for the Soviet Arctic. The high degree of correlation between T_a and Δh is surprising because shortwave radiation is the dominant term in the summer energy balance. Variations in cloud cover, surface albedo, ice concentration, and F_w would seem to be as important as T_a. The probable explanation is that the observations were taken close to shore and were strongly influenced by warm air from nearby land masses. It is unlikely that such relationships could be employed away from coastal areas where summer values of T_a are invariably close to the freezing point.

3. STRUCTURE AND SALINITY

A. Crystal Orientation

Ice crystals are hexagonal in form and are characterized by one principal hexagonal axis of symmetry (the c-axis) which is the optic axis of the crystal. Perpendicular to the c-axis is the *basal* (0001) *plane* defined by three crystallographic axes (the a-axes) of equal length with angles of 120° between the positive ends. Six crystal faces parallel the c-axis and are often called *prism* faces. The arrangement of atoms in an ice lattice is such that fracture along the basal plane requires the breaking of only two bonds, while fracture along any plane normal to this requires the breaking of four or more bonds. Slip and cleavage are thus most likely to occur parallel to the basal plane.

In natural sea ice the orientation of individual crystals tends to be highly organized. Only near the surface where the ice is composed of frozen slush or grease ice are crystal orientations random. Once congelation growth begins, crystals whose c-axis are parallel to the ice-water interface quickly begin to dominate the structure of the ice sheet. The explanation for this phenomenon is anisotropic growth on different crystal faces which results in a geometric selection of crystals with favorable orientations. The structure of the ice lattice is such that the density of potential bonding sites is greater on a prism face than on a basal plane. This means that, for a given degree of supercooling, growth parallel to the c-axis will be much slower than growth perpendicular to the c-axis. Observations (*Hallett*, 1960) show growth rate differences of as much as two orders of magnitude. Crystals whose c-axes are closer to the horizontal grow downward into the water faster than those with a more vertical orientation, wedging out the slower growing crystals. This process proceeds quite rapidly until only those crystals with c-axes parallel to the freezing interface remain. As we shall see later, this turns out to be an important factor in determining the structure and properties of sea ice.

The region over which the crystal orientation shifts from being random to having essentially all c-axes horizontal is termed the *transition zone* and typically occurs over a vertical distance of only 5-10 cm. The transition zone begins at the bottom of the frozen frazil layer and hence may be located anywhere in the upper meter of the ice cover, depending on the initial thickness of the frazil layer. Beneath the transition layer there is little interference between the growth of adjacent crystals and continued development of these crystals occurs primarily in the vertical. The region between the bottom of the transition zone and the ice-water interface is the so-called *columnar zone* and is characterized by crystals strongly elongated in the direction of the temperature gradient. Crystal diameter in the upper half meter of the columnar zone is typically about 1-2 cm. There is a definite tendency for average crystal diameter to increase with depth in a roughly linear fashion (*Weeks and Hamilton*, 1962; *Weeks and Ackley*, 1982). The reason appears to be associated with the decreasing growth rate of the ice as it thickens.

Until recently it was generally accepted that horizontal c-axis alignments were random throughout the columnar zone. However, several studies (e.g., *Cherepanov*, 1971; *Weeks and Gow*, 1978) now indicate that strong horizontal alignments exist over large portions of the Arctic. Near shore observations suggest that the c-axes are closely oriented in the direction of the average current at the bottom of the ice. Since the microscale roughness on the underside of the ice is greater when the current is parallel to the c-axis (see next section), *Weeks and Gow* (1978) argue that the resulting increase in turbulence decreases the thickness of the stable boundary layer at the growing interface, giving such crystals a slight growth advantage. Although this explanation is plausible, additional field and laboratory work is needed to verify it.

B. The Skeletal Layer and Brine Entrapment

Examination of the underside of growing sea ice reveals the presence of a delicate layer of thin ice platelets (Fig. 8a) arranged

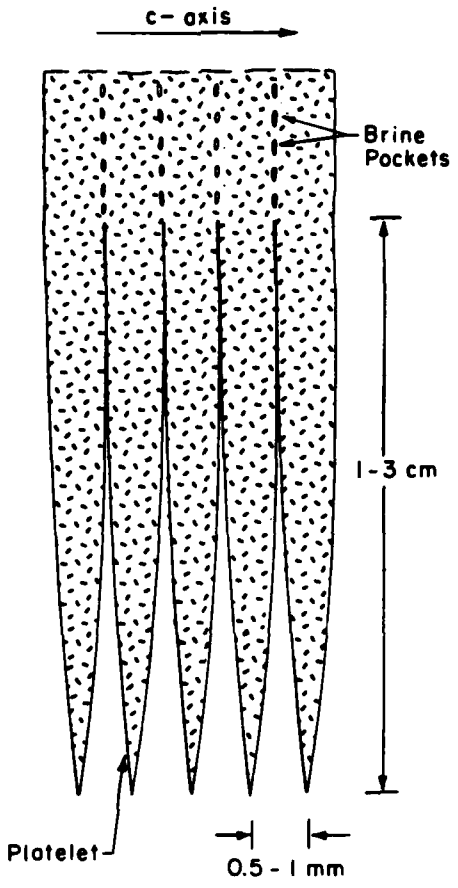

Fig. 8a. Schematic illustration of the platelet structure on the bottom of a growing ice crystal.

perpendicular to the c-axes of the individual crystals. The many platelets growing on the bottom of each exposed crystal are generally parallel (Fig. 8b) with a spacing (a_o) of 0.5-1.0 mm. The zone of platelet occurrence has a vertical dimension of about 1-3 cm and is frequently referred to as the *skeletal layer*. It has been found both theoretically and experimentally that a_o is proportional to $f^{-1/2}$. Clearly, flow parallel to the rows of platelets generates the least turbulence, allowing a slightly thicker boundary layer to develop beneath crystals with c-axes normal to the flow and possibly explaining the apparent growth advantage of crystals more closely aligned with the flow (*Weeks and Gow*, 1978).

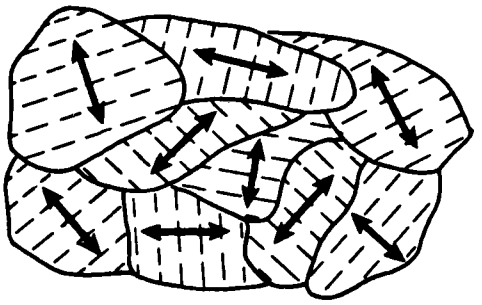

Fig. 8b. Plan view showing platelet arrangement at the underside of growing sea ice. Curved lines represent crystal boundaries and short straight lines the platelets. Note that platelets on an individual crystal tend to form in parallel sets normal to the horizontal direction of the c-axis (double ended arrow).

Absence of a skeletal layer beneath freshwater ice suggests that the complex microstructure found at the growing interface of sea ice is somehow related to the presence of salt in the water. When seawater freezes, most of the impurities (salts) are rejected from the ice lattice, resulting in the formation of a thin boundary layer of very salty water ahead of the advancing interface. The continual addition of salt causes the salinity at the top of this layer to be greater than the salinity beneath the layer. Because of the higher salinity, the temperature at the ice-water interface (T_h) will be lower than that in the underlying water. These conditions produce a downward flux of salt and an upward flux of heat through the layer. If we assume that the transport of heat and salt is primarily the result of diffusive processes, it follows that *constitutional supercooling* can occur in this boundary layer. Because of large differences in the rate at which heat and salt diffuse, the flux of heat through the boundary layer is much more rapid than the flux of salt, so that salinity undergoes an exponential type decrease below the interface whereas the temperature increase is more nearly linear. Since it is the salinity that determines the freezing point of the solution, the actual temperature will typically be below the freezing point (Fig. 9). Under such

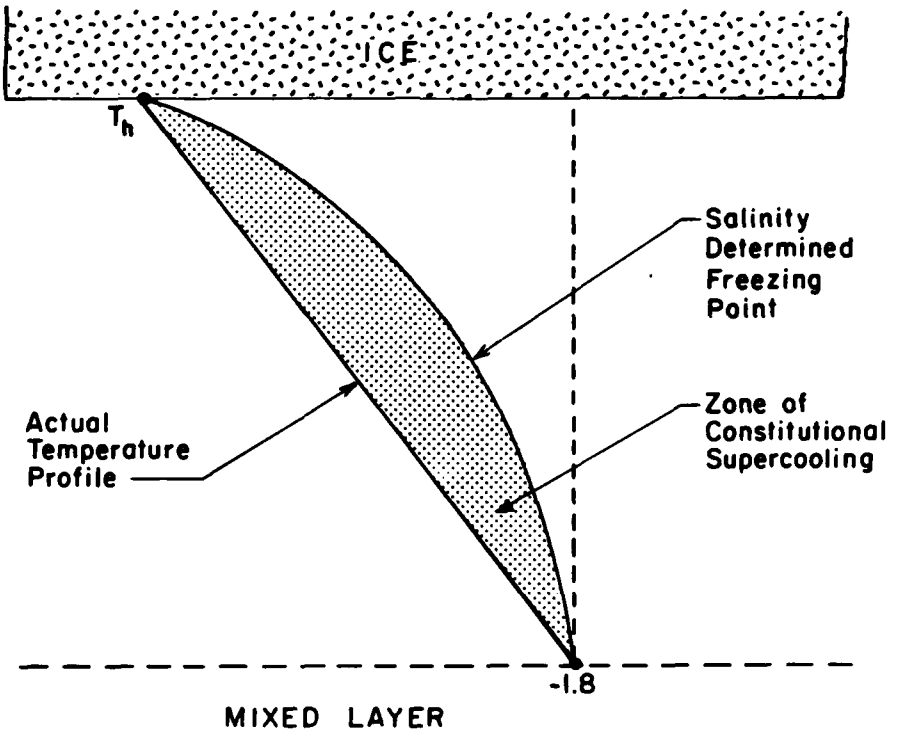

Fig. 9. Constitutional supercooling in the boundary layer ahead of an advancing ice interface.

conditions, laboratory observations (*Harrison and Tiller*, 1963) reveal that the ice-water interface initially develops an array of parallel knife-edged cells on which scallops form and deepen until the cells separate into a line of individual platelets. The length and spacing of these platelets act to minimize the amount of supercooling ahead of the interface. An approximate theory has been worked out to describe criteria for constitutional supercooling and the geometry of the interface (*Weeks and Ackley*, 1982). Efforts are under way to develop a more exact theory by allowing for free convection near the interface instead of only diffusion.

The significance of the skeletal layer is that it provides a mechanism for including substantial amounts of salt in the ice. As the platelets lengthen, they grow wider and periodically small ice bridges form between adjacent platelets, entrapping pockets of brine. These brine pockets are typically long and narrow, being on the order of

0.05 mm in diameter. Sea ice structure is thus characterized not only by the columnar crystals, but also by many vertical strings of liquid inclusions that mark the original boundaries between the platelets. As discussed in Section 4, these brine pockets dictate the bulk thermal and mechanical properties of the ice. Without this entrapment mechanism, there would be little to distinguish sea ice from freshwater ice.

Initially, the composition of the entrapped brine should have the same relative concentration of ions as normal seawater. However, as temperature decreases in the surrounding ice, solid salts begin to precipitate out of the brine solution. While mirabilite ($Na_2SO_4 \cdot 10H_2O$) begins to form at -8.2°C, the most important precipitate is sodium chloride ($NaCl \cdot 2H_2O$) which occurs below a temperature of -22.9°C. Appearance of the $NaCl \cdot 2H_2O$ causes the ice to take on a milky color and alters its optical properties. Other solid salts that may be present in small amounts include $CaCO_3 \cdot 6H_2O$, $MgCl_2 \cdot 8H_2O$, KCl, $MgCl_2 \cdot 12H_2O$, and $CaCl_2 \cdot 6H_2O$ (*Weeks and Ackley*, 1982).

In general, the salinity of the brine in a pocket is independent of the salinity of the original water because of mass changes taking place at the walls of the pocket. The temperature of the brine (T_b), which in the normal state of thermal equilibrium is the same as that of the surrounding ice, must be at the freezing point of the solution (T_f). If $T_b > T_f$, melting will occur on the ice walls, lowering the salinity of the brine (S_b) until $T_f = T_b$. Similarly, if $T_b < T_f$, freezing will occur in the brine, raising S_b until T_f and T_b coincide. This being the case, salinity in a brine pocket can be related to T_b through the following freezing point equations which are based on the work of *Assur* (1958):

$$S_b = \frac{1000\ T_b}{T_b - 54.11}, \quad T_b > -8.2°C \tag{7}$$

and

$$S_b = \frac{62.4 - 10.31\ T_b}{1.0624 - 0.01031\ T_b}, \quad -22.9 \leq T_b \leq -8.2°C, \tag{8}$$

where S_b is in $^o/oo$ and T_b in ^oC. Also fitting the data reasonably well are the approximate relations given by *Morey et al.* (1984): $S_b = 9.65 - 14.8\ T_b$ when $-8.2 \leq T_b \leq -2^oC$, and $S_b = 78.11 - 6.6\ T_b$ when $-22.9 \leq T_b \leq -8.2^oC$. The change in the $S_b(T_b)$ relationship below -8^oC is due to the precipitation of $Na_2SO_4 \cdot 10H_2O$ from the solution. Below -23^oC the data are somewhat ambiguous, and proper freezing point relations have not definitely been established. Since the temperature of the surrounding ice (T_i) will normally equal T_b, it is possible to calculate S_b by simply measuring T_i and applying (7) or (8).

C. Ice Salinity

The salt content of sea ice is usually described in terms of a *bulk salinity* (S_i) defined as

$$S_i = \frac{\text{mass of salt}}{\text{mass of ice + mass of brine}} \cdot 10^3 , \qquad (9)$$

where S_i is in $^o/oo$. The amount of salt initially entrapped by the growing ice depends strongly on growth rate and water salinity. Laboratory measurements by *Cox and Weeks* (1975) show two different regimes. When $f < 2 \cdot 10^{-5}$ cm s^{-1} ($\sim$1.7 cm d^{-1}),

$$S_i = S_w(0.8439 + 0.0529 \ln f), \qquad (10)$$

while for $f > 2 \cdot 10^{-5}$ cm s^{-1}

$$S_i = 0.26\ S_w[0.26 + 0.74 \exp(-7243f)]^{-1}. \qquad (11)$$

The flux of salt to the water beneath the growing ice can thus be written as $F_{salt} = \rho_i f(S_w - S_i)$ and estimated using (10) or (11).

If the brine did not migrate in the ice, we would expect to see stationary salinity profiles with a maximum near the surface and a continuous decrease with depth, reflecting the reduction in f as the ice thickened. Instead we find that $S_i(z)$ is highly time-dependent with a

shape that suggests substantial vertical movement of brine after entrapment. Figure 10 shows idealized salinity profiles for different ice thicknesses based on data from a variety of sources (*Weeks and Lee*, 1958; *Schwarzacher*, 1959; *Cox and Weeks*, 1974; *Nakawo and Sinha*, 1981; *Weeks and Ackley*, 1982). Actual salinity profiles exhibit considerable

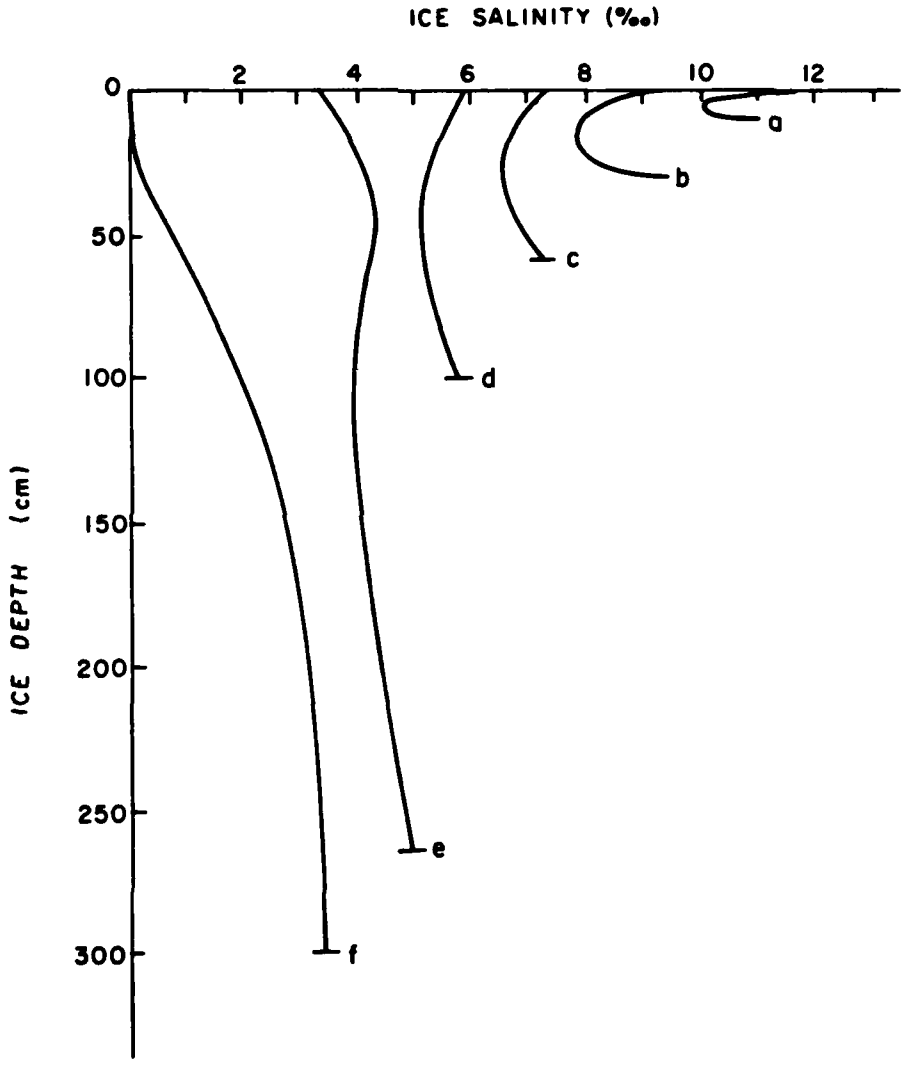

Fig. 10. Idealized salinity profiles in arctic sea ice of various thicknesses. Curves a-d represent first-year ice. The remaining curves illustrate the two classes of profiles found in multiyear ice: curve f shows S_i beneath hummocks and other elevated areas, while curve e shows S_i beneath low areas where the surface is close to the freeboard level.

vertical scatter, presumably correlated with changes in thermal forcing (see *Nakawo and Sinha*, 1981). Likewise, the magnitude of S_i can be quite different for ice of equal thickness because of differences in growth rate. Nevertheless, Fig. 10 illustrates several important points. Profiles in thinner ice tend to be C-shaped indicating salt enrichment in the lower half of the slab. The average salinity also decreases as the ice ages (i.e., becomes thicker), suggesting loss of brine to the ocean. Finally, there is a dramatic change in $S_i(z)$ in multiyear and melting first-year ice.

To explain the observed profiles, *Untersteiner* (1968) examined the role of four mechanisms that transport brine within the ice. *Brine pocket migration* will occur in the presence of a temperature gradient across the slab. Melting on the warm side of the pocket and ice accretion on the cool side cause the pocket to move opposite to the direction of heat flow. Under normal conditions, this mechanism is too slow to account for a significant amount of brine transport, although if the pocket is large enough to support convective heat transfer, movement can be quite rapid. Another mechanism is *brine expulsion* resulting from the pressure buildup in refreezing pockets. Again brine expulsion does not appear to play a major role in the desalination of sea ice. It is likely to be important only during the early stages of growth when the ice is undergoing rapid cooling. The "salt flowers" and extremely high salinities often found at the surface of young ice are probably the result of this process.

The mechanism primarily responsible for observed salinity changes in first-year ice is almost certainly *gravity drainage*. Because brine pockets typically form in vertical strings, they tend to become interconnected in response to temperature changes and internal stresses, forming long vertical tubes or *brine channels* which allow the vertical movement of brine through the ice. During most of the year temperature increases with depth, and colder denser brine in the upper part of the ice will sink downward to displace the warmer less dense brine. In addition, bottom growth causes the ice sheet to move upward, creating a hydrostatic head that forces brine downward in the channels and out of

the ice. Average brine channel diameters near the bottom of the ice are on the order of 0.4 cm. Depending on ice thickness, as many as 50-300 channels per square meter may exist along the bottom of the ice. The cold streamers of brine leaving the ice cause hollow tubes of ice to form around them. These "ice stalactites" have been observed to reach lengths of 6 m in the Antarctic, but lengths of 25-50 cm seem to be more representative in the Arctic. Brine movement within the ice causes complex changes within the channels. It has been noted (*Lake and Lewis*, 1970) that primary brine channels are often accompanied by smaller tributary channels which provide additional brine and form what is, in effect, a brine drainage system. Stalactite formation and flow in the primary channels have been extensively studied (*Martin*, 1974; *Eide and Martin*, 1975; *Niedrauer and Martin*, 1979), but few details are available regarding the formation and role of the tributary channels.

The final mechanism is *flushing* by surface meltwater. As surface temperatures approach the freezing point in spring and early summer, brine volume increases and the ice becomes extremely porous. Melting of the snow cover and the formation of ponds on the surface allow freshwater to percolate into the ice, resulting in a further decrease in S_i. Calculations (*Untersteiner*, 1968) indicate that the greatest salt loss occurs where brine volume is a maximum and that flushing appears to be sufficiently vigorous in the Arctic to explain the observed differences between salinity profiles in first-year and multiyear ice. Flushing does not appear to be a significant factor in the evolution of antarctic sea ice.

Data from a wide variety of sources and locations were compiled by *Cox and Weeks* (1974) to produce plots of average salinity versus ice thickness in the Arctic (Fig. 11). For cold ice the plots show a roughly linear decrease in $\overline{S}_i$ up to a thickness of about 40 cm, at which point the slope abruptly changes, possibly indicating a shift in the dominant desalination mechanism from brine expulsion to gravity drainage. It should be noted that, in spite of a wide range of growth conditions, $\overline{S}_i(h)$ shows surprisingly little scatter. Measurements of $\overline{S}_i$

when the ice is melting are complicated by brine leakage from the cores, but there is at best only a weak dependence on h.

Chemical studies (*Reeburgh and Springer-Young*, 1983) show that sulfate-chlorinity ratios in sea ice are different from the seawater ratio. On aging, sulfate in the ice is mobilized and removed in a constant ratio to chlorinity, indicating conservative behavior. Comparison of first-year and multiyear ice suggests that fractionation occurs during ice formation, but that further fractionation within the ice does not appear to take place. Because much of the entrapped brine ultimately returns to the ocean, there seems to be no lasting effect on

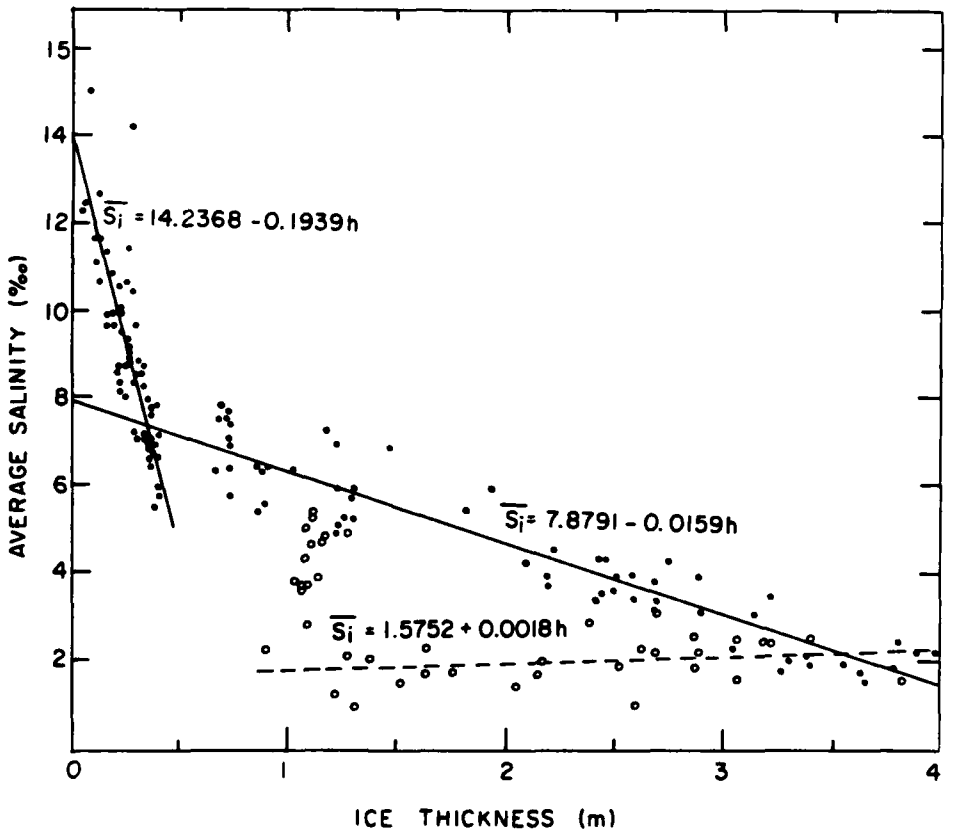

Fig. 11. Average salinity of arctic sea ice as a function of ice thickness (after *Cox and Weeks*, 1974). Solid lines show $\overline{S}_i(h)$ for cold ice, while dashed line shows $\overline{S}_i(h)$ for warm ice late in the melt season. Data points for the cold ice are given by dots and for the warm ice by open circles.

the chemical composition of the underlying water as a result of the freezing process.

The evolution of ice salinity can be summarized as follows. High initial growth rates entrap substantial amounts of brine, producing S_i values near the surface of 10-20 $^{o}/_{oo}$. As h increases, f decreases and less brine is entrapped. However, cooling of the upper part of the ice results in brine expulsion that allows S_i in the lower part of the ice to remain high. Substantial quantities of brine are lost to the underlying ocean during this period. By the time h approaches 40 cm, brine channels appear to be sufficiently developed for gravity drainage to control the rate of desalination. The ice continues to lose salt through this process until the onset of snow melting when flushing by freshwater occurs. Beneath elevated, drained areas there is a sharp drop in salinity whereas beneath low areas close to the freeboard level the decrease is much less pronounced. This pattern persists even in older multiyear ice where horizontal salinity gradients exist which are correlated with surface topography (*Cox and Weeks*, 1974).

D. Annual Layering in Sea Ice

Cores taken in multiyear arctic sea ice reveal the existence of horizontal layers which are suspected to develop during the annual thaw cycles (*Cherepanov*, 1957; *Schwarzacher*, 1959). These layers are of two different types. The first type is 2-5 mm thick, milky white in color, with a sharp upper boundary and an irregular lower boundary. The origin of this layer is uncertain, but it appears to form during the summer after the ice has stopped growing. It has been suggested that the milkiness of the ice may be associated with biological activity in the ocean (*Weeks and Ackley*, 1982). The second type is much thicker (1-10 cm) and appears to result from the freezing of surface meltwater that penetrates beneath the ice. The size of the crystals is much smaller than in the surrounding layers of normal congelation ice and the salinity much lower (1-1.5 $^{o}/_{oo}$). The presence beneath the ice of freshwater from surface melting can be explained by flow through natural

or artificial drain holes or by runoff into nearby leads that subsequently close. If vertical mixing is small, there will be a sharp interface between the freshwater at its freezing point (0°C) and the underlying seawater at its freezing point (∿-1.8°C). This results in supercooling in the freshwater near the interface and ultimately in the growth of ice crystals throughout the freshwater layer (*Martin and Kauffman*, 1974). Since freshwater does not necessarily occur beneath the ice each summer at a given location, the refrozen meltwater layers are often separated by one or more of the thin milky layers. These layers make it possible to estimate the age at various depths within the ice. Obtaining the total age of the ice cover by this method, however, is difficult because melting and refreezing near the surface tend to obliterate the uppermost layers.

4. PHYSICAL PROPERTIES OF SEA ICE

As the ice changes temperature, internal melting or freezing within the brine inclusions affect the brine volume of the ice. The fractional volume of brine in the ice (ν_b) can be written as

$$\nu_b = -\frac{\rho_i S_i}{\rho_b S_b} , \tag{12}$$

where ρ_i is the density of the ice and ρ_b is the density of the brine. From Eqs. (7) and (8) we know that S_b is dependent only on T_i, and hence ν_b will be a function of S_i and T_i. Application of (12) over a wide temperature range is complicated by the precipitation of solid salts and uncertainties in $\rho_b(T_i)$; however, a table of ν_b for standard sea ice has been tabulated by *Assur* (1958) down to a temperature of -54°C. In most cases values of sufficient accuracy can be obtained with a simple equation developed by *Frankenstein and Garner* (1967):

$$\nu_b \simeq S_i(0.0532 - \frac{4.919}{T_i}) , \quad -22.9 \leq T_i \leq -0.5°C , \tag{13}$$

where S_i is in °/oo and ν_b in percent. The brine volume at the bottom of growing sea ice can vary from about 8% to 40%. For multiyear ice ν_b is typically about 10%, except near the surface during the summer when values as high as 40-50% have been observed. As will be shown below, the magnitude of ν_b has a major impact on the bulk thermal, mechanical, optical, and electromagnetic properties of sea ice.

In addition to the entrapment of brine, growing sea ice also captures significant numbers of air bubbles. According to *Schwerdtfeger* (1963), the fractional volume of air bubbles in sea ice (ν_a) is given by

$$\nu_a = 1 - \rho_i\left(\frac{1 - S_i'}{\rho_o} + \frac{4.98S_i'}{T_i}\right), \quad T_i > -8.2°C , \tag{14}$$

where $\rho_o = 0.9178$ Mg m^{-3} is the density of pure ice, ρ_i is the bulk density of the sea ice, and $S_i = S_i/1000$ is the fractional salt content of the ice. Equation (14) can be rewritten and simplified to obtain an approximate relation for $\rho_i(\nu_a, T_i, S_i)$,

$$\rho_i \simeq (1 - \nu_a)\left(1 - \frac{0.00456S_i}{T_i}\right)\rho_o . \tag{15}$$

It can be seen from (15) that ρ_i is mainly determined by S_i at warm temperatures and by ν_a at lower temperatures. Because the major changes in thermal and mechanical properties occur when the ice is warm, air bubbles will be neglected in the following discussions.

A. Thermal Properties

If we remove heat from a block of sea ice, T_i decreases, causing brine to freeze in the pockets. This freezing releases latent heat which acts to warm the ice. As a result, sea ice cools more slowly than fresh ice. Alternatively, warming produces melting in the brine pockets which slows the rate at which T_i increases. Brine pockets thus behave as thermal buffers that retard the transport of heat in sea ice, which affects both conductivity and specific heat. These changes in brine volume also alter the latent heat of fusion of the ice.

1. Conductivity

The conductive heat flux in the ice (F_c) is given by $F_c = k_i(\partial T_i/\partial z)$, where k_i is the *thermal conductivity* of the ice. The magnitude of k_i and the temperature gradient thus determine the rate of

conductive heat transfer. In pure ice the conductivity (k_o) depends on temperature and is approximately $k_o = 9.828 \exp(-0.0057T)$, where T is in ^oK and k_o in W m^{-1} $^oK^{-1}$ (*Yen*, 1981). A typical value of k_o for warm ice would be 2.1 W m^{-1} $^oK^{-1}$ (0.005 cal cm^{-1} s^{-1} $^oK^{-1}$). There appears to be a slight difference between k_o measured parallel to the c-axis and that measured normal to it, but this difference is small (about 5%) and can usually be neglected. In sea ice, however, conductivity is substantially lower parallel to the c-axis than normal to it. This is because brine and air bubble layers are regions of lower conductivity, and more of these layers are intersected by heat conducted along the c-axis than perpendicular to it. Since horizontal temperature gradients in natural sea ice are usually negligible, only heat flow in the vertical (i.e., perpendicular to the c-axis) need be considered for practical purposes. Detailed theories for k_i, taking into account such factors as brine pocket distribution, air bubbles, and the precipitation of solid salts, have been worked out (*Anderson*, 1958; *Schwerdtfeger*, 1963). Tables of $k_i(T_i, S_i, \rho_i)$ are given in *Schwerdtfeger* (1963). An approximate expression for k_i was proposed by *Untersteiner* (1961),

$$k_i = k_o + \frac{\beta S_i}{T_i} , \tag{16}$$

where T_i is in ^oC and $\beta = 3.11 \cdot 10^{-4}$ cal cm^{-1} s^{-1} (0.13 W m^{-1}) is a constant. Although somewhat crude, (16) is particularly convenient in applications requiring a simple functional relationship between k_i, T_i, and S_i. Predicted values of $k_i(S_i, T_i)$ are shown in Fig. 12. Note that there is little dependence on temperature below about -4^oC. Under natural conditions, k_i may vary by 10-20% in perennial ice and by up to 50% in young ice.

At first glance it would appear that (16) predicts an infinite value for k_i as $T_i \rightarrow 0^oC$. This turns out not to be the case because T_i cannot approach 0^oC unless $S_i \rightarrow 0$. Whereas pure ice has a well defined

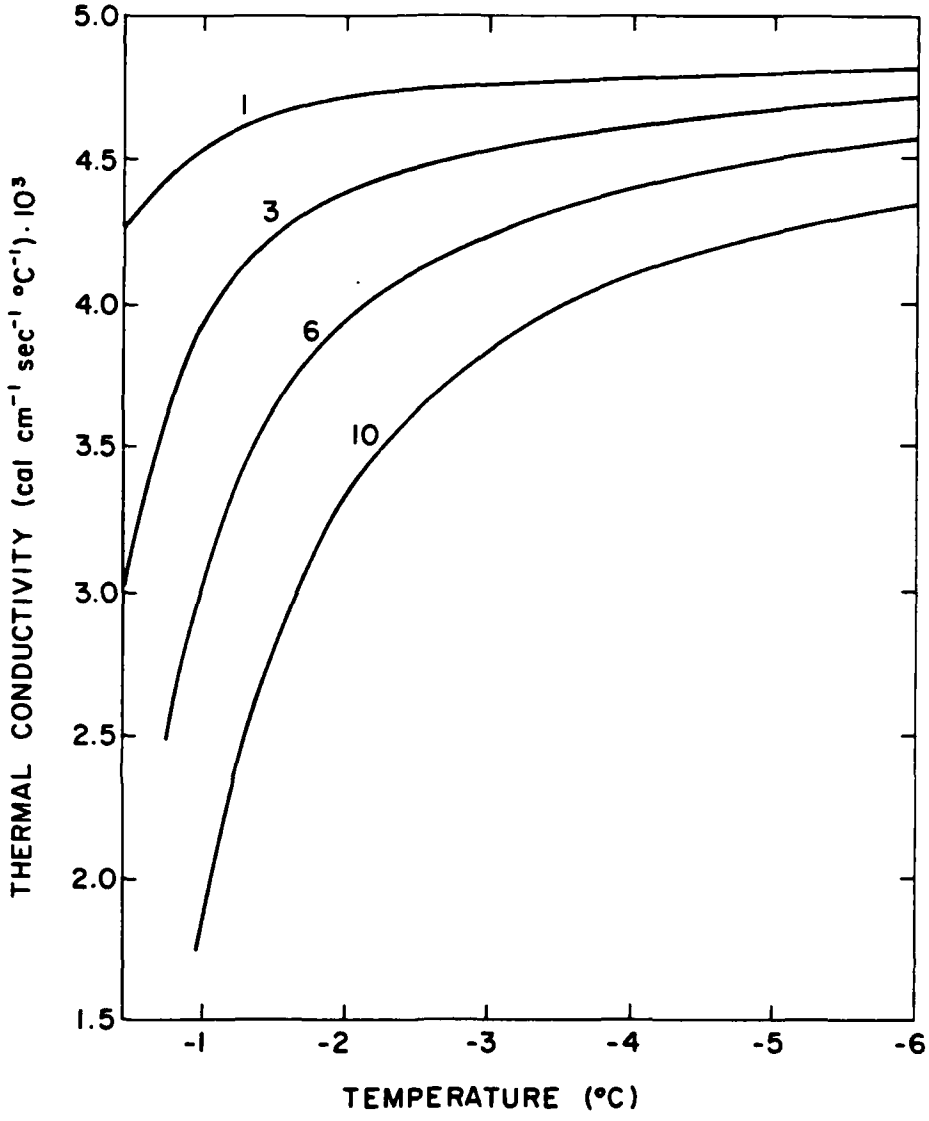

Fig. 12. Dependence of thermal conductivity in sea ice on ice salinity ($^{o}/_{oo}$) and temperature according to *Untersteiner* (1961).

temperature (0°C) at which phase transitions occur, sea ice does not. Any change in T_i produces internal phase changes. It can be shown, however, that for ice of a given salinity there is a temperature (T_m) above which the ice cannot exist without completely melting away. According to *Ono* (1967), $T_m \simeq -0.05411\ S_i$. This is consistent with the notion that the temperature of sea ice can reach 0°C only if $S_i = 0$.

2. Specific Heat

The *specific heat* of a substance is defined as the amount of heat necessary to raise a unit mass of the material 1°C, and is a fundamental property needed in calculating time-dependent temperature changes. The specific heat of sea ice (c_i) is the sum of the heat required to warm the ice and the brine plus that needed for melting in the brine pockets. *Ono* (1967) has derived a theoretical expression for c_i applicable to temperatures above -8°C:

$$c_i = c_o + aT_i + \frac{bS_i}{T_i^2} \quad , \tag{17}$$

where c_o = 0.505 cal g^{-1} $°C^{-1}$ (2113 J kg^{-1} $°C^{-1}$) is the specific heat of pure ice, a = 0.0018 cal g^{-1} $°C^{-2}$ (7.53 J kg^{-1} $°C^{-2}$) is a constant, and b = 4.3115 cal °C g^{-1} (0.018 MJ °C kg^{-1}) is also a constant. A slightly simpler form which gives similar results is the empirical formula of *Untersteiner* (1961): $c_i = c_o + (\xi S_i/T_i^2)$, where ξ = 4.1 cal °C g^{-1} (0.0172 MJ °C kg^{-1}). Tables and analytical expressions are also available (*Anderson*, 1958; *Schwerdtfeger*, 1963) for colder ice. Values of $c_i(T_i,S_i)$ are shown in Fig. 13. As with k_i, the largest changes in c_i occur at temperatures above -4 to -6°C, but the magnitude of the change is much larger. Under natural conditions c_i can vary by a factor of 20 or more. The figure demonstrates that it becomes increasingly difficult to change T_i as $T_i \to T_m$, primarily because mass changes in the brine pockets consume an increasing share of the available energy.

3. Latent Heat of Fusion

The *latent heat of fusion* (L_o) of pure ice is the amount of heat required to melt (or freeze) a unit mass of ice at 0°C. Because internal melting and freezing occur continuously over a wide temperature range, the traditional concept of absorption or release of latent heat at a constant temperature does not strictly apply to sea ice.

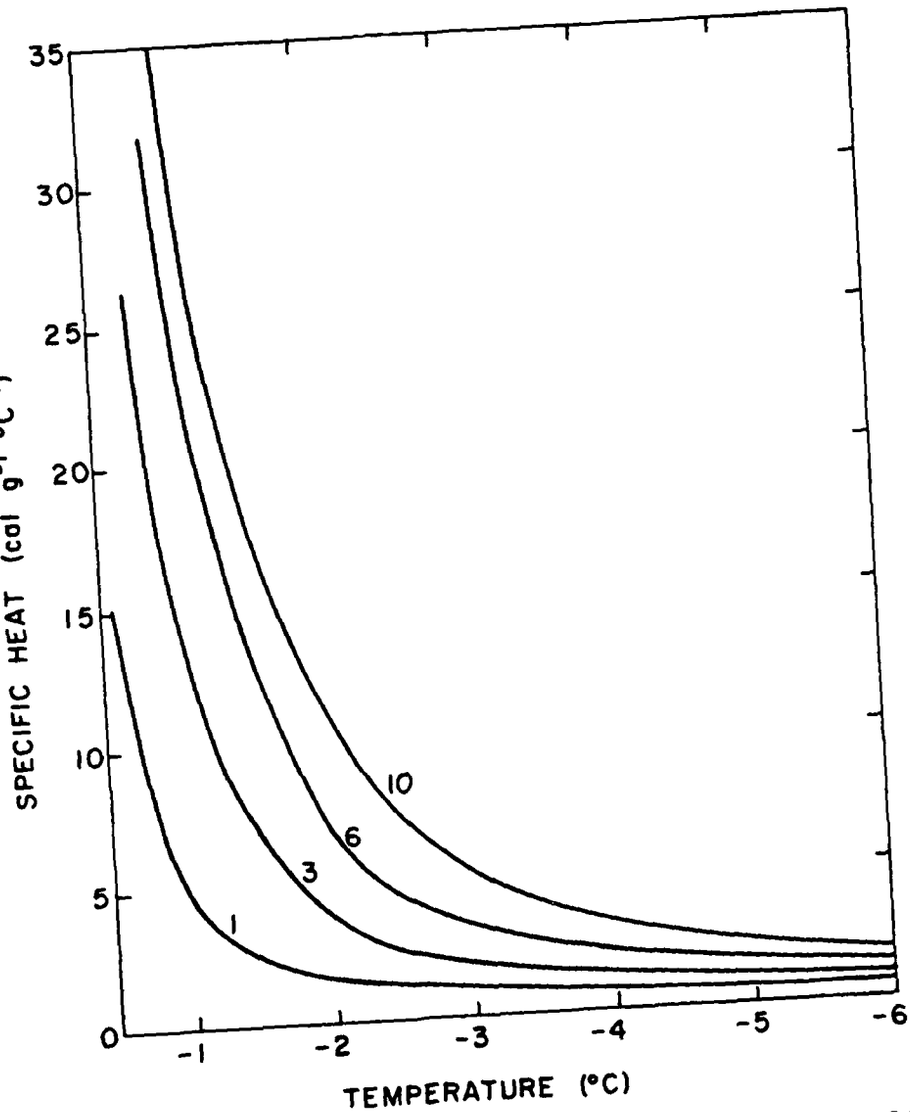

Fig. 13. Dependence of specific heat in sea ice on ice salinity ($^{o}/_{oo}$) and temperature according to data from *Ono* (1967).

Nevertheless, it is possible to calculate the amount of heat necessary to melt a sample of sea ice with temperature T_i and salinity S_i. It is this quantity that we will take to be the heat of fusion (L_i) of sea ice. A precise formula for L_i was derived by *Ono* (1967):

$$L_i = L_o - 0.505T_i - 0.0273S_i + 4.3115\frac{S_i}{T_i} + 0.0008S_iT_i - 0.0009T_i^2 , \quad (18)$$

where L_o = 79.68 cal g^{-1} (0.3335 MJ kg^{-1}). Simpler expressions are also possible. Since the amount of ice present in a unit mass of sea ice is $(1 - 0.01\nu_b)$, $L_i = (1 - 0.01\nu_b)L_o$, and from Eq. (13)

$$L_i \simeq [1 - S_i(0.000532 - \frac{0.04919}{T_i})]L_o \ . \qquad (19)$$

These equations can be used to estimate the heat of formation of sea ice. Suppose, for example, that salinity near the bottom of a growing ice cover is found to be 8 °/oo. Then, if T_f = -1.8°C, $\nu_b \simeq 22\%$ and L_i = 61.2 cal g^{-1}, where L_i represents the amount of heat that must be conducted away from the growing interface to form one gram of salty ice. As the ice cools below T_f, additional latent heat is released by freezing in the brine pockets, but that heat is accounted for in c_i and is not included in the heat of formation.

4. Diffusivity and Conductance

A parameter appearing frequently in the literature is the *thermal diffusivity*, $\kappa_i = k_i/\rho_i c_i$, a simple combination of previously discussed properties. This combination arises naturally from the form of the heat conduction equation (see Section 5B) and can be calculated directly from observations of the rate of change of temperature profiles in the ice (*Schwerdtfeger*, 1963). There is a very strong decrease in κ_i with temperature above -4°C. The most complete study of $\kappa_i(T_i,S_i)$ for sea ice was made by *Ono* (1968).

A useful quantity for estimating growth rates and heat conduction in snow-covered first-year ice is the *thermal conductance*, $\gamma = k_i k_s/(k_i h_s + k_s h)$. Because $k_s << k_i$, small amounts of snow can have a large effect on the amount of heat conducted to the surface (F_c). In situations where h_s undergoes significant changes in time or space, the insulating effect of the snow cannot be ignored. Equation (5) shows that surface temperature and γ are sufficient to obtain F_c when the ice is cold. If F_w is known or assumed to be negligible, the amount of

growth can be calculated directly from F_c and L_i. The dependence of γ on h and h_s is shown in Fig. 14 for values of k_i and k_s typical of winter conditions in the Arctic.

B. Mechanical Properties

Sea ice is subject to a variety of forces arising from the movement of air and water across its horizontal boundaries, and from internal stresses generated by the surrounding ice. The resulting deformations are of two types: elastic strains which are reversible when the stress is removed and inelastic strains which are irreversible. Ice is often described as a visco-elastic material, that is, when deformed rapidly or for brief periods it behaves elastically, while for sustained loadings it tends to creep with a rate depending on time and the amount of stress. The mechanical behavior on nonsaline ice depends on temperature, porosity, grain size, strain rate, and structure. Sea ice is further complicated by the presence of brine inclusions, strong crystal orientation, biological activity, and organized pore geometry.

Much of what is known about the rheology and strength of ice has been learned from laboratory measurements. Continual variations in the state of the material make such measurements difficult, and much work remains to be done. It is not the intent here to summarize the numerous (and sometimes contradictory) experimental data. Rather, we shall try to present a more qualitative picture of how sea ice responds to various types of mechanical forcing, and how this response depends on other physical properties of the ice. An excellent review of current knowledge regarding the mechanical behavior of sea ice, together with a discussion of the underlying continuum mechanics concepts, has been given by *Mellor* (1983). Additional information on the small scale physics can be obtained from *Doronin and Kheisin* (1975).

1. Elastic Constants

The theory of elasticity forms the basis for studies of deformable solids. A perfectly (or linearly) elastic material is one in which strain (ε) in the direction of the applied stress (σ) is directly

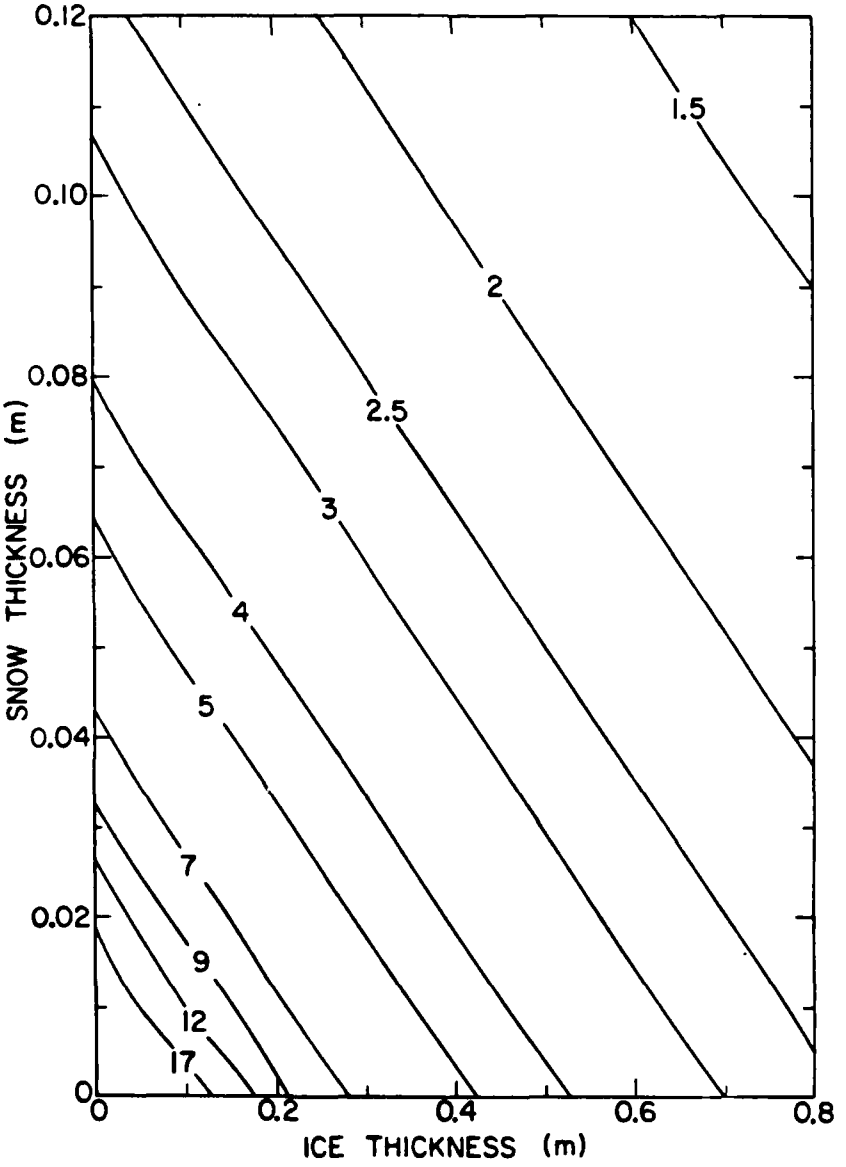

Fig. 14. Thermal conductance (W m^{-2} $^{o}C^{-1}$) of the arctic ice cover during winter and spring as a function of ice and snow thickness (after *Maykut*, 1978).

proportional to σ, i.e., $\sigma = E\varepsilon$, where E ≡ *Young's modulus*, the ratio of axial stress to strain. The ratio of the lateral strain to the axial strain is called the *Poisson ratio* (μ). Together, E and μ characterize the elastic behavior of a material. In nonsaline ice, E depends only weakly on T_i, but porosity (air bubble volume) has a significant effect. In sea ice, T_i strongly affects the porosity (brine volume) and hence E.

Small scale measurements (*Langleben and Pounder*, 1963) on first-year ice over a brine volume range of 0-8.5% indicate a relationship of the form, $E = a + b\nu_b$, where a and b are constants. These measurements also suggest that μ is relatively constant ($\sim$0.3) in sea ice and independent of T_i and S_i. Theoretical studies of the dependence of E on ν_b have been carried out by *Bergdahl* (1977) assuming that brine pockets and channels within the ice could be modeled as vertical rectangular tubes. For stresses along the tubes he found a relationship with the same form as the empirical studies. However, for stresses normal to the tubes, the relationship was of the form $E = a/(1 - b\nu_b)$, where b depends on the assumed geometry of the brine pockets. This result is supported by numerous observations indicating that the direction of applied stress is an important factor in the mechanical response of natural sea ice.

Conditions under which the ice behaves elastically are fairly limited and often are not satisfied in field and laboratory measurements reported in the literature. Nevertheless, elastic analysis is still applied in many problems that involve inelastic processes. Elastic moduli determined under these conditions are called "effective" moduli and are denoted by E' and μ'. Effective moduli have proved to be useful for many practical purposes, and a variety of studies have been made to determine their dependence on T_i, porosity, strain rate, and stress state. In general E' is substantially less than E, except at very low temperatures and high rates of stress or strain. Increasing porosity causes a much more rapid decline in E' than in E, there being roughly a 50% decrease in E' as temperature increases from -30 to -5°C. Values of μ' at very low stress rates approach 0.5 and vary between 0.35-0.4 for high stress rates. In contrast to fresh ice, there is a tendency in saline ice for μ' to increase with increasing T_i (and hence ν_b). In natural sea ice, where observations (*Wang*, 1981) indicate that μ' equals 0-0.2 in the vertical and 0.8-1.2 in the horizontal, sample orientation is of utmost importance.

2. Strength

The most useful property for engineering purposes is strength, the ratio of the minimum load necessary to fracture the ice to its cross-sectional area. Depending on temperature, structure, and the rate of deformation, either brittle or plastic fracture may occur. Several different parameters are commonly used to characterize ice strength. *Uniaxial compressive strength* (σ_c), the maximum stress that the ice can sustain in a particular direction without fracturing, is usually obtained by compression of ice cylinders at a specific rate of strain. Results show that in sea ice σ_c increases as strain rate ($\dot{\epsilon}$) to approximately the one-fourth power. As expected, σ_c decreases more strongly with temperature in sea ice than in either lake or river ice, and is much larger when force is applied in the direction of ice growth (vertical) than when applied in the horizontal. The ice is weakest when the stress is 45° to the horizontal plane. *Uniaxial tensile strength* (σ_T) can be measured by applying tension to carefully designed ice specimens, but practical difficulties with this approach have led most investigators to infer σ_T from observations of beam flexure. The behavior of both small ice beams in the laboratory and large ice cantilevers sawed in natural sea ice sheets has been studied. At low strain rates ($\dot{\epsilon} < 10^{-6}$ s^{-1}), σ_T and σ_c are roughly equal; however, for high rates of loading σ_T is much smaller than σ_c. As with σ_c, σ_T increases with decreasing temperature and salinity and is considerably greater for vertically oriented specimens of columnar ice than for horizontal specimens. Other measures of ice strength (e.g., flexural strength, shear strength, fracture toughness, bearing capacity) have also been investigated. Results from much of this work have been summarized by *Doronin and Kheisin* (1975) and *Mellor* (1983). Little has been published on the mechanical properties of multiyear ice. What evidence is available indicates that its strength is highly variable, with differences of an order of magnitude being observed in ice with similar strain rates. Much more work is needed before it will be possible to draw comparisons with the results from first-year ice.

Brine pockets and channels weaken sea ice, and fracturing tends to follow planes that pass through these features. This tendency has been used to simplify the treatment of pore geometry and fracture strength in theoretical sea ice models (*Weeks and Assur*, 1969; *Weeks and Ackley*, 1982). In these models brine pockets are assumed to be vertically oriented elliptical cylinders, elongated in the direction of the platelets, which occur in parallel rows. Model results show a relationship between fracture strength and ν_b of the form $\sigma_f = \sigma_o(1 - a\nu_b^k)$, where σ_o is the fracture strength of sea ice containing no brine, and a and k depend on the arrangement of the brine pockets and on how their shape changes with ν_b. Assuming that pockets enlarge in all directions to maintain a constant geometry results in $k = 2/3$, while assuming that expansion of the pockets primarily affects the degree of elongation results in $k = 1$. If, on the other hand, it is assumed that the relative length of the brine columns remains constant and that only the cross-sectional area changes with ν_b to maintain the same geometrical shape, it follows that $k = 1/2$, in agreement with observations (*Weeks and Ackley*, 1982).

A subject that has received surprisingly little attention is the effect of biological activity on the strength and breakup of an ice cover. It has long been known that many species of microalgae inhabit sea ice, but the degree to which their presence may alter the mechanical properties of the ice does not appear to have been generally appreciated. A particularly interesting series of observations was carried out by *Buynitskiy* (1968) during summer cruises in the Antarctic. He found that substantial quantities of algae were present in essentially all the ice between the extreme edge and the shore. Cell densities as high as 33,000 per cubic centimeter were recorded, with the average being about 4300 per cubic centimeter, roughly an order of magnitude larger than in the underlying water column. Late in the summer diatoms occurred throughout the ice cover, while earlier in the year they tended to concentrate in brine channels and in horizontal layers ranging from a few centimeters to tens of centimeters in thickness. The dark color of the algae enhances absorption of shortwave radiation, accelerating the

rate of internal melting near the algae and thereby weakening the ice. Ship travel through such ice was found to be substantially easier than through ice with little algae. In contrast to pure sea ice which splits mainly in directions normal to the plane of freezing, antarctic ice was observed to cleave frequently through horizontal planes populated by the algae. Strength tests were carried out on various ice samples containing algae. It was found that the flexural strength of such ice was reduced by an average of 40% over that of pure sea ice, with the greatest reduction in strength occurring for stresses applied perpendicular to the freezing interface. The bearing capacity of this ice was thus seriously decreased. Compressive tests indicated that σ_c was almost unchanged by the presence of diatoms for vertically applied stresses, but decreased by a factor of 2 for horizontal stresses. Information in the published account is inadequate to identify the exact mechanisms whereby the algae achieve this weakening, but it is probably due more to warmer temperatures and higher brine volumes in the vicinity of the horizontal layers than to any direct effect on the microstructure of the ice. Whether biological activity is high enough anywhere in the Arctic to produce similar effects is uncertain.

3. Large Scale Behavior

Although the large-scale mechanical behavior of a sea ice cover can be vastly different from that observed in small laboratory samples, the latter provide a basis for understanding and treating large-scale behavior. Small-scale strength measurements, for example, indicate that tensile forces generated by wind and water stresses are much too small to crack a floating sheet of unflawed ice. Fracture analysis similar to that used with the laboratory data shows that leads in natural sea ice must form as a result of the growth of small existing cracks. Such cracks can be produced by thermal stresses or wave action and are very common in natural ice covers. Compressive stresses are likewise inadequate to cause wide-scale crushing in an ice sheet, although they may produce buckling in areas of very thin ice. This suggests that other processes must be involved in the formation of pressure ridges. A

likely factor contributing to ridge building is overthrusting of the ice along a discontinuity (such as an old lead), causing flexural breakage to occur at much lower stress levels than needed for buckling. Overthrusting should take place primarily in thinner ice and does not explain how thicker ice can become involved in ridging. A possible explanation for this can be found in a ridging model developed by *Parmerter and Coon* (1972). Thin ice in an existing lead is assumed to break up as the lead closes in response to compressional forces. The resulting rubble is piled on and beneath the surrounding thick ice, disturbing its isostatic balance which then leads to flexural breakage adjacent to the lead. Incorporation of fragments from the parent ice into the rubble pile and further closure allow the process to continue until a limit height is attained. Additional activity then acts to widen the ridge, but not to increase its height. Whether this represents a quantitatively accurate simulation of the ridging process is not known; however, predicted limit values appear to be well correlated with ridge height data.

Central to the development of large-scale models of ice drift and deformation are (i) a constitutive law relating ice stress to deformation and (ii) some measure of the aggregate strength of the ice. Numerous attempts have been made to model the ice as a linear viscous fluid, but results from these models indicate that nonlinear effects are important. Physical considerations suggest that a plastic rheology should provide a more realistic description of large-scale dynamic behavior, and both elastic-plastic and viscous-plastic approaches have been used with some success (*Coon et al.*, 1974; *Hibler*, 1979).

The overall compressive strength (σ_c^*) of the ice pack is strongly affected by local variations in thickness. Converging motions cause the thinnest (weakest) ice to ridge, increasing its resistance to further compression. As convergence continues, σ_c^* increases and thicker ice becomes involved in the deformation. The magnitude of σ_c^* therefore depends on how thinner ice is distributed within the region. A formal theory has been developed (*Rothrock*, 1975) for the plastic rheology that relates the rate of work done on the ice through ridging to the strain

and state of stress providing a method of calculating σ_c^* for a given distribution of ice thickness. Numerical experiments indicate that values of σ_c^* are typically on the order of 10^4-10^5 N m^{-1}. A more detailed summary of work in this area can be found in *Hibler* (1980).

C. Optical Properties

The optical properties of a material define how it interacts with solar radiation. Shortwave energy exchange over the polar oceans is complicated by nonuniformities in the ice cover which cause its optical properties to exhibit large variations in both the horizontal and vertical. At the height of the melt season, for example, a relatively small area may contain leads, thin ice, surface melt ponds, drained white ice, and snow patches, all having significantly different optical properties. Both the surface and internal structure of the ice are altered by the absorption of shortwave radiation, so that its optical properties undergo temporal variations as well as spatial. Although the optical properties of the ice pack do change gradually during the winter months, the largest changes occur during the summer melt cycle with the decay of the snow cover and the formation of melt ponds. In contrast to snow and bare ice, ponds are areas of low reflectivity where large amounts of energy are absorbed and transmitted to the underlying ice and ocean. Accompanying the surface changes are changes in the transparency of the ice caused by internal melting and increasing brine volume. Quantitative knowledge of how light absorption, transmission, and reflection vary in time and space is of fundamental importance in a wide variety of studies involving the ice and upper ocean.

1. Albedo

The *albedo* (α) is defined as the ratio of reflected to incident shortwave radiation and is a measure of net solar input at the surface. Total (integrated over all wavelengths) albedo measurements of polar ice and snow have been made by many investigators (see *Grenfell and Maykut*, 1977). Albedos of cold polar snow are generally in the 0.80-0.85 range, dropping to 0.70-0.75 at the onset of melting. Snow-free multiyear ice

has an albedo of 0.70-0.75 when the surface temperature (T_o) is below freezing and 0.55-0.70 when $T_o = 0^oC$. Thicker (1-2 m) first-year ice has α values of 0.5-0.6 when cold and 0.3-0.5 when melting. The albedo of snow-free young ice exhibits a strong dependence on thickness which may be approximated by $\alpha = 0.44\ h^{0.28} + 0.08$, where h is in meters (*Maykut*, 1982). The higher reflectivity of multiyear ice is due to the presence of a decomposed surface scattering layer (typically 5-15 cm thick) and to greater vapor bubble density in the underlying ice. Melt pond albedos depend on water depth and the state of the underlying ice. Deep ponds remaining at the end of the melt season can have albedos as low as 0.15, while values of 0.4 are typical of the shallow ponds that form early in the melt season. Contamination by dirt or algae can reduce these values somewhat. Lead albedos vary with wave activity and sun angle, but average about 0.08.

While total albedos are easy to measure and apply, their usefulness is limited. For example, analysis of satellite observations, estimation of cloud effects on α, and calculations of light absorption in the ice require an understanding of how the radiative properties of the ice vary with wavelength (λ). Spectral albedos (α_λ) have been measured over many surface types in the Arctic (*Grenfell and Maykut*, 1977). Values for first-year and multiyear ice are shown in Fig. 15. Albedos are relatively constant in the visible region (400-700 nm), but begin to decrease in the near infrared at a rate that is related to the liquid water content in the surface layers. Melting first-year ice can be divided into two main types: (i) water-saturated blue ice (which includes shallow melt ponds), and (ii) white ice consisting of a 5-10 cm thick layer of drained ice underlain by blue ice. At longer wavelengths light penetration is small so that α_λ is determined by the properties of the surface layer; at shorter wavelengths backscattering from ice beneath the surface becomes important. This explains the similarity between α_λ in first-year white ice and melting multiyear ice at longer wavelengths, and the difference at shorter wavelengths that results from lower backscattering in the underlying first-year ice. The albedo of

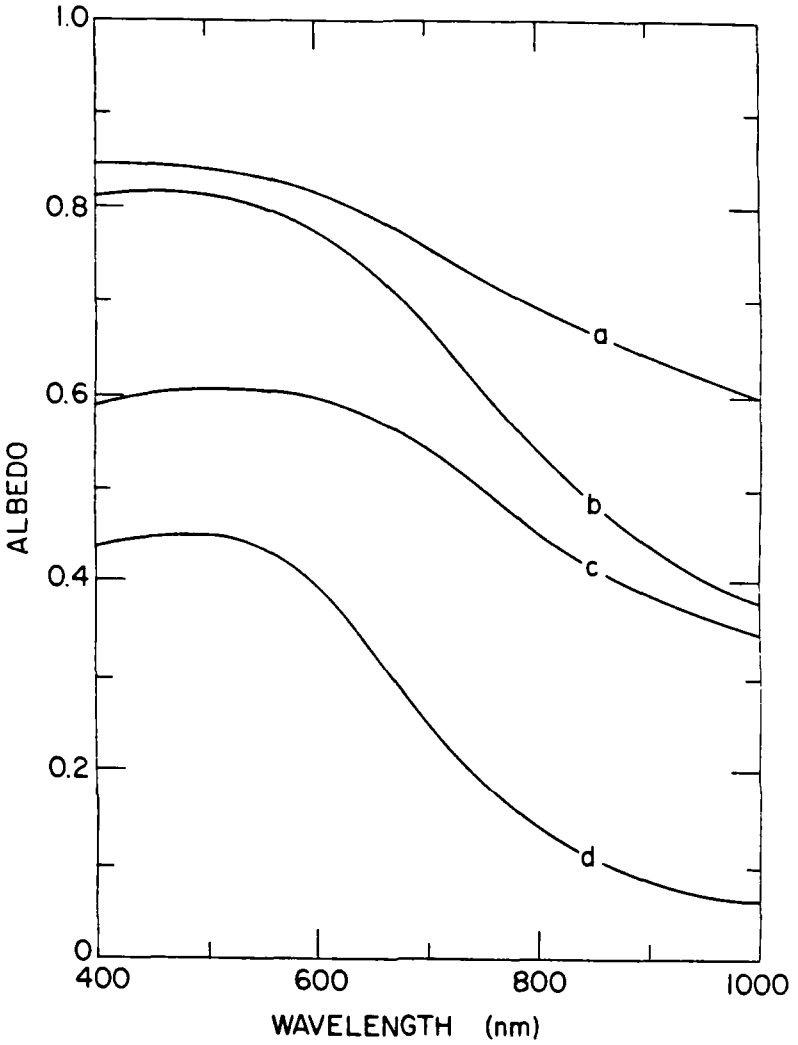

Fig. 15. Spectral albedos observed over bare sea ice in the Arctic: (a) frozen multiyear ice, (b) melting multiyear ice, (c) melting first-year white ice, and (d) melting first-year blue ice (after *Grenfell and Maykut*, 1977).

melting blue ice is substantially lower than that of first-year white ice at all wavelengths. At shorter wavelengths this is due to the absence of the white scattering layer, and at longer wavelengths to increased liquid water in the surface layers. Spectral albedos for snow and melt ponds are plotted in Fig. 16. The albedo of cold dry snow is high and has only a weak dependence on λ. Increasing density and liquid

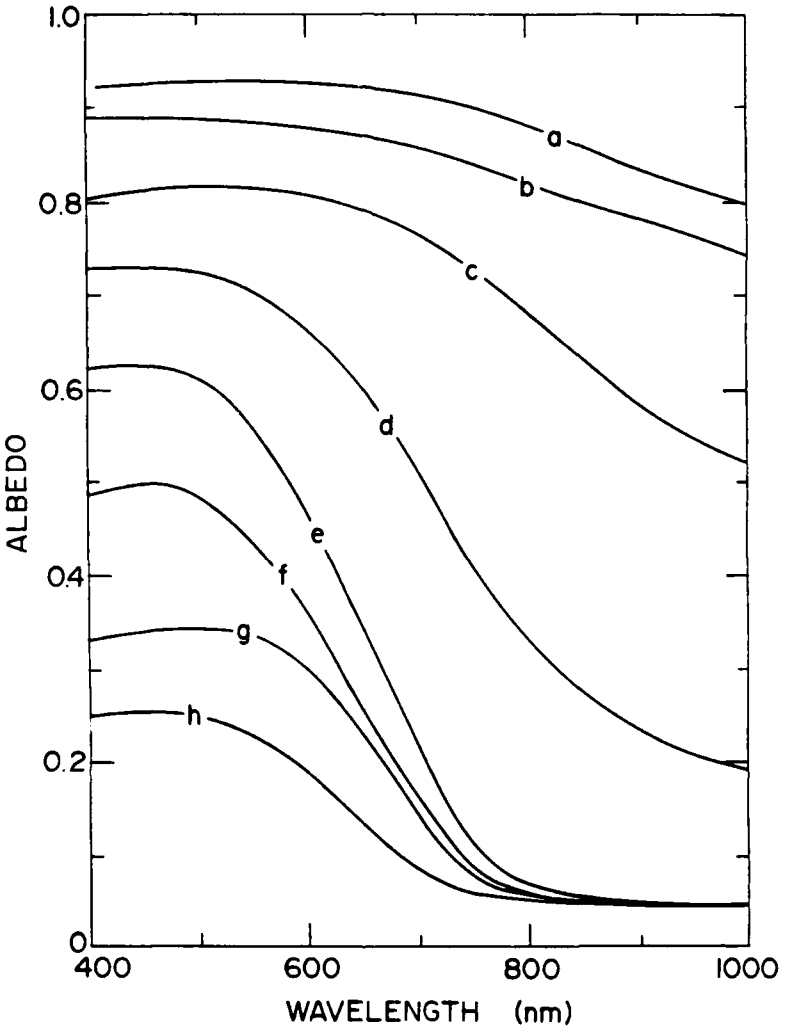

Fig. 16. Spectral albedos observed over snow and melt ponds in the Arctic: (a) dry snow, (b) wet new snow, (c) melting old snow, (d) frozen melt pond, (e) early season melt pond, (f) mature melt pond on multiyear ice, (g) melt pond on first-year ice, and (h) old melt pond on multiyear ice (after *Grenfell and Maykut*, 1977).

water content in the snow decrease α_λ, particularly in the infrared. Pond albedos tend to be high at shorter wavelengths with a sharp decrease between 500 and 800 nm. Because water in the ponds is relatively transparent at short wavelengths, albedos below 500 nm are determined primarily by the scattering properties of the underlying ice.

Between 500 and 800 nm α_λ becomes increasingly insensitive to the underlying ice as absorption in the water becomes the dominant factor. Above 800 nm α_λ is determined only by Fresnel reflection from the pond surface. Note that most of the albedo differences between individual ponds occur in the visible region and are readily apparent to the naked eye. Ice and snow albedos decrease strongly above 1000 nm, reaching values of 0.1 or less at 1400 nm after which the decrease becomes much more gradual (*Grenfell and Perovich*, 1984).

The total albedo can be expressed in terms of wavelength-dependent quantities as $\alpha = \int_0^\infty \alpha_\lambda F_r(\lambda)d\lambda \Big/ \int_0^\infty F_r(\lambda)d\lambda$, where $F_r(\lambda)$ is the downward flux of solar radiation reaching the surface at wavelength λ. The presence of clouds causes measured values of α to increase. The reason is that clouds remove proportionately more energy from $F_r(\lambda)$ at long wavelengths than at short ones, so that contributions from the more reflective shorter wavelength region are weighted more heavily in the integral when the sky is overcast. Typical increases observed for the relatively thin clouds found in the Arctic are about 15% (*Grenfell and Perovich*, 1984). Larger increases can be expected in regions where clouds have greater optical depths.

2. Extinction Coefficient

Because ice is a translucent material, light penetrates into the interior where, at any given level, some is absorbed and some transmitted. Light absorbed within the ice produces changes in the brine volume and provides energy for biological activity. Shortwave radiation transmitted completely through the ice is largely absorbed in the upper 10-20 m of the ocean, making an important contribution to the oceanic heat flux at the bottom of the ice. Light attenuation in the ice is characterized by its *spectral extinction coefficient* (κ_λ) defined as

$$\kappa_\lambda = - \frac{1}{F(\lambda,z)} \frac{dF}{dz} , \qquad (20)$$

where $F(\lambda,z)$ is the shortwave flux in the ice at wavelength λ and depth z. Measured values of κ_λ (*Grenfell and Maykut*, 1977) for various types of arctic ice and snow are presented in Fig. 17. All curves show

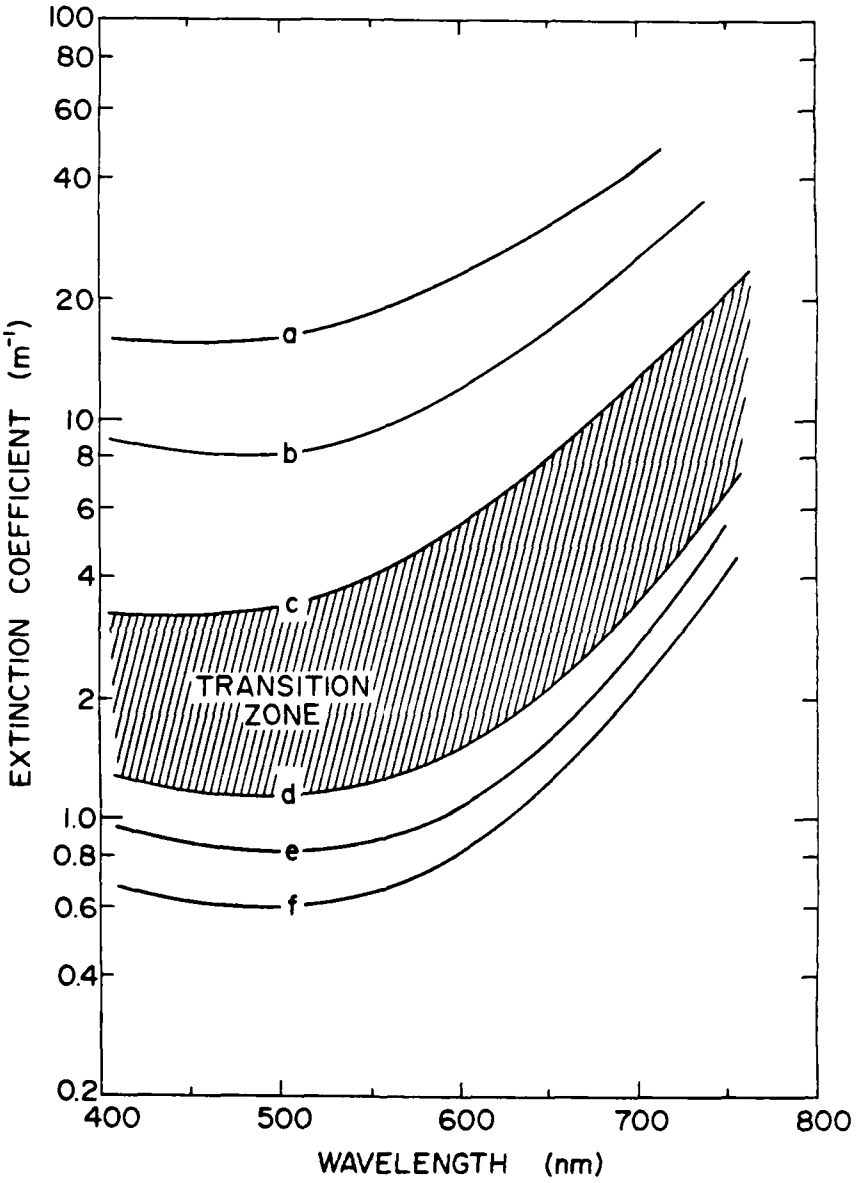

Fig. 17. Spectral extinction coefficients for various types of arctic ice and snow: (a) dry compact snow, (b) melting snow, (c) the surface scattering layer on melting multiyear ice, (d) interior multiyear ice, (e) interior first-year ice, and (f) ice beneath a late season melt pond (after *Grenfell and Maykut*, 1977).

relatively constant values of κ_λ in the 400-500 nm region, followed by strongly increased attenuation at longer wavelengths. The greatest attenuation was observed in cold dry snow where κ_λ's were about 20 times as large as those within the ice. The "transition zone" in Fig. 17 is a region of rapidly changing κ_λ that occurs within the 5-15 cm thick surface scattering layer on multiyear ice as it grades into the more uniform interior ice. Differences between κ_λ's in first-year and multiyear ice result from differences in brine volume and bubble density. Minimum values (curve f) were found beneath a mature melt pond where brine volume in the upper part of the ice exceeded 50%.

The strong attenuation at longer wavelengths causes the spectral composition of the light to undergo rapid changes as it passes through the ice. Measurements of downwelling irradiance taken beneath first-year sea ice (*Maykut and Grenfell*, 1975) show energy maxima occurring in the 470-480 nm wavelength band, corresponding to the peak in the incident solar spectrum. Red wavelengths are quickly absorbed in the surface layers of the ice so that the amount of energy reaching the ocean is negligible above 700-800 nm, even when the ice is very thin. Maximum transmission by the ice occurs in the 450-550 nm region, regardless of the surface conditions or ice thickness. The nature of the surface is, however, the dominant factor in determining the *amount* of energy reaching the ocean. These points are illustrated by Figs. 18 and 19 which show the spectral distribution of light beneath different thicknesses of first-year melt pond/blue ice and white ice. Because the spectral composition of the incident radiation field is rarely measured, it is useful to be able to estimate $F(\lambda,h)$ from more commonly available data. Values in Figs. 18 and 19 have thus been expressed as a percent of the total incoming shortwave radiation measured under typical arctic cloud conditions. The presence of snow on the ice drastically reduces the amount of transmitted light as illustrated in Fig. 20.

In many regions a thick layer of algae forms on the underside of the ice in late spring, intercepting most of the transmitted light. With the onset of bottom ablation, this layer tends to slough off; however,

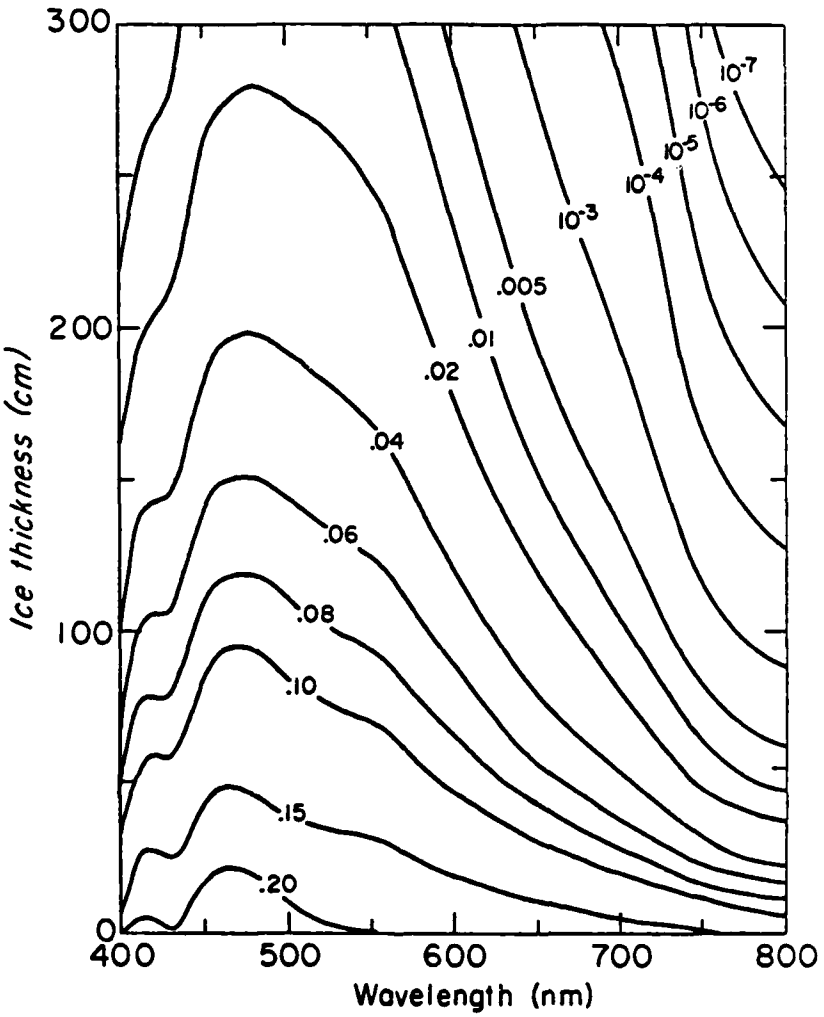

Fig. 18. Spectral distribution of downwelling irradiance beneath first-year melt pond/blue ice (after *Maykut and Grenfell*, 1975). Isopleths are expressed in percent per nanometer of the total incident irradiance at the surface.

algae remaining within the ice are still sufficient to affect the spectral distribution of the transmitted light. The characteristic signature of these algae is a broad peak in the transmission spectra between 450-550 nm and a secondary peak or shoulder at about 540 nm (*Maykut and Grenfell*, 1975). Bottom melting and brine drainage act to reduce the density of interstitial algae, and the transmission spectra slowly return to a fairly narrow maximum at 470-480 nm later in the melt

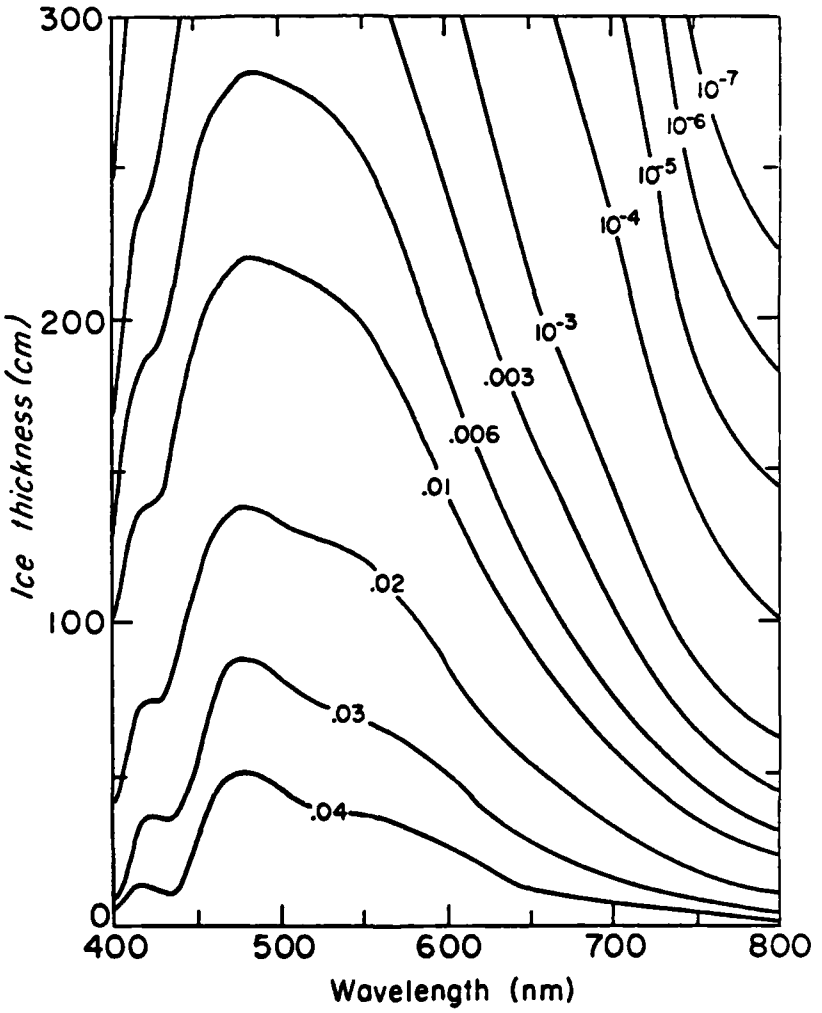

Fig. 19. Spectral distribution of downwelling irradiance beneath first-year white ice (after *Maykut and Grenfell*, 1975).

season. Differences in transmission spectra measured with and without algae indicate that the algae cause maximum absorption at 435 nm, with a secondary peak at about 670 nm.

The spectral distribution of shortwave radiation within the ice can be calculated by integrating Eq. (20) to obtain

$$F(\lambda,z) = F(\lambda,0)e^{-\kappa\lambda z} , \qquad (21)$$

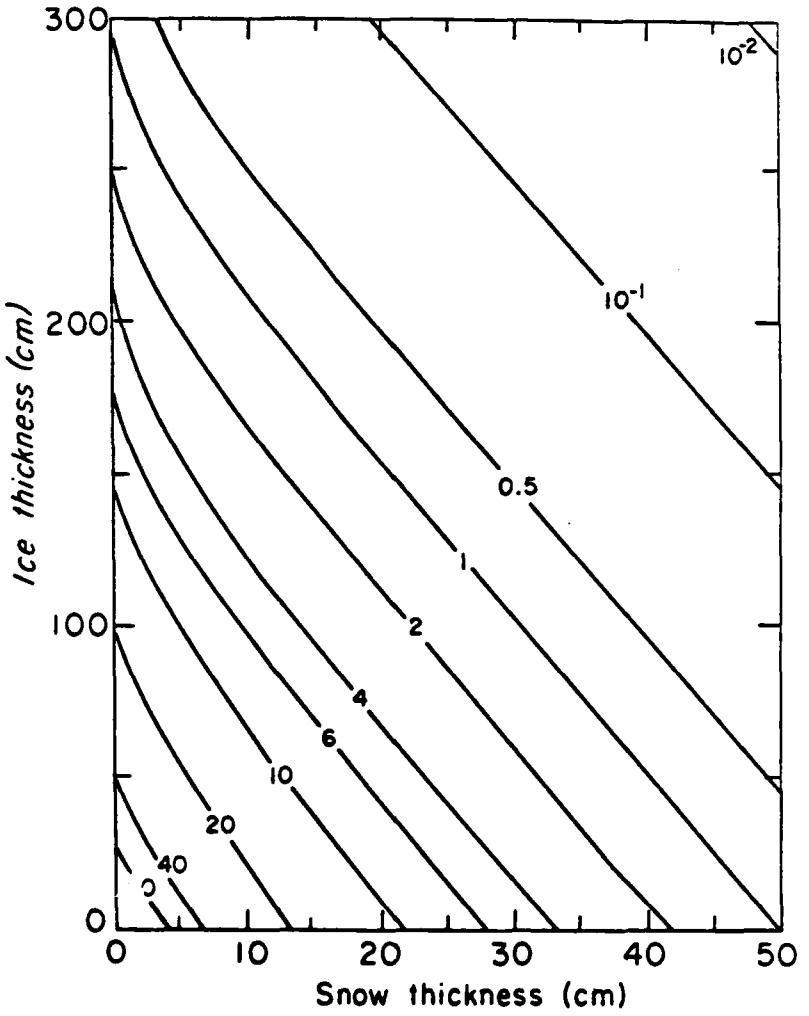

Fig. 20. Total downwelling irradiance beneath first-year arctic sea ice as a function of ice thickness and snow depth (after *Maykut and Grenfell*, 1975). Isopleth values are given as a percentage of the total incident irradiance at the surface under overcast conditions.

where $f(\lambda,0) = (1 - \alpha_\lambda)F_r(\lambda)$ = the net surface flux of shortwave radiation at wavelength λ. Equation (21) is known as *Beer's law*. In most practical applications it is the total flux, $F_z = \int_0^\infty F(\lambda,z)d\lambda$, which is of interest. By defining a *bulk extinction coefficient* (κ_z) as $\kappa_z = -\int_0^\infty \kappa_\lambda F(\lambda,0)e^{-\kappa\lambda z}d\lambda / \int_0^\infty F(\lambda,0)e^{-\kappa\lambda z}d\lambda$, it is possible to rewrite Beer's law as

$$F_z = F_o \exp(-\int_o^z \kappa_z dz) \quad , \tag{22}$$

where $F_o = \int_o^\infty F(\lambda,o)d\lambda = \int_o^\infty (1-\alpha_\lambda)F_r(\lambda)d\lambda$ is the net total shortwave radiation at the surface. *Grenfell and Maykut* (1977) have examined the variation of κ_z with depth in both first-year and multiyear ice. They found that κ_z decreases by as much as a factor of 50 in the upper 10-20 cm of the ice, after which it exhibits only a weak dependence on z. Very little difference was found between κ_z's in the interior of first-year and multiyear ice. For purposes of estimating F_z, the ice can be thought of as consisting of two layers: an upper layer that filters out nearly all the energy at longer wavelengths, and a lower layer where κ_z does not depend strongly on either ice type or cloud conditions. Shortwave energy absorbed in the upper layer is assumed to contribute immediately to temperature or mass changes at the surface, while energy absorbed in the lower layer returns slowly to the surface through conduction. This picture provides a simple method of estimating F_z. If we define i_o to be the fraction of F_o that passes through the upper layer, then

$$F_z = i_o F_o e^{-\bar{\kappa}(z-z_o)} \quad , \tag{23}$$

where $\bar{\kappa}$ is the average bulk extinction coefficient in the lower layer and z_o is the thickness of the upper layer. Equation (23) provides the best fit to observations when $\bar{\kappa} = 0.015$ cm^{-1}. The value of i_o depends on both the ice type and the spectral distribution of the incident radiation (i.e., on cloudiness). Using $z_o = 10$ cm, *Grenfell and Maykut* (1977) calculate that i_o for melting white ice is 0.35 when overcast and 0.18 when clear; for blue ice it is 0.63 when overcast and 0.43 when clear. With (23) it is possible to calculate the amount of energy transmitted to the ocean by setting $z = h$, while the amount of energy absorbed at a depth $z(z > z_o)$ is simply $\bar{\kappa}F_z$.

D. Ice Thickness and Floe Size Distributions

It was pointed out earlier that continual deformation and growth produce an ice cover that is a mixture of many different thicknesses of ice. Because many of the physical properties of the ice cover depend strongly on h, it is useful to have a way to quantify thickness variations within a particular region. To accomplish this, *Thorndike et al.* (1975) have introduced a probability density function g(h) called the *ice thickness distribution*, where $\int_{h_1}^{h_2} g(h)dh$ is the fractional area covered by ice in the thickness range $h_1 \leq h < h_2$. Processes that act to change g(h) are thermodynamic growth, ice advection, ridging, and divergence. A thickness distribution model that includes these processes has been developed and tested using data from the Central Arctic (*Thorndike et al.*, 1975). While producing reasonable results, the model parameterizes a number of complex and poorly understood processes related to the mechanical redistribution of h. Considerable work on the mechanical response of the ice to various strain states needs to be carried out before it will be possible to specify these processes with any degree of confidence. Nevertheless, g(h) provides a framework for coupling the dynamics and thermodynamics of the ice pack that has proved to be very useful in a variety of modeling efforts and large-scale studies of the ice.

Although the large-scale behavior of the ice is directly influenced by the distribution of ice thickness, data on g(h) are difficult to obtain. At present the only practical way to measure g(h) directly is with upward-looking submarine sonar. Figure 21 shows distributions of ice draft derived from submarine transects north of Fram Strait in October (*Wadhams*, 1981). As might be expected, there is a strong peak at about 3 cm, close to the thermodynamic equilibrium thickness, and a secondary peak at about 50 cm originating from young ice formed earlier in the fall. Level (presumably undeformed) ice makes up about 50% of the ice in the region. The distribution of deformed ice follows a negative exponential at drafts greater than 8-10 m. Measurements in the Beaufort Sea (*Wadhams and Horne*, 1980) show similar characteristics, although the secondary peak in g(h) occurs at about 2 m rather than 50

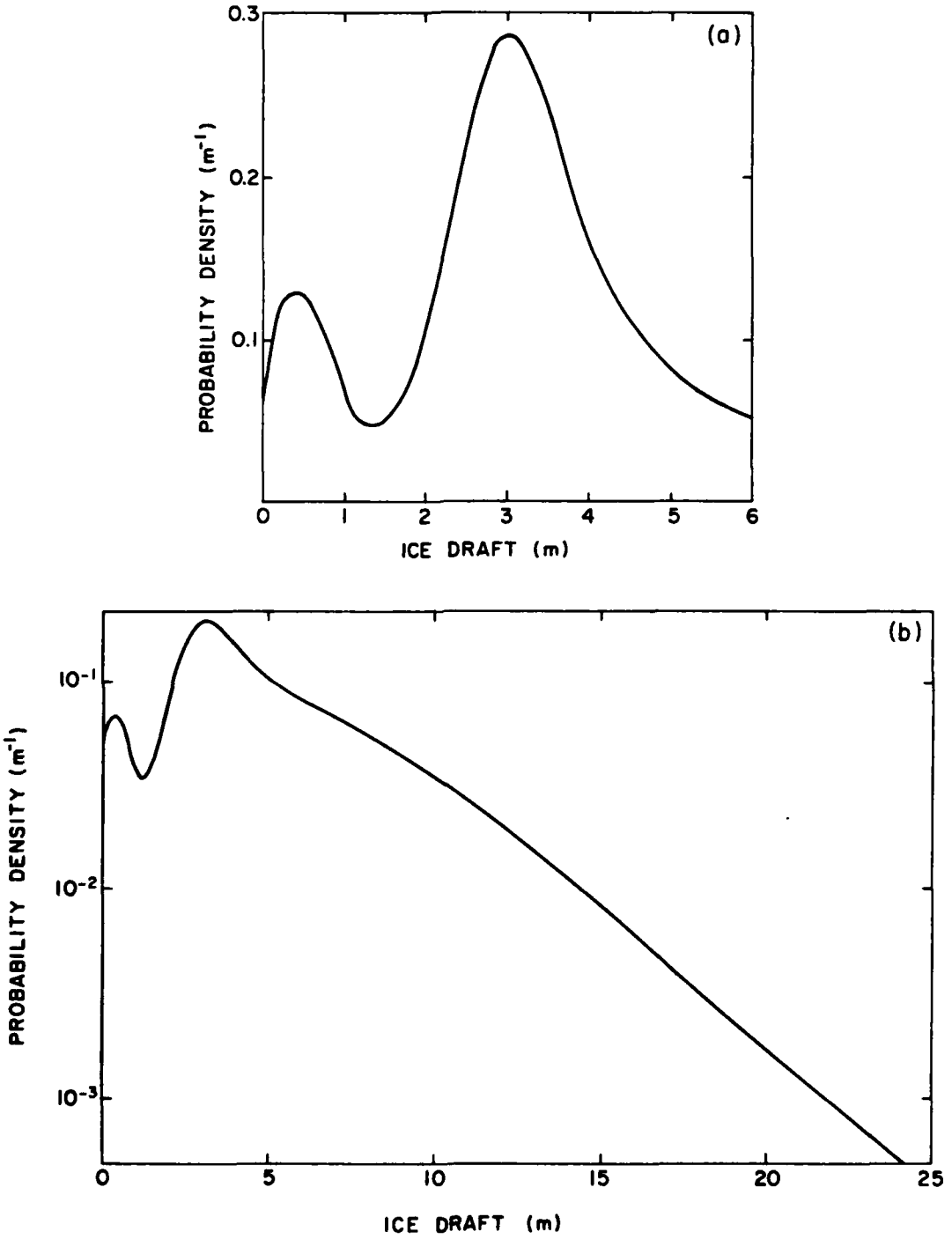

Fig. 21. October ice thickness distributions observed in the Arctic Ocean north of Fram Strait (after *Wadhams*, 1981): (a) the distribution of level ice, and (b) the complete distribution including ridged ice.

cm, probably representing second-year ice from the previous season. While a systematic analysis of spatial variations in g(h) has not been carried out, LeShack (see *Hibler*, 1980) has utilized submarine data to calculate the average thickness ($\bar{h}$) at many locations in the Arctic Basin (Fig. 22). The dominant feature of the $\bar{h}$ distribution is a sharp increase in thickness north of Greenland and the Canadian Archipelago that is almost certainly the result of greater ridging activity in the region. Comparable data are not available for the Antarctic and little is known about g(h) there.

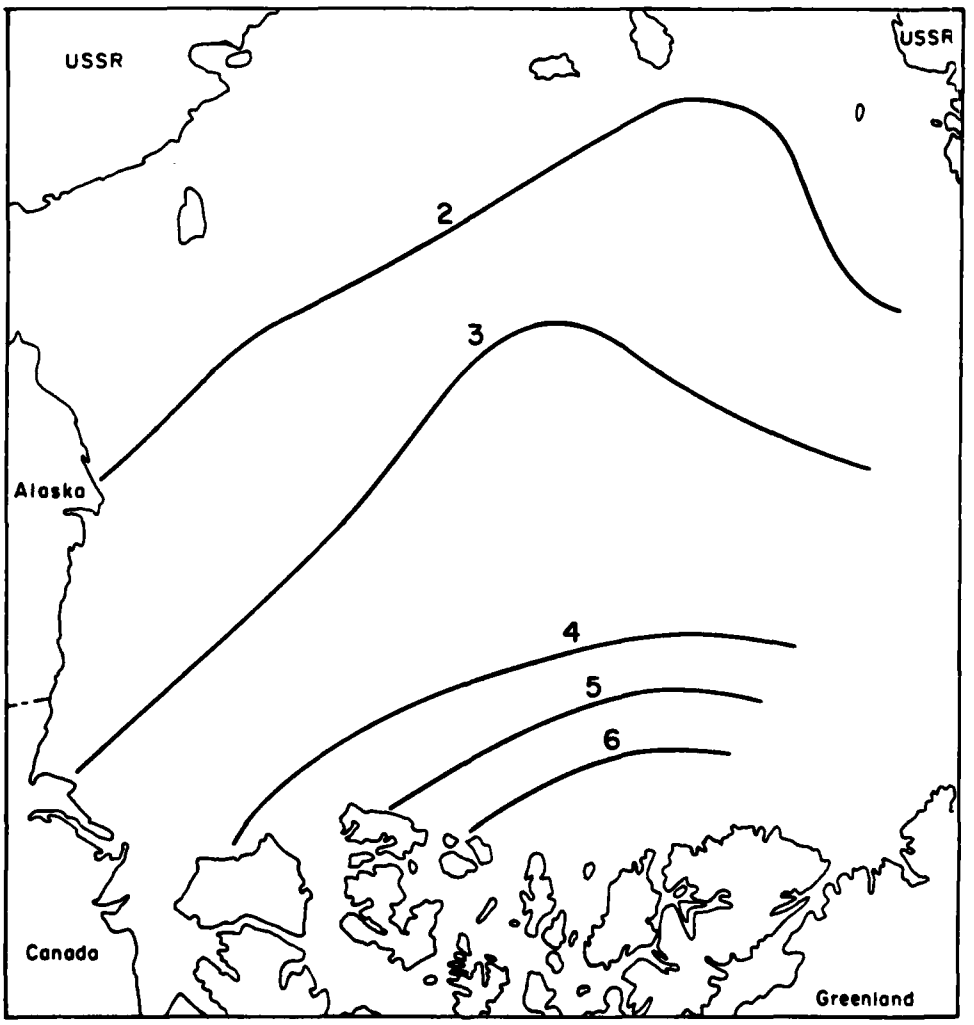

Fig. 22. Contours (in meters) of mean ice thickness in the Arctic Basin derived from submarine sonar data by LeShack (after *Hibler*, 1980).

While providing adequate definition of variations in the amount of thicker ice, submarine sonar data are not sufficiently dense in time to resolve the large and rapid changes that occur in the distribution of young ice. Yet knowledge of temporal changes in g(h < 1 m) is of fundamental importance because such areas not only make a major contribution to regional ice production and heat exchange, but also control the mechanical behavior of the ice pack. Without routine submarine transects or satellite instruments capable of resolving young ice thicknesses to within 10-20 cm, g(h) must be inferred from other data. The most feasible approach is to predict g(h) theoretically by combining models of ice growth and thickness distribution with heat balance and ice velocity data. Thermodynamic forcing for the models is often derived from climatology, modified on the basis of buoy or satellite observations. Information on the velocity field of the ice can be obtained directly from the motion of drifting buoys (*Colony and Thorndike*, 1983), or calculated from atmospheric pressure data using a dynamic ice model (*Coon et al.*, 1974; *Hibler*, 1979).

A geometric property of the ice cover that has received relatively little attention is the *floe size distribution*, N(d), defined as the number of floes of mean diameter d per unit area. Floe size distribution is believed to be a significant factor in problems related to the summer ice pack. Part of the shortwave energy deposited in the upper few meters of a lead goes to lateral melting on floe edges causing a decrease in ice concentration (A_i) and an increase in the amount of open water (A_w). This positive feedback between solar input to the ocean and the rate of change of A_i can have a large effect on the summer decay and retreat of the ice (*Langleben*, 1972). As the ice cover becomes more broken up, there is a decreasing probability that heat absorbed in the leads will be lost to the atmosphere or underlying ocean, and a corresponding increase in the amount of heat transferred to floe edges. Simple model experiments (*Perovich*, 1983) show that, for a given ice concentration, the rate of lateral decay depends directly on the number of leads present, i.e., on the total floe perimeter. Ice concentration alone is thus inadequate to characterize the state of the

summer ice cover. N(d) provides a measure of total floe perimeter and, unlike g(h), is relatively simple to obtain from aerial photography. N(d) appears to be particularly important in modeling the Marginal Ice Zone, where it affects not only lateral melting but also drag coefficients, melt pond coverage, and open water distribution. The equation governing N(d) is analogous to that for g(h), containing terms to describe advection, thermodynamics (lateral melting), and mechanical processes (breaking). Except near the ice edge where wave activity fractures the ice in a predictable fashion, processes involved in floe breakup are not well understood. Measurements of floe size distribution have been made in several locations (*Wadhams*, 1973; *Vinje*, 1977; *Rothrock and Thorndike*, 1984). Figure 23, for example, shows mid-August values in the central Beaufort Sea. For this case the decrease in N with d roughly follows a power law between 0.05 and 10 km. In the Marginal Ice Zone, N(d) tends to assume a negative exponential distribution (*Vinje*, 1977; *Wadhams*, 1980), but in the interior ice N(d) is much more variable and no single analytical form can be used to fit all the data (*Rothrock and Thorndike*, 1984). No systematic studies have yet been carried out to define how N(d) evolves during the summer or how this evolution differs from one region to another.

E. Electromagnetic Properties

In recent years there has been increasing interest in the electrical properties of sea ice in the 0.1-100 GHz region. Because of the extensive cloud cover and long periods of darkness, satellite imagery in the visible and infrared are of limited value in monitoring the state of the polar ice pack. Signals in the microwave region, however, are not affected by darkness and are attenuated only slightly by clouds. Microwave imagery thus provides a reliable method of observing the ice throughout the year. Both active and passive microwave measurements have been carried out over the ice. Active methods transmit a radar signal to the ice and measure the resulting reflection. At lower frequencies (0.1-0.5 GHz) maximum reflections occur at the top and

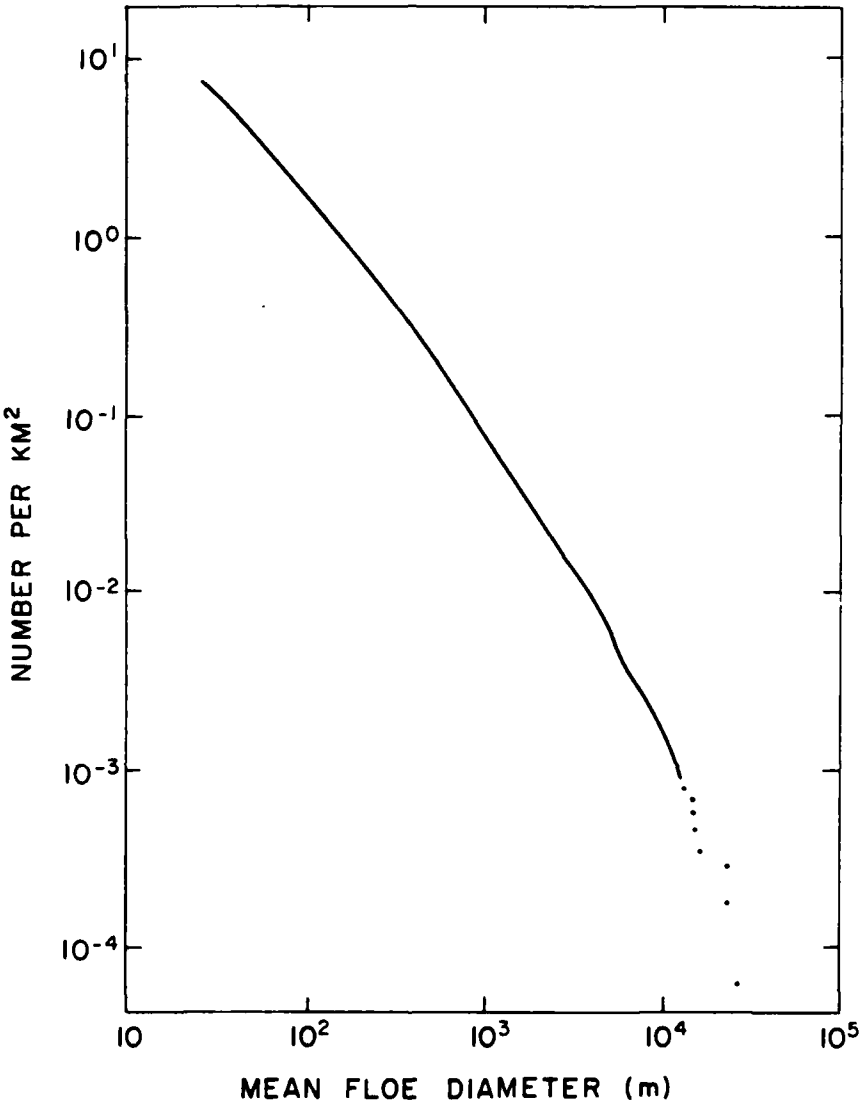

Fig. 23. Floe size distribution observed in the central Beaufort Sea during mid-August (based on measurements by *Rothrock and Thorndike*, 1984).

bottom of the ice, providing in principle a means to obtain thickness information. At higher frequencies (several GHz) radar images primarily show differences in surface roughness. Passive methods measure thermal emission from the ice, generally in the 3-100 GHz range. A serious limitation with passive observations is lack of spatial resolution. Whereas satellite-borne radar can resolve surface elements tens of

meters across, passive resolution varies from 150 km at 6 GHz to 30 km at 37 GHz. On the plus side, passive techniques can distinguish several different ice types because of distinct differences in thermal emission. Understanding microwave signatures from various types of ice requires information on the *dielectric constant*, a complex quantity whose real part describes surface reflection and backscattering and whose imaginary part describes attenuation within the ice. Dielectric properties of sea ice depend on the properties of its constituents (ice, brine, air, solid salts), and various expressions have been derived to express bulk values in terms of temperature, brine volume, and pore geometry (*Weeks and Ackley*, 1982; *Morey et al.*, 1984).

The availability of routine microwave data from polar orbiting satellites has made it possible to procure quantitative information on ice conditions in the polar oceans (e.g., *Carsey*, 1982; *Zwally et al.*, 1983) that cannot be obtained by other techniques. Most of the microwave data have been in the form of passive "brightness temperatures" which, after suitable analysis, can give ice concentration, ice extent, and the relative amounts of first-year and multiyear ice. Unfortunately, the procedure for translating brightness temperature measurements into quantitative estimates of ice state is not straightforward. A single brightness temperature is a spatial integral of energy emitted from a region that is large (30-150 km across) compared to the scale of individual features such as leads and floes. Even though such features cannot be resolved by passive microwave imagery, it is possible to estimate their contribution to an observed brightness temperature and so infer their relative abundance. The method makes use of frequency-dependent differences in microwave *emissivity*, the ratio of energy actually emitted to that emitted by a blackbody under identical conditions. In the Arctic, multiyear ice, first-year ice, and seawater exhibit markedly different changes in emissivity with frequency (Fig. 24). At lower frequencies first-year and multiyear ice appear much the same, while leads and open water have much lower brightness temperatures owing to a lower emissivity. At higher frequencies first-year ice

appears to be much warmer than multiyear ice. The reason why emissivity decreases with frequency in multiyear ice and not in first-year ice is related to differences in the distribution of brine which controls the depth from which the radiation emanates. Multiyear arctic ice typically

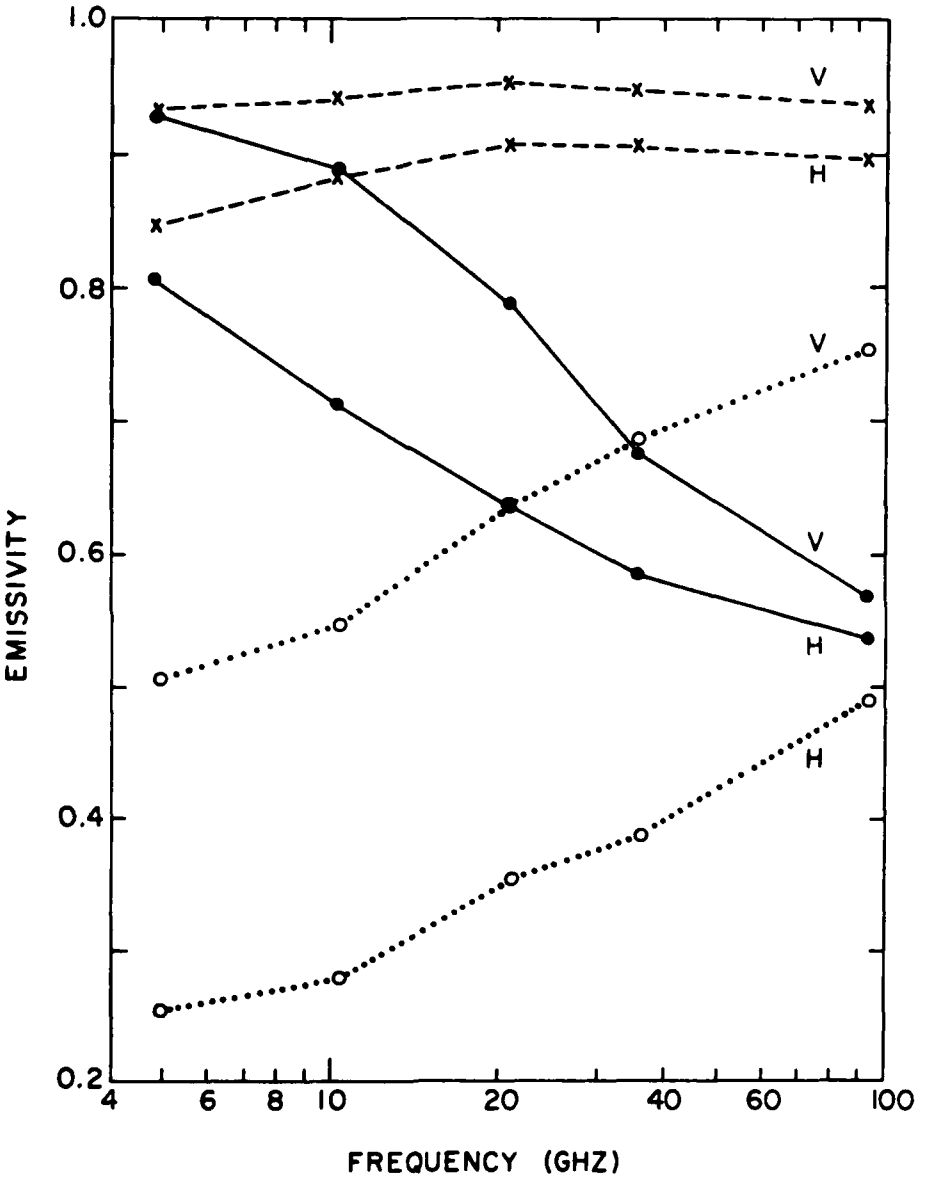

Fig. 24. Microwave emissivities of multiyear ice (solid lines), first-year ice (dashed lines), and calm seawater (dotted lines) in the Greenland Sea as a function of frequency (after *Svendsen et al.*, 1983). The symbols H and V refer to values obtained from horizontally and vertically polarized radiation.

has a surface layer containing little brine, but many air pockets. Radiation emitted from brine deeper in the ice is subject to scattering by the air pockets as it moves upward through the ice. The degree of scattering increases with frequency, and hence the observed decrease in emissivity. In first-year ice, brine is present very close to the surface so that the emitted radiation undergoes little scattering, and as a result is relatively independent of frequency. It is thus possible to use lower frequency data to determine ice concentration and extent, and higher frequency data to calculate first-year/multiyear ratios. The method is of limited value during the summer because melting erases any distinction between ice types and because leads cannot be distinguished from surface melt ponds. Ice extent, however, can still be found, regardless of season or the location of the edge.

Uncertainties inherent in the determination of ice concentration are larger than the amount of open water normally present within the arctic ice pack during the growing season, so microwave data are primarily used to map the distribution of first-year and multiyear ice in the Northern Hemisphere. Because of weak surface melting during the summer, differences in microwave emission from first-year and multiyear ice tend to be subdued or totally lacking in the Antarctic, particularly in the Weddell Sea region. Although signatures similar to multiyear ice have been seen in the Ross, Amundsen, and Bellingshausen seas, little is yet known regarding the physical characteristics of this ice. For this reason, microwave analyses of ice conditions in the Southern Hemisphere are generally focused on seasonal and spatial variations in ice concentration (e.g., *Zwally et al.*, 1983).

5. HEAT AND MASS BALANCE

Although an ice cover reduces momentum transfer between the air and the water, thermal processes associated with its growth and movement have the greatest impact on the ocean. In particular, solar input to the upper ocean is drastically reduced, limiting biological activity beneath the ice. The cold dense brine rejected by growing ice promotes convective overturning, causing any heat contained in the mixed layer to be transported upward where it is lost to the ice. Thus, unlike the open ocean, heat storage in the upper part of the water column is minimal. Heat and mass balance measurements have been carried out from land-based stations in the Arctic and Antarctic, as well as from manned and unmanned drifting stations in the Arctic Basin. Conditions in the coastal regions, however, are influenced by the proximity of the nearby land masses and are not necessarily representative of the ice pack as a whole. As a result, our understanding of interactions between the ice, ocean, and atmosphere is based largely on what has been seen in the perennially ice-covered portions of the Arctic Basin. The extent to which such information applies to more dynamically active areas such as the Marginal Ice Zone and the antarctic ice pack is unknown.

A. Energy Fluxes

1. Radiation

Radiation dominates heat exchange in the polar regions throughout the year. All matter radiates energy in proportion to the fourth power of its absolute temperature, i.e., $F^* = \varepsilon\sigma T_o^4$, where F^* is the flux of emitted radiation, ε is the surface emissivity, and σ is the Stefan-Boltzmann constant = $5.67 \cdot 10^{-8}$ W m^{-2} $^oK^{-4}$ ($4.88 \cdot 10^{-9}$ cal cm^{-2} s^{-1} $^oK^{-4}$). Most of the radiation reaching the earth's surface lies in two spectral bands: *shortwave radiation*, which originates from the sun and has a narrow intensity maximum near λ = 500 nm, and *longwave radiation*, which originates from the earth and atmosphere with a broad intensity maximum near λ = 12000 nm. Because there is little overlap in the spectral

distribution of radiation derived from these two sources, there is a natural separation in their measurement and treatment.

Downward longwave radiation (F_L) emitted from clouds and water vapor in the atmosphere is a major component in the surface heat balance. During most of the winter and fall incoming shortwave radiation (F_r) is negligible and, even at the height of the melt season, F_r is only slightly larger than F_L (Table 1). On an annual basis F_L is more than double F_r in the Central Arctic. Despite the magnitude of F_L, the net effect of longwave radiation is to remove heat from the ice. This is because the radiative temperature of the ice usually exceeds that of the atmosphere so that longwave radiation emitted by the ice ($F^{\uparrow}$) is almost always greater than F_L. Measurements of F_L and $F^{\uparrow}$ are difficult in the polar regions because of constant problems with dew and frost formation on the instruments. Fortunately, both can be estimated from other information. Surface temperature data are frequently used to calculate $F^{\uparrow}$ according to the formula, $F^{\uparrow} = \varepsilon_L \sigma T_o^4$, where ε_L is the longwave emissivity which equals 0.99 for snow and 0.97 for bare ice and melt ponds. Because a large part of the incoming longwave radiation is emitted by clouds and water vapor close to the ground, F_L can be approximated fairly well from surface observations of air temperature

Table 1. Monthly and annual radiation totals (MJ m^{-2}) over perennial ice in the Central Arctic (after *Marshunova, 1961; Maykut and Untersteiner,* 1971). Numbers in parentheses include the effects of summer melt ponds.

	JAN	FEB	MAR	APR	MAY	JUN	JUL	AUG	SEP	OCT	NOV	DEC	YEAR
Incoming longwave radiation [F_L]	435	430	430	495	630	750	800	780	690	580	475	450	6945
Outgoing longwave radiation [$F^{\uparrow}$]	-520	-500	-505	-600	-725	-830	-835	-820	-720	-610	-535	-520	-7720
Net longwave radiation [$F_L+F^{\uparrow}$]	-85	-70	-75	-105	-95	-80	-35	-40	-30	-30	-60	-70	-775
I coming shortwave radiation [F_r]			100	420	730	785	575	370	155	20			3155
Absorbed shortwave radiation [$(1-\alpha)F_r$]			15	80	145	170	245 (295)	115 (165)	35	5			810 (910)
Net radiation	-85	-70	-60	-25	50	90	210 (255)	75 (120)	5	-25	-60	-70	35 (125)

(T_a), partial pressure of water vapor (e_a), and fractional cloud cover (C). Longwave parameterizations have the form, $F_L = \varepsilon^* \sigma T_a^4$, where ε^* is the effective emissivity of the atmosphere. Several empirical expressions have been suggested for ε^* in the Arctic. The simplest,

$$\varepsilon^* = 0.7829(1 + 0.2232C^{2.75}) \tag{24}$$

obtained by *Maykut and Church* (1973) from observations at Point Barrow, Alaska, gives estimates of F_L accurate to within about 7% under overcast skies and 12% under clear skies. No correlation was found between ε^* and e_a. More complex expressions depending on e_a, C, T_a, and a seasonally varying empirical parameter have been obtained by *Marshunova* (1961) and *Idso and Jackson* (1969).

The sun being continuously above or below the horizon for periods of 2-6 months at a time produces seasonal changes in F_r that are much larger than those in F_L. In spite of extensive clouds and low sun angles, monthly totals of F_r in the Arctic can exceed those measured at many midlatitude stations (e.g., New York, Chicago) during the summer. Spatial variations in F_r poleward of 65°N tend to be small during the summer months (*Marshunova*, 1961). Because of the extreme summer cloudiness ($\bar{C}$ = 0.8-0.9), most of the shortwave radiation reaching the surface is diffuse rather than direct. Clouds over the polar oceans tend to be thin and so typically reduce F_r by 30-50% as compared to the 80-90% often observed at lower latitudes. The relatively low water vapor content of arctic clouds allows substantial amounts of near infrared energy to reach the surface. Under clear skies about 55% of F_r lies outside the visible region (400-700 nm), while under overcast skies this figure decreases to about 35%. Shortwave parameterizations used in large-scale heat balance studies and numerical models are generally written in the form $F_r = a^* F_{ro}$, where F_{ro} is the incoming shortwave radiation at the surface in the absence of clouds and a^* is the fractional attenuation by clouds. Although both F_{ro} and a^* can be calculated theoretically, the procedures are too involved for many

applications and empirical relationships are frequently employed. A particularly convenient form for F_{ro} was given by *Zillman* (1972),

$$F_{ro} = \frac{S_o \cos^2 z}{1.085 \cos z + (2.7 + \cos z)e_a \cdot 10^{-3} + 0.1}, \qquad (25)$$

where S_o is the solar constant, e_a is in millibars and z is the solar zenith angle, a function of latitude, day, and hour. Limited tests with arctic data (*Maykut*, in press) suggest that (25) tends to underestimate F_{ro} at high latitudes. The reason is probably related to the smaller amount of water vapor in the polar atmosphere and to backscattering of radiation reflected from the ice. This suggests that a high latitude correction may be desirable for formulas based on observations at lower latitudes. On the basis of model calculations, *Shine* (1984) reports that improved performance can be obtained from (25) over ice and snow if the denominator is changed to $1.2 \cos z + (1.0 + \cos z)e_a \cdot 10^{-3} + 0.046$. Expressions for a^* have been obtained by *Marshunova* (1961) [$a^* = 1 - kC$, where k increases from 0.15 in March to 0.5 in July] and *Laevastu* (1960) [$a^* = 1 - 0.6C^3$]. A parameterization for the net shortwave flux over ice and snow, claimed to be accurate to within a few percent under cloudy arctic conditions, has also been derived by *Shine* (1984) in terms of solar zenith angle, surface albedo, and the optical thickness of the cloud cover.

As mentioned earlier, the summer melt cycle over perennial ice is driven almost entirely by absorbed shortwave radiation. Although F_r reaches a maximum in June, the largest values of net shortwave radiation occur in July because of the decrease in α following removal of the snow cover. The presence of melt ponds significantly increases the net shortwave radiation and hastens the rate of decay and retreat of seasonal ice. In areas of perennial ice, ponds increase shortwave input to the ice by 20-40% (Table 1), but have only a small effect on the annual average ice thickness (*Maykut and Untersteiner*, 1971). Ice concentration is also an important parameter because leads admit large

quantities of energy to the ocean. Once the snow cover has vanished, the amount of energy available for primary production in the underlying water is largely determined by the relative area occupied by leads and melt ponds. Table 2 compares how 1 m thick layers of melt pond/blue ice and white ice distribute F_r for different ice concentrations. When A_i is high, transmission through blue ice accounts for most of the energy absorbed beneath the ice. As A_i decreases, leads quickly begin to dominate solar input to the water beneath the ice.

Table 2. The effect of ice concentration and surface type on absorption and transmission of incoming shortwave radiation in a region of 1 m thick bare ice. Values are expressed as percentages of F_r, weighted by relative area.

Ice concentration	Surface type	Net input at surface	% Absorbed $0 \leq z \leq 1$ m	% Transmitted below 1 m	Regional input
0.9	blue ice	61	48	13	70
	white ice	27	25	2	36
	leads	9	4	5	
0.5	blue ice	34	27	7	80
	white ice	15	14	1	61
	leads	46	19	27	

2. Turbulent Exchange

Apart from outgoing longwave radiation, the only means of transferring energy from the ice to the atmosphere is through turbulent exchange. The *sensible heat flux* (F_s) results from temperature differences between the ice and atmosphere, while the *latent heat flux* (F_e) is produced by the release of latent heat associated with evaporation, condensation, and sublimation. These fluxes are frequently dismissed as being unimportant because they are typically 1-2 orders of magnitude smaller than the radiation fluxes. This argument is misleading, however, because the net radiation balance is small in comparison to its individual components (Table 1). In fact, the magnitude of $F_s + F_e$ in the Central Arctic is on the order of 20-50% of

the total net radiation. Theoretical calculations (*Maykut and Untersteiner*, 1969) have demonstrated that the equilibrium thickness of multiyear ice is very sensitive to changes in F_s and F_e during the summer. Turbulent fluxes near the boundaries of the ice pack tend to be larger and appear to be a significant factor in the summer decay cycle there.

The rate of turbulent heat transfer depends on surface roughness, wind speed, boundary layer stability, and the gradients in temperature and water vapor near the surface. Commonly used parameterizations for these fluxes are: $F_s = \rho_a c_p C_s u(T_a - T_o)$ and $F_e = \rho_a L_v C_e u(q_a - q_o)$, where ρ_a is the density of the air, c_p is the specific heat of the air, u is the wind speed, L_v is the latent heat of vaporization, q_a and q_o are specific humidities in the air and at the surface, and C_s and C_e are bulk transfer coefficients which vary with stability and surface roughness. Eddy correlation measurements over multiyear ice (*Thorpe et al.*, 1973) indicate that $\overline{C}_s = 1.2 \cdot 10^{-3}$ and $\overline{C}_e = 0.55 \cdot 10^{-3}$, while observations in the unstable boundary layer over a refreezing lead (*Lindsay*, 1976) give values of $2.0\text{-}2.5 \cdot 10^{-3}$ for both C_s and C_e. Differences in surface geometry (ridges, hummocks, floe sizes) can be expected to produce local variations in C_s and C_e of at least a factor of 2.

Studies of turbulent heat exchange over perennial sea ice (*Doronin*, 1963; *Badgley*, 1966; *Leavitt et al.*, 1978) show that, unlike the situation over temperate and tropical oceans, F_e is negligible during much of the polar year (November-April in the Arctic). Even during the summer, latent heat losses are only slightly larger than those from sensible heat. During the winter when there is a persistent temperature inversion close to the surface, F_s supplies heat to the ice, compensating for one-third to one-half the net longwave loss. Although daily totals of F_s during the summer are comparable in magnitude to the winter values, monthly averages are small as a result of frequent alternations in the direction of F_s. All studies in the Central Arctic show a net turbulent heat loss for the summer that acts to reduce the amount of surface melting. Without these turbulent heat losses, surface ablation

would be 20-100% larger and the equilibrium thickness reduced by up to 50% (*Maykut and Untersteiner*, 1969). At the margins of the ice pack, F_s and F_e are generally downward and contribute substantial amounts of heat to the surface. During May and June, for example, the turbulent fluxes can account for as much as one-third of the net heat input to coastal ice (*Langleben*, 1966).

3. Heat Conduction

Even during the melt season, there is an upward conduction of heat in the ice [$F_c = k_I(\partial T/\partial z)$] which supplies much of the energy needed to balance the longwave loss at the surface. In thin ice $F_c(z = 0) \simeq F_c$ $(z = h)$, greatly simplifying the treatment of young ice growth. In thicker ice internal phase changes and heat storage become important and growth calculations must take into account nonlinearities in the temperature profile. Over an annual cycle the amount of heat conducted to the surface of multiyear ice is the sum of the sensible heat input from the ocean (F_w), the latent heat released by net bottom accretion, and the shortwave energy temporarily stored in brine pockets and surface melt ponds. For perennial arctic ice $F_c \simeq 6.6$ kcal cm^{-2} $year^{-1}$ (8.8 W m^{-2}), of which 23% is supplied by the ocean, 39% by bottom accretion, 29% by release of stored heat in the brine pockets, and 9% by the refreezing of surface meltwater (*Maykut*, in press). F_c can be more than two orders of magnitude larger in young ice than in multiyear ice. Over the course of the entire growth season the amount of heat conducted to the surface of seasonal ice is roughly 2-3 times the annual total for perennial ice.

4. Oceanic Heat Flux

A variety of observational and theoretical evidence points to a significant input of heat from the ocean to the ice, but direct measurements of this flux (F_w) have not been successful. In the Antarctic where surface ablation is small, the seasonal disappearance of the ice must be caused almost entirely from energy contained in the water.

Certainly shortwave radiation absorbed in the upper ocean is a major component of F_w there; however, heat from the deeper ocean is also important. *Gordon* (1981) estimates that up to 50% of F_w could be derived from water below the pycnocline, but the uncertainty in this estimate appears to be large. In the Central Arctic F_w is about 1.5 kcal cm^{-2} $year^{-1}$ (2 W m^{-2}). The source of this heat was originally believed to be the layer of relatively warm Atlantic water that occurs across much of the Arctic Basin. More recently it has been suggested that temperature changes in the Atlantic layer are largely due to mixing with colder shelf water (*Aagaard et al.*, 1981) and that F_w is determined almost entirely by shortwave input through leads and areas of thin ice (*Maykut*, 1982). In areas of seasonal ice the upper part of the water column at the onset of freezing can contain 1-2 kcal cm^{-2} (40-80 MJ m^{-2}) which is slowly lost as the mixed layer deepens in response to salt rejection by the growing ice. The largest values of F_w in the Arctic probably occur in the Fram Strait region where the Atlantic enters the basin and is still close to the surface.

B. Response of the Ice to Environmental Changes

Because sea ice appears to be an integral part of the global climate system, there are numerous questions that need to be answered regarding its long-term response to various environmental factors. For example, how will the polar ice pack be affected by the increasing concentration of carbon dioxide in the atmosphere? Can man artificially alter ice conditions to limit these effects? How does the state of the ice pack change over a glacial cycle? Although some information on historical changes in the ice pack can be gained from the fossil record and oxygen isotope analysis of ocean sediments, sensitivity studies with coupled ocean-ice-atmosphere models are needed to fully understand the response of the ice. Such models are, however, still in a relatively crude state of development and do not adequately simulate many system interactions and feedbacks that are likely to affect ice extent and thickness.

Even though prediction of future changes in the state of the ice cannot yet be made with any real degree of confidence, it is possible to determine with some accuracy how specific changes in such factors as air temperature, snowfall, cloudiness, and oceanic heat flux will alter ice thickness. This is the first step needed in addressing the more difficult problem of ice extent. To estimate thickness changes, it is first necessary to formulate energy balance equations at the upper and lower boundaries of the ice. The flux balance at the surface is

$$(1 - \alpha)(1 - i_o)F_r + F_L - F^{\uparrow} + F_s + F_e + k_i(\frac{\partial T_i}{\partial z})_o + F_m = 0 \ , \quad (26)$$

where $F_m = \rho_i L_i (dh/dt)_o$ = the heat loss due to surface melting. When T_o is below freezing, $F_m = 0$; when T_o is at the melting point, any surplus of energy will be balanced by melting and a change in h. At the bottom of the ice

$$\rho_i L_i (\frac{dh}{dt})_h - k_i (\frac{\partial T_i}{\partial z})_h + F_w = 0 \ . \quad (27)$$

Equations (26) and (27) are coupled via the heat conduction terms, $k_i(\partial T_i/\partial z)_o$ and $k_i(\partial T_i/\partial z)_h$, whose calculation requires knowledge of the vertical temperature distribution within the ice. Changes in $T_i(z)$ can be calculated using a form of the thermal diffusion equation modified to include the effects of internal heating from solar radiation

$$\rho_i c_i \frac{\partial T_i}{\partial t} = \frac{\partial}{\partial z} (k_i \frac{\partial T_i}{\partial z}) + \bar{\kappa}_i i_o (1 - \alpha) F_r e^{-\bar{\kappa}_i (z - z_o)} \ . \quad (28)$$

Simultaneous solution of (26)-(28) then makes it possible to determine the thermal response of the ice to any of the parameters explicitly or

implicitly contained in the equations. Inclusion of a snow cover adds an additional boundary condition and heat conduction equation, but does not significantly complicate the solution. Large-scale simulations of the ice cover generally retain (26) and (27), but simplify the problem either by eliminating (28) through the assumption of a linear temperature profile in the ice, or by resolving $T_i(z)$ only crudely.

Model results (*Maykut and Untersteiner*, 1971) indicate that the equilibrium thickness (see Section 2B) is especially sensitive to factors that affect the amount of summer melting: air temperature, surface albedo, incoming radiation, and turbulent heat exchange. Complete disappearance of perennial arctic ice would, for example, occur with increases of 3-5°C in T_a, 25-30% in incident solar radiation, or a 15-20% decrease in summer albedo. Changes in cloudiness affect both the shortwave and longwave radiation. Decreased cloudiness lowers the amount of incoming longwave radiation while increasing the downward shortwave flux. A decrease in cloudiness thus acts to cool the ice during the winter, but has only a weak effect during the summer because the opposing changes in incident radiation tend to balance. Year to year variations in arctic cloudiness are presently on the order of 25% and do not appear to change h_e significantly.

Theoretical predictions of how variations in snowfall and oceanic heat flux affect h_e in the Central Arctic are shown in Figs. 25 and 26. In spite of the large effect that snow depth has on ice temperatures and growth rates, differences in snowfall are found to have little impact on h_e until depths exceed about twice the present day average of 40 cm. With less snow the ice is colder and winter growth greater, but summer ice melting is also greater because of earlier removal of the snow. Changes in surface melting and bottom accretion approximately balance until snow depths become so large that ice ablation is delayed until late in the summer when F_r begins to decrease rapidly with time. Above $h_s \simeq 80$ cm the decrease in ice ablation is greater than the decrease in accretion, and h_e increases steeply with increasing h_s. Under present surface conditions the thickness of undeformed perennial ice will not

AD-A166 140 AN INTRODUCTION TO ICE IN THE POLAR OCEANS(U) 2/2
WASHINGTON UNIV SEATTLE APPLIED PHYSICS LAB G A MAYKUT
SEP 85 APL-UW-8510 N00014-84-C-0111

UNCLASSIFIED F/G 8/12 NL

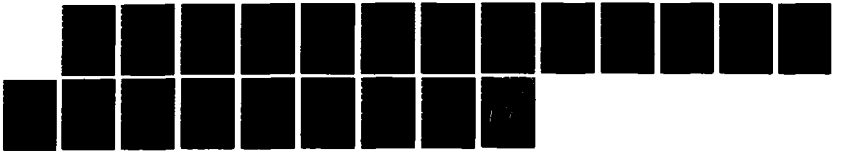

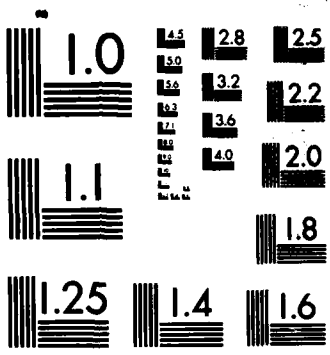

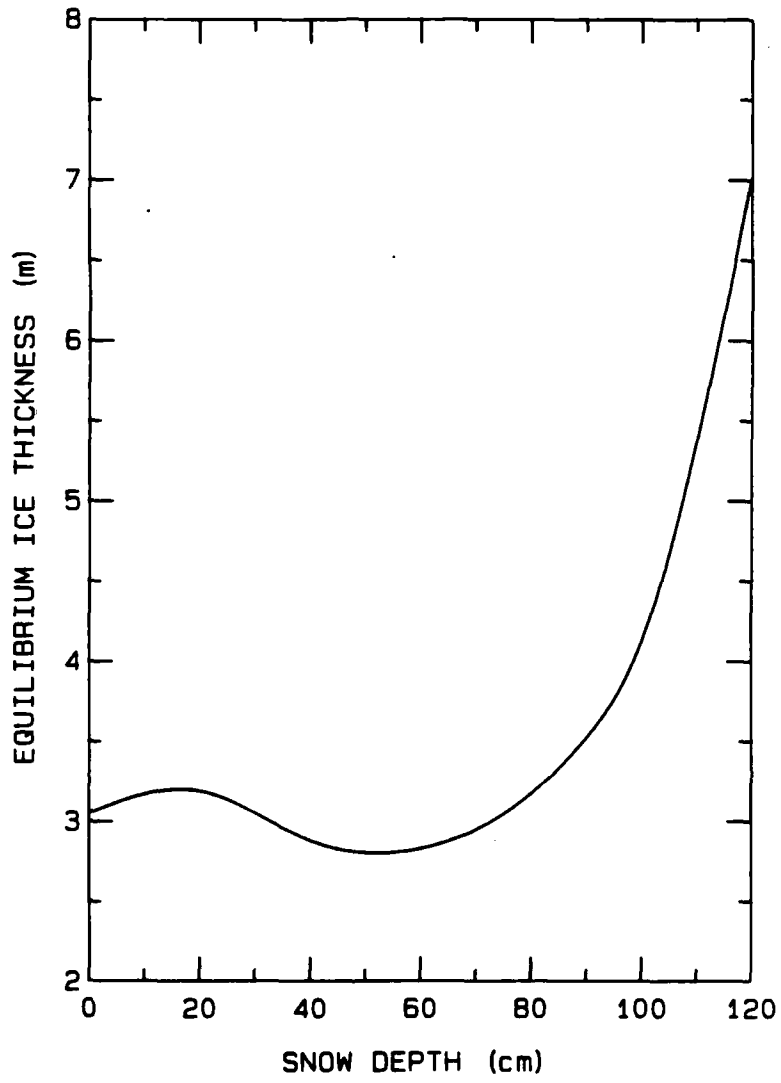

Fig. 25. Average equilibrium thickness of perennial arctic sea ice as a function of maximum annual snow depth (after *Maykut and Untersteiner*, 1971).

exceed 7 m in the Central Arctic, even in regions where the oceanic heat flux is negligible (Fig. 26). However, if h_s is in excess of about 120 cm, summer melting in the Arctic is generally insufficient to remove the snow cover completely, and equilibrium ice will grow from above and ablate from below, becoming in effect a "floating glacier." The combination of small F_w and high snowfall can produce ice of almost any thickness and has been used to explain the origin of very thick ice found in Nansen Sound and along the north coast of Ellesmere Island

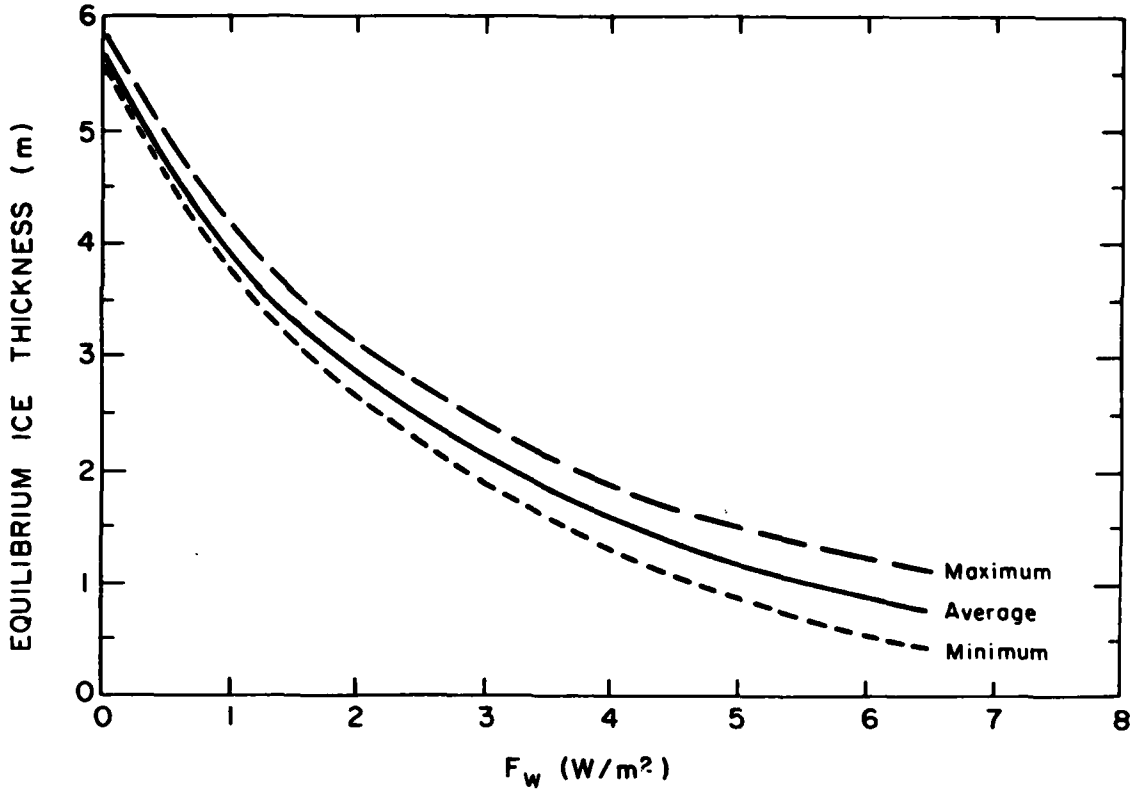

Fig. 26. Equilibrium thickness of arctic sea ice as a function of the average annual oceanic heat flux. Average annual thickness, as well as the absolute annual maximum and minimum, are shown (after *Maykut and Untersteiner*, 1971).

(*Walker and Wadhams*, 1979). The calculations also predict that the arctic ice cover would be seasonal if F_w totaled more than about 5.5 kcal cm^{-2} $year^{-1}$ (7.3 W m^{-2}). It is suspected that average values of F_w in many parts of the Southern Ocean may exceed this value by at least a factor of 2-3 (*Gordon et al.*, 1984).

C. Effects of Ice Thickness on Surface Heat Exchange

It was shown in Fig. 5 that, for constant thermal forcing, winter growth rates in young ice are strongly dependent on thickness. The same holds true for the surface heat balance. Surface temperatures in thin ice decrease rapidly with increasing thickness (Fig. 27), affecting the conductive heat flux, the turbulent exchange, and the longwave loss. In

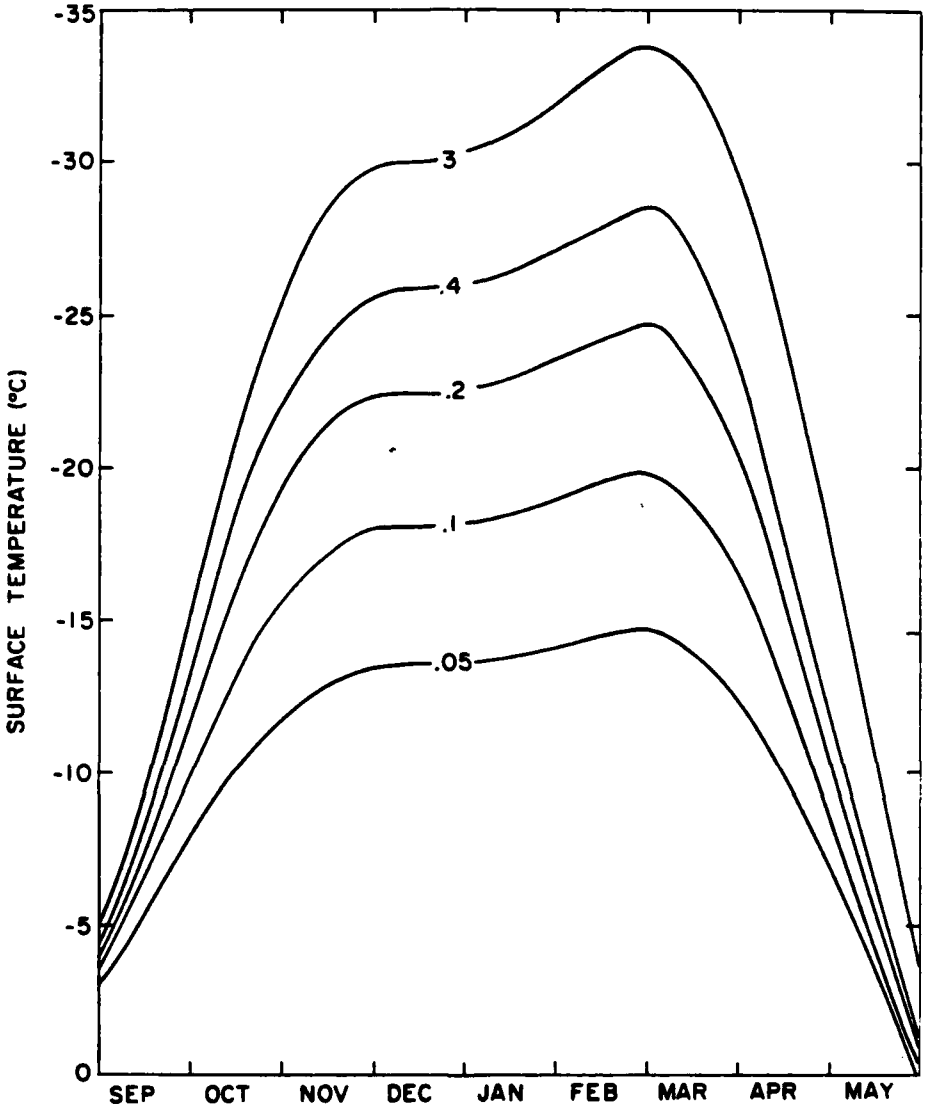

Fig. 27. Seasonal variations in surface temperature for various ice thicknesses (in meters) in the Central Arctic (after *Maykut*, 1978).

addition, the increase of albedo with thickness produces a decrease in shortwave absorption as the ice grows. Heat exchange over thin ice tends to be much more vigorous than over thicker ice. Turbulent heat losses over a refreezing lead, for example, can be more than two orders of magnitude larger than those over nearby thick ice. Thus, relatively small areas of thin ice and open water can have a significant impact on regional heat, mass, and salt balances.

Theoretical calculations have been carried out to quantify how thickness affects the surface heat balance in regions of perennial arctic ice (*Maykut*, 1978). Results are summarized in Table 3. When the ice is thin, heat input at the surface is controlled by F_c, and temperatures are relatively insensitive to changes in atmospheric

Table 3. Surface heat balance components in the Central Arctic as a function of ice thickness (after *Maykut*, 1978). Energy fluxes are given in W m^{-2} and apply to conditions on the first day of the month.

	Sept.	Oct.	Nov.	Dec.	Jan.	Feb.	March	April	May	June
					Open Water					
Net shortwave radiation	89	24					7	83	209	281
Net longwave radiation	−28	−69	−114	−138	−142	−147	−149	−140	−98	−43
Sensible heat flux	−68	−259	−458	−540	−543	−575	−615	−520	−276	−33
Latent heat flux	−34	−108	−139	−145	−145	−147	−150	−144	−112	−31
Oceanic heat flux	130	436	711	823	830	869	914	804	486	107
					0.05 m					
Available shortwave energy*	60	16					5	56	141	189
Net longwave radiation	−22	−42	−70	−87	−91	−93	−93	−93	−76	−51
Sensible heat flux	−44	−142	−261	−311	−312	−334	−362	−313	−179	−74
Latent heat flux	−31	−50	−49	−47	−46	−45	−44	−51	−62	−47
Conductive heat flux	37	218	380	445	449	472	494	401	176	−17
					0.1 m					
Available shortwave energy	56	15					4	52	131	175
Net longwave radiation	−20	−33	−55	−69	−73	−75	−73	−77	−68	−50
Sensible heat flux	−36	−101	−186	−222	−222	−238	−262	−232	−143	−73
Latent heat flux	−27	−34	−30	−27	−26	−25	−24	−31	−47	−47
Conductive heat flux	27	153	271	318	321	338	355	288	127	−5
					0.2 m					
Available shortwave energy	53	14					4	49	124	166
Net longwave radiation	−19	−25	−41	−53	−57	−58	−55	−62	−61	−49
Sensible heat flux	−29	−64	−115	−137	−136	−147	−165	−154	−109	−68
Latent heat flux	−23	−22	−16	−14	−14	−13	−12	−17	−34	−46
Conductive heat flux	18	97	172	204	207	218	228	184	80	−3
					0.4 m					
Available shortwave energy	48	13					4	46	114	153
Net longwave radiation	−17	−19	−31	−41	−45	−45	−42	−51	−55	−47
Sensible heat flux	−22	−36	−62	−72	−70	−77	−91	−93	−82	−60
Latent heat flux	−19	−14	−9	−6	−6	−6	−5	−10	−26	−44
Conductive heat flux	10	56	102	119	121	128	134	108	49	−2
					0.8 m					
Available shortwave energy	45	12					3	42	104	140
Net longwave radiation	−16	−16	−24	−33	−37	−37	−34	−43	−51	−46
Sensible heat flux	−17	−18	−27	−30	−27	−31	−42	−53	−61	−54
Latent heat flux	−16	−9	−4	−3	−2	−2	−2	−5	−19	−39
Conductive heat flux	4	31	55	66	66	70	75	59	27	−1
					3.0 m					
Available shortwave energy	16	4					1	17	42	59
Net longwave radiation	−14	−12	−18	−26	−31	−29	−25	−32	−38	−35
Sensible heat flux	−5	0	6	11	17	16	12	9	−2	−8
Latent heat flux	−9	−4	0	0	0	0	0	0	−4	−10
Conductive heat flux	12	12	12	15	14	13	12	6	2	−6

*$(1 - i_o)(1 - \alpha) F_r$

forcing. Heat exchange with the atmosphere over young ice is dominated by the sensible heat flux. In March, for example, F_s ranges from a small heat *gain* over thick ice to a loss over open leads that is about 3.5 times the total of the incident radiation fluxes. While F_e over open leads is comparable to the radiation fluxes during most of the winter, its importance decreases rapidly with h owing to a steep decline in saturation vapor pressure below 0°C. Over thicker first-year ice F_s is comparable to the net longwave radiation. Energy needed to support the large energy fluxes over young ice is derived largely from latent heat released by the growth of ice, and not by heat transport in the ocean. In all cases the relative differences in heat exchange tend toward zero in the spring as the ice approaches the melting point. The calculations also demonstrate that the surface heat balance becomes insensitive to thickness once h exceeds 80-100 cm.

D. Regional Fluxes

Large changes in the amount of thin ice and open water can occur on time scales of hours to days, producing corresponding changes in the regional heat and mass balance which are independent of the incident energy fluxes. For obvious reasons most field data have been gathered from thick, relatively stable sea ice. However, because they do not take into account contributions made by areas of thin ice and open water, such data are not necessarily representative of the region as a whole. The large spatial variability in local values makes direct determination of regional fluxes difficult. An alternate approach is to utilize theoretical models to infer large-scale values from routine local observations. The method works as follows. Let ϕ be any property that depends on h (e.g., the salt flux to the ocean). The contribution made by a particular thickness category is found by multiplying the fractional area covered by that category times the magnitude of ϕ over that thickness. Summing over all possible thicknesses then gives a total for the region, i.e.,

$$\bar{\phi} = \int_0^\infty \phi(h)g(h)dh \quad . \tag{29}$$

$\bar{\phi}$ is defined to be the *regional* or *large-scale* average. In practice it is usually necessary to work with discrete thickness categories. If g(h) is partitioned into n categories, (29) can be approximated by

$$\bar{\phi} = \sum_{i-1}^{n} \bar{\phi}_i \Delta G_i \quad , \tag{30}$$

where $\bar{\phi}_i$ is the average value of ϕ in the i^{th} category, $\Delta G_i = \bar{g}_i \Delta h_i$, $\Delta h_i = h_i - h_{i-1}$, and $\bar{g}_i$ is the average value of g in the i^{th} category. Since ϕ and g are also usually functions of time, we use the notation $\langle\phi\rangle = \int_0^t \bar{\phi}(t)dt$ to denote spatial averages integrated over time. Application of (29) or (30) requires general heat balance and ice movement information. A thermodynamic ice model is used with heat balance data to obtain growth rates and energy fluxes over all thicknesses of ice. Growth rates and ice velocities are then used to drive an ice thickness distribution model and calculate g(h) for the region, thereby allowing the determination of $\bar{\phi}$ from (30).

A study of the effects of thickness variations on regional fluxes has been carried out using data from the central Beaufort Sea (*Maykut*, 1982). Results are summarized in Table 4 and Figs. 28 and 29. The calculations clearly demonstrate that relatively small amounts of thin ice can play a major role in the overall heat and mass balance of a region. Between October and April refreezing leads generally covered no more than 0.5% of the area, while thin ice ($10 < h < 40$ cm) covered only 2-3%. Greater divergence and melting of thin ice caused a large increase in the amount of open water during the spring and summer. Freezing of the open water in late August produced a September peak in the distribution of young ice, but ridging and continued growth combined to move most of this ice into the 80^+ cm category by October. The

Table 4. Area weighted fluxes of heat (MJ m^{-2} mo^{-1}) and salt (kg m^{-2} mo^{-1}) in the central Beaufort Sea (after *Maykut*, 1982).

	Ice Thickness Category	JAN	FEB	MAR	APR	MAY	JUN	JUL	AUG	SEP	OCT	NOV	DEC	Annual
Net radiation	0-0.1	-0.6	-0.4	-0.6	0.6	7.4	21.6	44.4	46.6	5.5	-0.7	-1.2	-0.8	121.8
	0.1-0.2	-0.8	-0.5	-0.8	1.4	6.7	2.1	1.5	1.7	3.5	-0.7	-1.6	-1.3	11.2
	0.2-0.4	-2.0	-1.1	-1.1	2.7	11.7	4.4	3.1	2.8	2.9	-0.9	-2.7	-3.3	16.5
	0.4-0.8	-4.1	-2.4	-0.9	1.9	18.0	10.8	5.9	5.0	2.1	-1.3	-3.3	-5.9	25.8
	0.8 - ∞	-74.2	-65.2	-50.2	-10.9	48.5	85.6	181.8	86.5	-1.7	-30.8	-55.4	-60.9	53.1
	TOTAL	-81.7	-69.6	-53.6	-4.3	92.3	124.5	236.7	142.6	12.3	-34.4	-64.2	-72.2	228.4
	3 m	-79.0	-67.8	-52.4	-10.8	56.5	94.3	207.9	111.2	-1.8	-33.1	-60.2	-67.6	97.2
Sensible heat flux $<F_s>$	0-0.1	-2.1	-1.4	-2.9	-2.9	-4.7	-1.0	-1.2	-0.7	-8.1	-2.9	-4.4	-2.7	-35.0
	0.1-0.2	-2.3	-1.6	-3.4	-3.2	-3.5	-0.2	-0.1	-0.2	-5.0	-2.6	-4.7	-3.8	-30.6
	0.2-0.4	-3.9	-2.6	-4.4	-4.0	-5.7	-0.6	-0.1	-0.3	-5.0	-2.7	-6.3	-7.4	-43.0
	0.4-0.8	-4.7	-3.6	-2.8	-2.6	-9.3	-1.9	-0.3	-0.6	-3.1	-3.0	-4.7	-8.2	-44.8
	0.8 - ∞	43.7	32.8	27.8	11.1	-13.4	-15.2	-11.8	-12.0	-5.7	4.6	20.5	30.9	113.3
	TOTAL	30.7	23.6	14.3	-1.6	-36.6	-18.9	-13.5	-13.8	-26.9	-6.6	0.4	8.8	-40.1
	3 m	46.5	34.1	29.0	11.3	-15.6	-16.7	-13.6	-15.7	-7.5	4.9	22.3	34.3	113.3
Latent heat flux $<F_e>$	0-0.1	-0.3	-0.2	-0.4	-0.7	-2.2	-1.3	-2.5	-3.1	-4.8	-0.8	-0.8	-0.4	-17.5
	0.1-0.2	-0.3	-0.2	-0.3	-0.7	-1.5	-0.2	-0.1	-0.3	-2.9	-0.6	-0.6	-0.4	-8.1
	0.2-0.4	-0.4	-0.2	-0.4	-0.8	-2.5	-0.6	-0.3	-0.5	-2.7	-0.6	-0.7	-0.8	-10.5
	0.4-0.8	-0.5	-0.3	-0.2	-0.5	-4.3	-1.8	-0.6	-0.9	-1.8	-0.9	-0.5	-0.8	-13.1
	0.8 - ∞	0.0	0.0	0.0	-3.2	-16.2	-26.1	-24.0	-20.5	-12.7	-7.3	-0.1	0.0	-110.1
	TOTAL	-1.5	-0.9	-1.3	-5.9	-26.7	-30.0	-27.5	-25.3	-24.9	-10.2	-2.7	-2.4	-159.3
	3 m	0.0	0.0	0.0	-3.5	-18.8	-28.4	-27.5	-26.7	-16.8	-7.9	-0.1	0.0	-129.7
Conductive heat flux $<F_c>$	0-0.1	3.1	2.0	4.1	4.1	6.1	0.1	0.0	3.3	13.7	4.6	6.4	3.9	51.4
	0.1-0.2	3.4	2.3	4.7	4.2	3.6	0.0	0.0	0.1	8.1	3.9	6.7	5.5	42.5
	0.2-0.4	6.3	3.9	6.2	4.6	4.1	0.0	0.0	0.0	7.8	4.4	9.8	11.4	58.5
	0.4-0.8	9.3	6.2	4.2	2.3	3.6	0.0	0.0	0.0	4.4	5.5	8.5	14.9	58.9
	0.8 - ∞	30.6	32.4	22.4	3.1	-19.0	-4.5	0.0	0.0	20.1	33.5	35.0	29.9	183.5
	TOTAL	52.7	46.8	41.6	18.3	-1.6	-4.4	0.0	3.4	54.1	51.9	66.4	65.6	394.8
	3 m	32.5	33.7	23.4	3.0	-22.1	-5.0	0.0	0.0	26.1	36.1	38.0	33.3	199.0
Salt flux	0-0.1	.14	.09	.18	.21	.27	-.05	.00	-.06	.83	.26	.30	.18	2.35
	0.1-0.2	.20	.14	.28	.25	.14	-.05	-.06	-.04	.51	.26	.42	.34	2.39
	0.2-0.4	.42	.26	.40	.27	.13	-.13	-.13	-.08	.51	.31	.66	.76	3.38
	0.4-0.8	.66	.44	.29	.15	.07	-.35	-.29	-.18	.29	.40	.61	1.06	3.15
	0.8 - ∞	2.43	2.65	2.38	1.59	.71	-3.96	-6.20	-1.91	-.20	.57	1.33	2.06	1.45
	TOTAL	3.85	3.58	3.53	2.47	1.32	-4.54	-6.68	-2.27	1.94	1.80	3.32	4.40	12.72
	3 m	1.57	1.77	1.84	1.71	1.25	-3.60	-7.30	-2.09	-.45	-.41	.21	1.24	-4.26

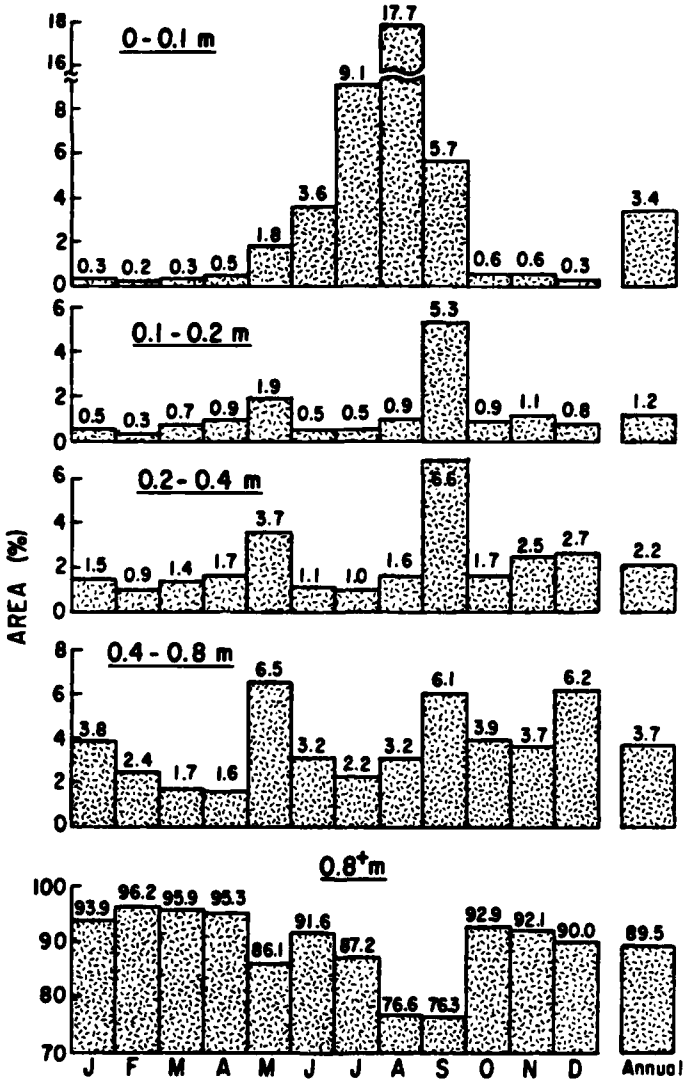

Fig. 28. Calculated distribution of ice thickness in the central Beaufort Sea (after *Maykut*, 1982).

annual net radiation balance for the region was more than double what would have been expected on the basis of measurements over thicker ($h > 1$ m) ice. Most of this additional energy input came from solar radiation absorbed in summer leads and ultimately went to lateral melting on floe edges and to F_w. The amount of solar radiation absorbed beneath the ice during the summer was about 105 MJ m^{-2}, more than a factor of 50 greater than the amount that would be absorbed beneath a continuous 3 m thick ice cover. Conduction of heat to the surface

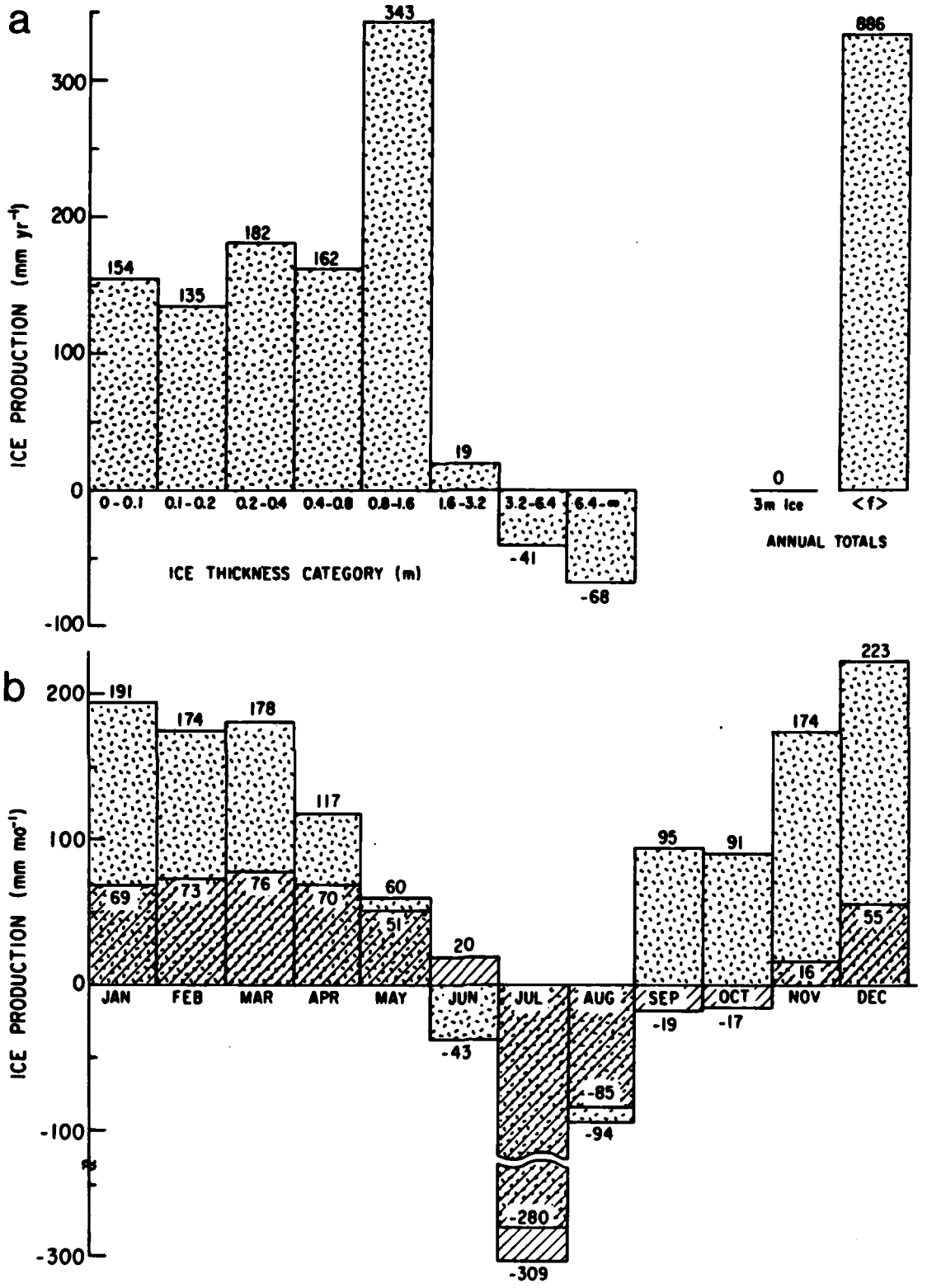

Fig. 29. Regional ice production in the central Beaufort Sea: (a) annual totals in each thickness category, (b) monthly totals taking into account ice thickness variations (stippled) and assuming a uniform 3 m thick ice cover (cross-hatched) (after *Maykut*, 1982).

increased by a factor of 2 when thickness variations were taken into account. Most of this heat was lost to the atmosphere during the fall and winter via larger turbulent fluxes. Turbulent heat input to the atmosphere totaled about 200 MJ m^{-2} for the year, due in large part to greater sensible heat losses associated with young ice formation in the fall. It is notable that the open water category (0-10 cm) did not dominate the balance, rather it was the intermediate thicknesses of young ice (10-80 cm) that were responsible for over half the total loss.

Total ice production within the region <f> was also dramatically larger when contributions from young ice were considered. Figure 29a shows annual ice production in each of the thickness categories. The mass produced in the 0-10 cm category, for example, was equivalent to a 15.4 cm thick layer covering the entire region. For the year <f> totaled about 89 cm, in contrast to the zero mass balance expected for 3 m ice. Growth in areas of first-year ice accounted for essentially all of the net ice production. Despite the extremely large growth rates in new leads, only about 15% of the first-year ice production occurred in the 0-10 category, reflecting the very small area occupied by open water during the winter. As expected, the greatest production took place following the fall freezeup. Seasonal variations in the flux of salt to the ocean paralleled the ice production. Net salt input began in mid-September, the observed time of minimum salt content in the mixed layer. Without young ice, the salt content of the mixed layer would not begin to increase significantly until early December.

Numerical experiments were also conducted to determine how uncertainties in specified strains might affect regional heat and mass fluxes. It was found that the average divergence of the ice was poorly correlated with monthly or annual heat flux totals, but that <f> was related to the time average of the strain components. Ice typically alternates between diverging and converging motions over periods of days, producing continual changes in the amount of open water, ice production, and ridging activity. It appears that these short-term variations in strain are more important to the thermodynamics than the

longer term averages. The tendency for <f> to increase with increased divergence suggests that variations in the export of ice from the Arctic Basin may not have a great impact on total ice volume because of the compensating changes in ice production.

These calculations have shown that thin ice and open water resulting from differential ice movement cause interactions between the ocean and atmosphere to be much more vigorous than would be the case for a uniform, static ice cover. Further, it is evident that care must be exercised when interpreting local measurements made in areas of nonuniform ice. Failure to consider thickness variations and how they affect area averages can lead to substantial errors in understanding large-scale interactions between the ice, ocean, and atmosphere.

REFERENCES

Aagaard, K., L. K. Coachman and E. Carmack, On the halocline of the Arctic Ocean, *Deep Sea Res., 28*, 529-45, 1981.

Ackley, S. F., Mass-balance aspects of Weddell Sea pack ice, *J. Glaciol., 24*(90), 391-405, 1979.

Ackley, S. F. and T. Keliher, Antarctic sea ice dynamics and its possible climatic effects, *AIDJEX Bull., 33*, 53-76, 1976.

Alexander, V., Interrelationships between the seasonal sea ice and biological regimes, *Cold Regions Sci. Tech., 2*, 157-78, 1980.

Allison, I., Antarctic sea ice growth and oceanic heat flux, in *Sea Level Ice and Climatic Change*, I. Allison (ed.), IAHS Publ. 131, Washington, D.C., 161-70, 1981.

Anderson, D. L., A model for determining sea ice properties, in *Arctic Sea Ice*, National Academy of Sciences, NRC Publ. 598, Washington, D.C., 148-52, 1958.

Anderson, D. L., Growth rate of sea ice, *J. Glaciol., 3*, 1170-72, 1961.

Andreas, E. L. and S. F. Ackley, On the differences in ablation seasons of the arctic and antarctic sea ice, *J. Atmos. Sci., 39*, 440-47, 1982.

Armstrong, T., B. Roberts and C. Swithinbank, *Illustrated Glossary of Snow and Ice*, Scott Polar Research Institute, Cambridge, 60 pp., 1973.

Assur, A., Composition of sea ice and its tensile strength, in *Arctic Sea Ice*, National Academy of Sciences, NRC Publ. 598, Washington, D.C., 106-38, 1958.

Badgley, F. I., Heat balance at the surface of the Arctic Ocean, in *Proc. Symposium Arctic Heat Budget and Atmospheric Circulation*, J. O. Fletcher (ed.), RAND Corp. Memorandum RM-5233-NSF, Santa Monica, 267-77, 1966.

Bauer, J. and S. Martin, Field observations of the Bering Sea ice edge properties during March 1979, *Mon. Weather Rev., 108*, 2045-56, 1980.

Bergdahl, L., *Physics of Ice and Snow as Affects Thermal Pressure*, Chalmers University, Dept. Hydraulics, Rept. Series A:1, Goteborg, Sweden, 158 pp., 1977.

Bilello, M. A., Formation, growth and decay of sea ice in the Canadian Arctic Archipelago, *Arctic, 14*, 3-24, 1961.

Budd, W. F., Antarctic sea ice variation from satellite sensing in relation to climate, *J. Glaciol., 15*, 417-28, 1975.

Buynitskiy, V. Kh., The influence of microalgae on the structure and strength of antarctic sea ice, *Oceanology, 8*, 771-76, 1968.

Campbell, W. J., P. Gloersen, W. J. Webster, T. T. Wilheit and R. O. Ramseier, Beaufort Sea ice zones as delineated by microwave imagery, *J. Geophys. Res., 81*, 1103-10, 1976.

Carsey, F. D., Microwave observations of the Weddell Sea polynya, *Mon. Weather Rev., 108*, 2032-44, 1980.

Carsey, F. D., Arctic sea ice distribution at the end of summer 1973-76 from satellite microwave data, *J. Geophys. Res., 87*(C8), 5809-35, 1982.

Cavalieri, D. J., S. Martin and P. Gloersen, Nimbus 7 SMMR observations of the Bering Sea ice cover during March 1979, *J. Geophys. Res., 88*, 2743-54, 1983.

Central Intelligence Agency, *Polar Regions Atlas*, GC 78-10040, U.S.G.P.O., Washington, D.C., 66 pp., 1978.

Cherepanov, N. V., Using the method of crystal optics for determining the age of drift ice (in Russian), *Probl. Arkt., 2*, 179-84, 1957.

Cherepanov, N. V., Spatial alignment of sea ice crystal structure (in Russian), *Probl. Arkt. Antarkt., 38*, 176-81, 1971.

Colony, R. and A. S. Thorndike, An estimate of the mean field of arctic sea ice motion, in *Proc. Eighth Conference on Probability and Statistics in Atmospheric Sciences*, American Meteorological Society, Boston, 10-15, 1983.

Coon, M. D., G. A. Maykut, R. S. Pritchard, D. A. Rothrock and A. S. Thorndike, Modeling the pack ice as an elastic-plastic material, *AIDJEX Bull., 24*, 1-105, 1974.

Cox, G. F. N. and W. F. Weeks, Salinity Variations in Sea Ice, *J. Glaciol., 13*, 109-20, 1974.

Cox, G. F. N. and W. F. Weeks, *Brine Drainage and Initial Salt Entrapment in Sodium Chloride Ice*, CRREL Research Report 345, Hanover, 85 pp., 1975.

Dayton, P. K., G. A. Robillard and A. L. DeVries, Anchor ice formation in McMurdo Sound, Antarctica, and its biological effects, *Science*, *163*, 273-74, 1969.

Doronin, Yu. P., On the heat balance of the Central Arctic (in Russian), *Tr. Arkt. Antarkt. Nauchno-Issled. Inst.*, *253*, 178-84, 1963. (Transl. in *Soviet Data on the Arctic Heat Budget and Its Climatic Influence*, J. O. Fletcher, B. Keller and S. M. Olenicoff, eds., RAND Corp. Memorandum RM-5003-PR, Santa Monica, 193-205, 1966.)

Doronin, Yu. P. and D. E. Kheisin, *Sea Ice*, Gidrometeoizdat Publishers, Leningrad, 323 pp., 1975. (Transl. by NSF, TT75-52088, 1977.)

Eide, L. and S. Martin, The formation of brine drainage features in young sea ice, *J. Glaciol.*, *14*, 137-54, 1975.

Frankenstein, G. E. and R. Garner, Equations for determining the brine volume of sea ice from -0.5° to -22.9°C, *J. Glaciol.*, *6*(48), 943-44, 1967.

Gill, A. E., Circulation and bottom water production in the Weddell Sea, *Deep-Sea Res.*, *20*, 111-40, 1973.

Gordienko, P., Arctic ice drift, in *Proc. Conference on Arctic Sea Ice*, National Academy of Sciences Publ. 598, Washington, D.C., 210-22, 1958.

Gordon, A. L., Seasonality of southern ocean sea ice, *J. Geophys. Res.*, *86*, 4193-97, 1981.

Gordon, A. L., C. T. A. Chen and W. G. Metcalf, Winter mixed layer entrainment of Weddell deep water, *J. Geophys. Res.*, *89*, 637-40, 1984.

Grenfell, T. C. and G. A. Maykut, The optical properties of ice and snow in the Arctic Basin, *J. Glaciol.*, *18*(80), 445-63, 1977.

Grenfell, T. C. and D. K. Perovich, Spectral albedos of sea ice and incident solar irradiance in the southern Beaufort Sea, *J. Geophys. Res.*, *89*(C3), 3573-80, 1984.

Hall, R. T., Seasonal photo mosaic of the AIDJEX triangle, *AIDJEX Bull.*, *39*, 79-84, 1978.

Hallett, J., Crystal growth and the formation of spikes in the surface of supercooled water, *J. Glaciol.*, *3*, 698-702, 1960.

Harrison, J. D. and W. A. Tiller, Controlled freezing of water, in *Ice and Snow*, W. D. Kingery (ed.), MIT Press, Cambridge, 215-25, 1963.

Herbert, W., The first surface crossing of the Arctic Ocean, *Geogr. J., 136*, 511-33, 1970.

Hibler, W. D. III, A dynamic thermodynamic sea ice model, *J. Phys. Oceanogr., 9*, 815-46, 1979.

Hibler, W. D. III, Sea ice growth, drift, and decay, in *Dynamics of Snow and Ice Masses*, S. C. Colbeck (ed.), Academic Press, New York, 141-209, 1980.

Idso, S. B. and R. D. Jackson, Thermal radiation from the atmosphere, *J. Geophys. Res., 74*, 5397-403, 1969.

Kovacs, A. and M. Mellor, Sea ice morphology and ice as a geological agent in the Southern Beaufort Sea, in *The Coast and Shelf of the Beaufort Sea*, J. C. Reed and J. E. Sater (eds.), AINA, Arlington, 113-24, 1974.

Laevastu, T., Factors affecting the temperature of the surface layer of the sea, *Commentat. Phys. Math., Soc. Sci. Fenn., 25*(1), 8-134, 1960.

Lake, R. A. and E. L. Lewis, Salt rejection by sea ice during growth, *J. Geophys. Res., 75*, 583-97, 1970.

Langleben, M. P., On the factors affecting the rate of ablation of sea ice, *Canadian J. Earth Sci., 3*, 431-39, 1966.

Langleben, M. P., The decay of an annual ice cover, *J. Glaciol., 11*, 337-44, 1972.

Langleben, M. P. and E. R. Pounder, Elastic parameters of sea ice, in *Ice and Snow*, W. D. Kingery (ed.), MIT Press, Cambridge, 69-78, 1963.

Larsen, L., Sediment-laden sea ice: concepts, problems, and approaches, *Outer Continental Shelf Environmental Assessment Program, NOAA, Arctic Project Bulletin, 29*, 59-69, 1980.

Leavitt, E., M. Albright and F. D. Carsey, Report on the AIDJEX meteorological experiment, *AIDJEX Bull., 39*, 121-48, 1978.

Lindsay, R. W., *Wind and Temperature Profiles Taken During the Arctic Lead Experiment*, M.S. Thesis, Dept. Atmospheric Sciences, University of Washington, Seattle, 89 pp., 1976.

Marshunova, M. S., Principal characteristics of the radiation balance of the underlying surface and of the atmosphere in the Arctic, in *Soviet Data on the Arctic Heat Budget and Its Climatic Influence*, J. O. Fletcher *et al.* (eds.), RAND Corp. Memorandum RM-5003-PR, Santa Monica, 51-131, 1966. (Transl. from *Proc. Arct. Antarc. Res. Inst.*, *229*, 5-53, 1961.)

Martin, S., Ice stalactites: comparison of a laminar flow theory with experiment, *J. Fluid Mech.*, *63*, 51-79, 1974.

Martin, S., Frazil ice in rivers and oceans, *Annu. Rev. Fluid Mech.*, *13*, 379-97, 1981.

Martin, S. and P. Kauffman, The evolution of underice melt ponds, or double diffusion at the freezing point, *J. Fluid Mech.*, *64*, 507-27, 1974.

Martin, S. and P. Kauffman, A field and laboratory study of wave damping by grease ice, *J. Glaciol.*, *27*(96), 283-313, 1981.

Maykut, G. A., Energy exchange over young sea ice in the Central Arctic, *J. Geophys. Res.*, *83*(C7), 3646-58, 1978.

Maykut, G. A., Large-scale heat exchange and ice production in the Central Arctic, *J. Geophys. Res.*, *87*(C10), 7971-84, 1982.

Maykut, G. A., The surface heat and mass balance, in *The Geophysics of Sea Ice*, N. Untersteiner (ed.), Chapter 5, Plenum Publ. Corp., New York (in press) 1985.

Maykut, G. A. and P. E. Church, Radiation climate of Barrow, Alaska, 1962-66, *J. Appl. Meteorol.*, *12*(4), 620-28, 1973.

Maykut, G. A. and T. C. Grenfell, The spectral distribution of light beneath first-year sea ice in the Arctic Ocean, *Limnol. Oceanogr.*, *20*(4), 554-63, 1975.

Maykut, G. A. and N. Untersteiner, *Numerical Prediction of the Thermodynamic Response of Arctic Sea Ice to Environmental Changes*, RAND Corp. Memorandum RM-6093-PR, Santa Monica, 173 pp., 1969.

Maykut, G. A. and N. Untersteiner, Some results from a time dependent, thermodynamic model of sea ice, *J. Geophys. Res.*, *76*(6), 1550-75, 1971.

McPhee, M. G., Physical oceanography of the seasonal sea ice zone, *Cold Regions Sci. Tech.*, *2*, 93-118, 1980.

McPhee, M. G., Greenland Sea ice/ocean margin, *EOS*, *64*, 82-3, 1983.

Mellor, M., *Mechanical Behavior of Sea Ice*, CRREL Monograph 83-1, Hanover, 105 pp., 1983.

MIZEX West Study Group, MIZEX West: Bering Sea marginal ice zone experiment, *EOS*, *64*, 578-79, 1983.

Morecki, V. N., Underwater sea ice (in Russian), *Probl. Arkt. Antarkt.*, *19*, 32-8, 1965. (English transl., Def. Res. Board Canada, Transl. T497 R, 1968.)

Morey, R. M., A. Kovacs and G. F. N. Cox, *Electromagnetic Properties of Sea Ice*, 32 pp., CRREL Rept. 84-2, Hanover, 32 pp., 1984.

Muench, R. D. and K. Ahlnas, Ice movement and distribution in the Bering Sea from March to June 1974, *J. Geophys. Res.*, *81*, 4467-76, 1976.

Nakawo, M. and N. K. Sinha, Growth rate and salinity profile of first-year sea ice in the high Arctic, *J. Glaciol.*, *27*, 315-30, 1981.

Neumann, G. and W. J. Pierson, *Principles of Physical Oceanography*, Prentice-Hall, Englewood Cliffs, p. 43, 1966.

Newbury, T. K., Under landfast ice, *Arctic*, *36*, 328-40, 1983.

Niedrauer, T. M. and S. Martin, An experimental study of brine drainage and convection in young sea ice, *J. Geophys. Res.*, *84*, 1176-86, 1979.

Ono, N., Specific heat and heat of fusion of sea ice, in *Physics of Snow and Ice, 1*, H. Oura (ed.), Inst. Low Temp. Sci., Hokkaido, Japan, 599-610, 1967.

Ono, N., Thermal properties of sea ice IV: Thermal constants of sea ice (in Japanese), *Low Temp. Sci., A26*, 329-49, 1968.

Paige, R. A., *Crystallographic Studies of Sea Ice in McMurdo Sound, Antarctica*, US Naval Civil Engineering Lab. Tech. Rept. R494, Washington, D.C., 31 pp., 1966.

Parmerter, R. R. and M. D. Coon, Model of pressure ridge formation in sea ice, *J. Geophys. Res.*, *77*, 6565-75, 1972.

Perovich, D. K. *On the Summer Decay of a Sea Ice Cover*, Ph.D. Thesis, Geophysics Program, University of Washington, Seattle, 176 pp., 1983.

Reeburgh, W. S. and M. Springer-Young, New measurements of sulfate and chlorinity in natural sea ice, *J. Geophys. Res.*, *88*, 2959-66, 1983.

Rothrock, D. A., The energetics of the plastic deformation of pack ice by ridging, *J. Geophys. Res.*, *80*(33), 4514-19, 1975.

Rothrock, D. A. and A. S. Thorndike, Measuring the sea ice floe size distribution, *J. Geophys. Res.*, *89*(C4), 6477-86, 1984.

Schwarzacher, W., Pack ice studies in the Arctic Ocean, *J. Geophys. Res.*, *64*, 2357-67, 1959.

Schwerdtfeger, P., The thermal properties of sea ice, *J. Glaciol.*, *4*, 789-807, 1963.

Semtner, A. J., A model for the thermodynamic growth of sea ice in numerical investigations of climate, *J. Phys. Oceanogr.*, *6*, 379-89, 1976.

Shine, K. P., Parameterization of shortwave flux over high albedo surfaces as a function of cloud thickness and surface albedo, *Q.J.R. Meteorol. Soc.*, *110*, 747-61, 1984.

Streten, N. A., Satellite observations of the summer decay of the antarctic sea ice, *Arch. Meteorol. Geophys. Bioklimatol.*, *A22*, 119-34, 1973.

Svendsen, E., K. Kloster, B. Farrelly, O. M. Johannessen, J. A. Johannessen, W. J. Campbell, P. Gloersen, D. Cavalieri and C. Matzler, Norwegian remote sensing experiment: Evaluation of the Nimbus 7 scanning multichannel microwave radiometer for sea ice research, *J. Geophys. Res.*, *88*(C5), 2781-91, 1983.

Thorndike, A. S., D. A. Rothrock, G. A. Maykut and R. Colony, The thickness distribution of sea ice, *J. Geophys. Res.*, *80*(33), 4501-13, 1975.

Thorpe, M. R., E. G. Banke and S. D. Smith, Eddy correlation measurements of evaporation and sensible heat flux over arctic sea ice, *J. Geophys. Res.*, *78*, 3573-84, 1973.

Tucker, W. B. and J. W. Govoni, Morphological investigations of first-year sea ice pressure ridge sails, *Cold Regions Sci. Tech.*, *5*, 1-12, 1981.

Tucker, W. B., W. F. Weeks and M. Frank, Sea ice ridging over the Alaskan continental shelf, *J. Geophys. Res.*, *84*, 4885-97, 1979.

Tucker, W. B., W. F. Weeks, A. Kovacs and A. J. Gow, Nearshore ice motion at Prudhoe Bay, Alaska, in *Sea Ice Processes and Models*, R. S. Pritchard (ed.), University of Washington Press, Seattle, 261-72, 1980.

Untersteiner, N., On the mass and heat budget of arctic sea ice, *Arch. Meteorol. Geophys. Bioklimatol., A12*, 151-82, 1961.

Untersteiner, N., Natural desalination and equilibrium salinity profile of perennial sea ice, *J. Geophys. Res., 73*, 1251-57, 1968.

Vinje, T. E., *Sea Ice Studies in the Spitzbergen-Greenland Sea Area*, Landsat Rept. E77-10206, US Dept. Commerce, Washington, D.C., 1977.

Wadhams, P., *The Effect of a Sea Ice Cover on Ocean Surface Waves*, Ph.D. thesis, University of Cambridge, England, 223 pp., 1973.

Wadhams, P., Ice characteristics in the seasonal sea ice zone, *Cold Regions Sci. Tech., 2*, 37-87, 1980.

Wadhams, P., Sea-ice topography of the Arctic Ocean in the region 70°W to 25°E, *Philos. Trans. R. Soc. London, A302*, 45-85, 1981.

Wadhams, P. and R. J. Horne, An analysis of ice profiles obtained by submarine sonar in the Beaufort Sea, *J. Glaciol., 25*, 401-24, 1980.

Walker, E. R. and P. Wadhams, Thick sea-ice floes, *Arctic, 32*, 140-47, 1979.

Walsh, J. E. and C. M. Johnson, An analysis of arctic sea ice fluctuations, 1953-77, *J. Phys. Oceanogr., 9*, 580-91, 1979.

Wang, Y. S., Uniaxial comparison testing of arctic sea ice, *International Conference on Port & Ocean Engineering under Arctic Conditions, POAC*, Vol. 1, Quebec, 346-55, 1981.

Weeks, W. F. and S. F. Ackley, *The Growth, Structure, and Properties of Sea Ice*, CRREL Monograph 82-1, Hanover, 130 pp., 1982.

Weeks, W. F. and A. Assur, *Fracture of Lake and Sea Ice*, CRREL Research Rept. 269, Hanover, 77 pp., 1969.

Weeks, W. F. and A. J. Gow, Preferred crystal orientations along the margins of the Arctic Ocean, *J. Geophys. Res., 84*, 5105-21, 1978.

Weeks, W. F. and W. L. Hamilton, Petrographic characteristics of young sea ice, Point Barrow, Alaska, *Am. Mineral., 47*, 945-61, 1962.

Weeks, W. F. and O. S. Lee, The salinity distribution in young sea ice, *Arctic, 15*, 93-108, 1958.

Yen, Y. C., *Review of Thermal Properties of Snow, Ice, and Sea Ice*, CRREL Research Rept. 81-10, Hanover, 27 pp., 1981.

Zillman, J. W., A study of some aspects of the radiation and heat budgets of the southern hemisphere oceans, *Meteorol. Studies, 26*, Bureau of Meteorol., Dept. of Interior, Canberra, Australia, 562 pp., 1972.

Zubov, N. N., *L'dy Arktiki (Arctic Ice)*, Izdatel'stvo Glavsevmorputi, Moscow, 491 pp., 1945. (Translated from Russian by U.S. Naval Oceanographic Office and American Meteorological Society, 1965.)

Zwally, H. J., J. C. Comiso, C. L. Parkinson, W. J. Campbell, F. D. Carsey and P. Gloersen, *Antarctic Sea Ice, 1973-1976: Satellite Passive-Microwave Observations*, Chapter 5, NASA SP-459, Washington, D.C., 206 pp., 1983.

END

DTIC

5-86